A Tutorial on:

Fire Safety Issues of "Adiabatic" Processes in Real- and Ideal-Oxidant Systems

Barry L. Werley

This publication is in a series meant to finalize, and archive materials that were openly available for use or comment on the author's web site in the period 2000-2011. These were and are voluntary "as is" and "use at your own risk" analysis during the author's retirement and as such are non-profit, public-service opinion for use at your own discretion, and any costs are those of reproduction. A digital electronic PDF is also being prepared to be included with numerous other related materials for free and open unaltered distribution in print or electronic form. It may be reproduced and quoted to any degree.

As public opinion, expected to outlive the author, there is no long-term earthly publisher location to cite or contact.

Other related materials from the web site include commentary on fire and explosion limit analysis, suggested technical content for oxygen safety standards, computer software utilities (all again as is and use at your own risk basis) and source code.

25 September 2016.

Table of Contents

Blank Transition Page

Abstract

REFERENCE: Werley, B. L., **" A Tutorial on Fire Safety Issues of 'Adiabatic' Processes in Real and Ideal Oxidant Systems"**, ©2007, ©2016, Public Domain 2016, 140 pages.

ABSTRACT: Rapid oxidant compression calculations are often predicated on ideal gas assumptions. Comparable real-gas calculations and estimates are offered based on data in National Institute of Standards and Technology databases, in comparison to other efforts. The math is reviewed in detail and simplified, and a simplified algorithm for making estimates is proposed. Real and ideal calculations are performed for a series of common oxidant safety parameters and for the series of oxidants: O_2, F_2, NF_3 and N_2O, and selected diluents and oxygen mixtures with several diluent gases. Context is proposed for use of these data by oxidant system designers and users.

KEY WORDS: adiabatic compression, isentropic compression, heat of compression, temperature of compression, oxygen, fluorine, nitrogen trifluoride, nitrous oxide, argon, helium, carbon dioxide, tetrafluoromethane.

Introduction

Rapid compression and rapid expansion of oxidants are important concerns of Oxidant Safety Practitioners (OSPs). Both can lead to fires, injuries and system and mission damage. Among them, rapid compression has received the most attention.

In common circumstances familiar to OSPs, when a gas (including an oxidant gas) is rapidly compressed, it warms and can get hot. This is well known and has been successfully demonstrated in many laboratory tests. Sometimes, the high temperature and the heat it can transfer can cause ignition and fire of some materials. This too has been demonstrated in the laboratory, and it is often cited as a cause of some accidents. The ignition and fire are more likely if the transient gas temperature is high, protracted, and transfers a large heat. The tendency to do this depends on the actual properties of the oxidant gas and system, and the compression method.

Attempting to understand, estimate and analyze this effect is not easy, and it is a non-trivial challenge that has always confronted OSPs. Assumptions and simplifications (that to some of us are not so simplifying and can even serve to obscure) are like the layers on an onion. Those layers are described with words like adiabatic, isentropic, reversible, ideal. It can be very confusing.

Progress has been made to be sure, but yet in many cases where fires are attributed to rapid compression, lab simulations have been wanting. Often when one rapidly pressurizes a system that is expected to ignite, to simulate one that may have in fact ignited thusly, it doesn't. Similarly, there are a number of test procedures, including two from ASTM G-4 [***1-2***][1], that seek to expose materials and components to rapid compression as a way to pursue safety. These also are not yet definitive. Components that pass the test may not be totally immune to these fires.

On the other hand, when a gas is rapidly expanded, it cools but often produces high velocities that can propel particles into collisions that can also initiate fires. International standards recommend limits on allowable oxygen velocities to control this risk [***3***].

The book on rapid compression and expansion is not closed. There is a macro understanding that is pretty good, but much still lies in the details. This tutorial is written from the mid-level of the intellectual food chain and seeks to understand and simplify some of the more complex analyses out there and to advance still others. The writer has tried to do this before with this and other topics to better (or at least more simply or more thoroughly) review the current analyses of several fluid mechanical processes [***4,5***]. Unencumbered again by any commercial publication limits on size and content, this commentator will seek to find and learn information that is not hidden but might as well be for some of us. This opinion will belabor many rapid compression issues in perhaps extreme detail and ad nauseam in hopes of providing another useful, and different, perspective in that same spirit. To some this may seem too much, an overdose, of the subject.

The most commonly pursued need of OSPs, is the prediction of the peak temperature that occurs during compression. To a large extent, this is in hopes of establishing whether the maximum achievable will be below the minimum ignition temperatures of materials in use. However, this is not to say that the peak temperature in well-designed systems always is or always should be limited this way. In many oxygen systems, it is certain that the maximum possible is well above the minimum ignition temperature by large margins and, at least most of the time, ignition still does not seem to occur even with this extreme provocation.

This owes in part to the fact that minimum ignition temperatures are measured for a specimen with a uniform (bulk) temperature throughout. Rapid compression exposes only the surface of the material to a transient high temperature. And this should be less prone to ignition in many, but perhaps not all, cases. So this is one factor auguring for a mismatch between the peak rapid compression temperature and the minimum autogenous ignition temperature. There are other factors, as well.

[1] Italic numbers in brackets refer to the reference list at the end of the paper.

The writer has also made rough attempts [***6,7***] at also estimating the amount of heat that might transfer during rapid compression to also improve understanding of where the worst-case rapid compression conditions might obtain. These attempted to estimate whether the heat transfer might exceed the minimum ignition energy required before the peak temperature produced decays below the *in-situ* ignition temperature, for where this constraint may also be desirable to impose in some systems. Wilson, et al. [***8***] have attempted a much more detailed but also much more complex analysis that, for the cases examined, exhibits trends similar to the earlier qualitative and semi-quantitative approaches.

It is common practice to estimate the behavior of many gases, including oxygen, during rapid compression using the ideal gas equations:

$$P_i V_i^{\gamma} = P_f V_f^{\gamma}, \quad (P_f/P_i) = (V_i/V_f)^{\gamma} = (V_f/V_i)^{-\gamma} \tag{1}$$

$$T_f/T_i = (P_f/P_i)^{(\gamma-1)/\gamma} \tag{2}$$

$$T_f/T_i = (V_i/V_f)^{(\gamma-1)} = (V_f/V_i)^{(1-\gamma)} \tag{3}$$

Where P is the absolute pressure, V is the volume, T is the absolute temperature, the subscripts *i* and *f* indicate the initial and final states, and the parameter γ (usually taken as 1.4 for oxygen) is a constant ratio of the specific heats, C_p/C_v where C_p is the specific heat at constant pressure and C_v is the specific heat at constant volume. Figure 1 exhibits these three equations for oxygen at an initial atmospheric pressure and room temperature and a final pressure of 5000 psia[2]. Beside each plot is a log-log analog to show how this perfectly linearizes the curves for ideal gases of constant γ. Note that the slope of the three curves, respectively, is given by $-\gamma$, $(\gamma-1)/\gamma$, and $-(\gamma-1)$. For a γ of 1.4, these three slopes would be about –1.4, 0.286, and –0.4, respectively.

These equations are ubiquitous, easy to misuse, and make assumptions, not all of which are clearly specified in standard texts. Some of the assumptions are misleading and the writer feels some of the most common assumptions (albeit few in number) are ill-advised (including as to implications relating to whether the gas is ideal).

ASTM Committee G-4 on Compatibility and Sensitivity of Materials in Oxygen-Enriched Atmospheres suggests this same approach in its numerous standards, and for a time provided a balloted PC utility (G4Math12.exe)[3] for aiding the calculation, and it is similarly

[2]The author grew up, and is most familiar, with the now disdained fps system of units. He has often published papers with dual units and embarrassed himself with errors in the conversion to SI. Therefore, in this paper the fps system will predominate except where citing other work. Humble apologies for this concession to accuracy.

[3]G4Math is a PC utility (algorithm) that ASTM G4 adopted in the early 1990s and expanded several times through 1998. It has been distributed freely globally. It had been provided and was taught in G4 oxygen training classes. At present the status of G4Math is "abandoned". It was 16-bit software useable only on 32-bit Windows PCs, G4 has no energies to maintain it, and ASTM has become concerned about liability issues. Nonetheless, it is used as support and background for many of the calculations herein. Furthermore, in 2016 its source code was converted to 32-bit format so that it can be run on 64-bit Windows PCs in "Compatibility mode" and the ASTM G4 logo and imprimatur was removed (with resulting loss of credibility and prestige).

Eq (1): $P_f = P_i(V_i/V_f)^{\gamma}$ $\quad\quad$ $\mathrm{Log}_{10}P_f = \mathrm{Log}_{10}P_i - \gamma\ \mathrm{Log}_{10}(V_f/V_i)$

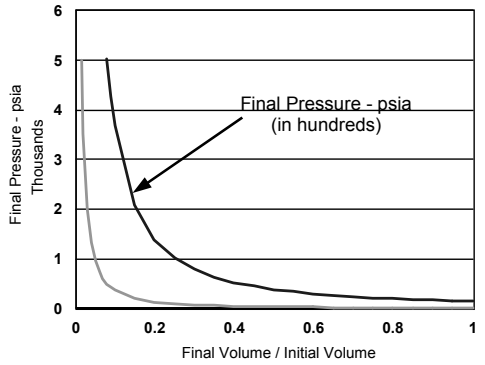

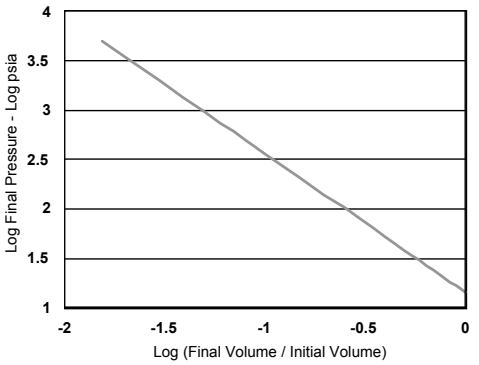

Eq (2): $T_f = T_i(P_f/P_i)^{(\gamma-1)/\gamma}$ $\quad\quad$ $\mathrm{Log}_{10}T_f = \mathrm{Log}_{10}T_i + [(\gamma-1)/\gamma]\ \mathrm{Log}_{10}(P_f/P_i)$

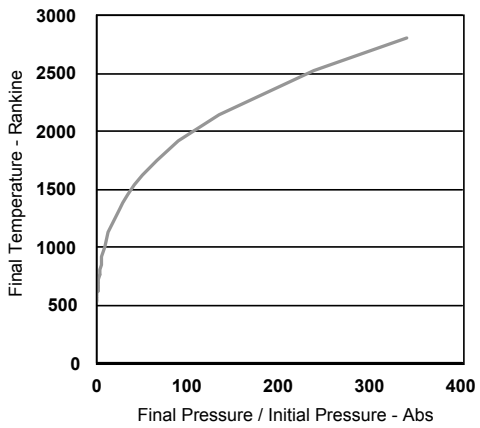

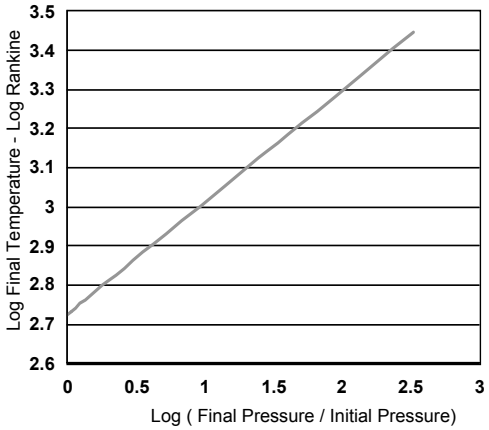

Eq (3): $T_f = T_i(V_i/V_f)^{\gamma-1}$ $\quad\quad$ $\mathrm{Log}_{10}T_f = \mathrm{Log}_{10}T_i - (\gamma-1)\ \mathrm{Log}_{10}(V_f/V_i)$

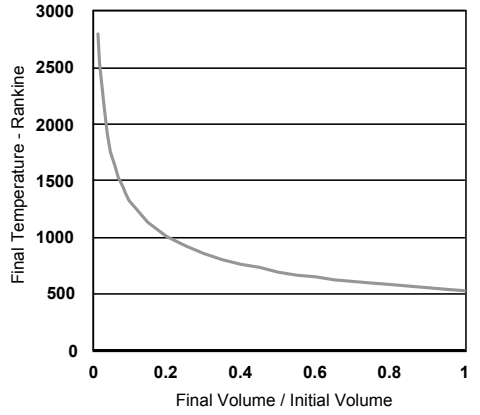

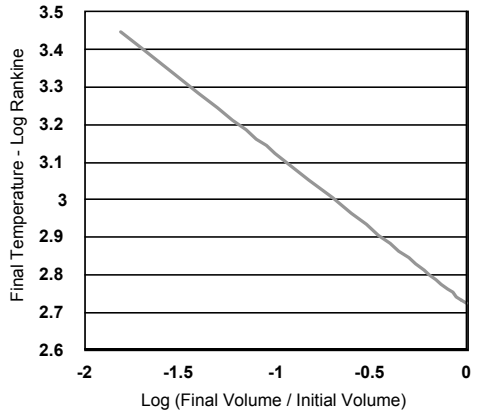

FIG. 1—*Interrelationships of parameter pairs during adiabatic processes for ideal gas of constant γ = 1.4. (Initial pressure = atm, 14.7 psia, Final pressure =5000 psia, Initial temperature = 70°F, 530°R)*

somewhat misleading. Oxygen is *not* precisely an ideal gas nor does it precisely meet other apparent underlying assumptions to equations (1-3), nor do a number of other things apply precisely during rapid oxygen pressurization in a real system.

Occasionally, a question arises as to how much error may be present in these temperature estimates. At least four papers [***9-11, 8***] have been presented in the ASTM collegium in 1989, 1999, 2000 and 2003 specifically examining what may be happening more precisely during rapid compression heating, and one of them [***10***] also looked at expansion and other related parameters. Three of these papers and their estimates will be elaborated upon. In addition, this tutorial will also attempt to expand upon them and the writer's prior efforts, and extend them all to other gases and other properties such as maximum gas velocities, TNT equivalency, and others.

Leslie (STP 1111)

In 1989, Leslie [***9***] published what is apparently the first thermodynamic and fluid mechanic analyses in the ASTM body of work. In the first part of his analysis, he compared adiabatic compression predictions three ways:

- Estimating peak temperature from adiabatic compression of room temperature, atmospheric pressure oxygen ("isentropic ideal gas model") using Equation (2) except that he used a value for γ of 1.395 instead of 1.4.

- Repetition of the above calculation but using "a curve allowing for variations in specific heat" obtained from page 688 in van Wylen [***12***] but assuming ideal-gas behavior implied in the equation:

$$P = P_o \exp\left[(1/R) \int \{C_p(T)/T\} dT\right] \tag{4}$$

- Calculations using van der Waals equation of state "with the two constants calculated using the critical point method." in combination with the equation:

$$(\partial T/\partial P)_S = (\partial v/\partial T)_p T/C_p \tag{5}$$

Leslie offered two conclusions. First, the influence of variations in the specific heat at constant pressure, $C_p(T)$, on the final temperature is large. Second, the consequence of compressibility effects is not significant. He calculated that oxygen compressed isentropically from ambient conditions to 34.5 MPa (5000 psi) by the three methods would achieve final temperatures of 1568K, 1339K, or 1365K, respectively. At this pressure ratio of 340 over ambient, the calculated final absolute temperature of the real gas estimates (the second and third calculations) were 14.6% and 12.9% less, respectively.

If Leslie had chosen to apply a γ of 1.4 with equation (2), he would have calculated a

final temperature of 1593K instead of 1568K. In this case a 0.36% change in γ results in a 1.6% change in the result. Clearly choosing the optimum γ is significant.

When he plotted all three equations on log-log paper, he found they are all fairly straight lines. He then calculated least-squares-fit slopes for the three methods for those who might wish to perform simplified "real-gas" calculations based on an empirical equation similar to equation (2). His values for "n" (which will be referred to as m_{TV} in later text), the real exponent which would analogous to [(γ-1)/γ] in Equation (2), were 0.2829, 0.2632, and 0.2599. However, Leslie did stress that: "The values on n for the last two cases strictly apply to T_i = 300K and P_i = 100kPa; (about 80°F, ambient pressure), small deviations from these values should cause little error". Clearly using his empirical "n" over smaller temperature ranges or in segments with adjustments to "n" for each would yield greater accuracy.

The writer obtained a copy of the source [***12***] Leslie used for $C_p(T)$ data and on page 688 in its Table A.9E (English units) and A.9SI (SI units), "Constant Pressure Specific Heats of Various Ideal Gases" are the following equations for oxygen:

$$C_{po} = 8.9465 + (4.8044 \times 10^{-3}\theta^{1.5}) - (42.679\theta^{-1.5}) + (56.615\theta^{-2}) \quad (6)$$

For use over the range 540-6300 R, with C_{po} in Btu/lb-mole-R, and θ in T(Rankine)/180.

$$C_{po} = 37.432 + (0.0201020\theta^{1.5}) - (178.57\theta^{-1.5}) + (236.88\theta^{-2}) \quad (7)$$

For use over the range 300-3500 K, with C_{po} (specific heat at zero pressure) in kJ/kmol-K, and θ in T(Kelvin)/100. Both of the equations are further attributed to T. C. Scott and R. E. Sonntag, Univ. of Michigan, 1971.

Barragan et al. (STP 1395)

Barragan et al. [***11***] is the most recent of the three papers in the ASTM collegium. The goal of these writers was to examine real-fluid effects and identify an optimal equation of state for real-gas calculations. They also compared their choice with other alternatives.

They compared the Peng-Robinson and Soave-Redlich-Kwong equations of state and found Peng-Robinson preferable. Using it and some heavy-duty mathematics, they calculated isentropic compression temperatures for single-phase, single component pressure ratios up to 1000 (in tabular form) and plotted results up to a pressure ratio of 100.

They compared the results to isentropic compression using the virial equation, and ideal-gas constant-specific-heat calculations of equation (2) and finally similar calculation for an ideal gas with a temperature-dependent heat capacity, using a variation of Eq. (4):

$$\int \{C_p(T)/T\}dT - R\ln(P_f/P_i) = 0 \quad (8)$$

The temperature dependence used for $C_p(T)$ in these cases (in J/mol K) was apparently speci-

fied in their Table 4 as:

$$C_p \text{ (vapor)} = 25.46 + 1.519 \times 10^{-2}T - 0.7151 \times 10^{-5}T^2 + 1.311 \times 10^{-9}T^3 \qquad (9)$$

This yields results as J/mol K, and the source of the equation is a cited text [***13***].

They concluded that the three alternatives to Equation (2) provide similarly different results to it at pressure ratios of 1000 for initial room temperature, atmospheric pressure starting conditions, and therefore, commended the use of the Peng-Robinson (PR) approach to OSPs as a "real gas" alternative that is now available.

In comparison to the Leslie approximations, this PR equation presumably also has merit for starting conditions, $P_{initial}$, other than atmospheric pressure and/or $T_{initial}$ other than room temperature (however, this is not explicitly stated and there are no such calculations presented in the paper). They argue use of this equation would therefore be a more general tool than Equations (1-3), for those comfortable with its solution.

However, linearly interpolating their results in their table 5, for a pressure ratio of 340 over ambient in order to compare them with the 340 pressure ratio of Leslie [***9***], their calculations by Equation (2) [their equation (10)] do not compare well with his. Their difference between the results from Equation (2) and "real oxygen" are about twice Leslie's. This appears to be due to an error in their use of Equation 2, in which they appear to have employed a γ of about 1.44 (perhaps an inadvertent double-key-tap on the "4" or key bounce in entering the value of γ?). At a pressure ratio of 500 this yields 2022 K for them versus 1730 K for Leslie (17% higher). In comparison, the values they calculate for real-oxygen final absolute temperature are closer to predictions by Leslie's empirical equation, and they are about 5% lower at a pressure ratio of 500 (1444.2 K for Barragan vs. 1530 K for Leslie). Table 1 presents a recalculation of their Table 5, adding data using a γ of 1.4, that is close in agreement to Leslie's results and data in Table 2 in a later paper from several of these same authors [***8***] for the same calculations[4] that are also in better agreement. Coincidentally, this again illustrates the dramatic difference that a mere 3% difference in γ (from 1.395 to 1.44) can yield, increasing the result by about 12-14% (from 1730K to 2022K). Using the optimum exponent is clearly important to precise results.

[4]Table 2 in [***8***] reports isentropic compression temperatures for oxygen and Nitrox (O_2/N_2 mixtures) at various "Compression Ratios", however, the writer believes "compression ratios" to have been a confusing and ill-advised word choice for the parameter that is more commonly called "pressure ratios" which the data reflect. The parameter "compression ratio" is widely applied in the automotive industry to reflect the geometric ratio of the max and min contained volume in a piston engine's cylinders, and interpreted in that way would yield much higher temperatures than are reported.

TABLE 1—*Recalculation of Isentropic Compression Temperature Values for Equation 10 in Table 5 of* Reference [***11***] Compared to Reference [***8***] *(Equation numbers refer to the original reference)*

	P_f/P_i[a]								
T_f Method Using:	**2**	**5**	**10**	**20**	**50**	**100**	**200**	**500**	**1000**
"Equation 10"	369	489	606	750	995	1232	1525	2022	2503
"Equation 10" (Recalculated)	363	472	576	701	912	1111	1354	1760	2145
Data from [*8*] Table 2[b]	363		572	696		1097	1335		
"Equation 11"	362	464	557	666	837	990	1166	1441	1686
"Equation 6"	362.2	464.8	558.3	667.3	838.8	992.3	1169.2	1444.2	1687.4

[a] T_i = 298.15, P_i = 101.3 kPa.
[b] T_i = 298, P_i = 101.3 kPa.

Koeller (March 1999 ASTM G4 Seminar)

In 1999, the writer suggested then-associate Koeller [***10***] perform "real-gas" calculations using a presumably reasonable numerical estimating technique in combination with "real γ" data from a proprietary software resource: Computer-Aided Physicochemical Properties (CAPP)[5] at Air Products and Chemicals, Inc., and then use of them to assess the effects of this estimated real gas on a number of common oxygen compatibility analyses. Another goal was to find a way to produce a simple PC algorithm for Oxygen Safety Practitioner use. However, she later compared the suggested method to direct isentropic temperature predictions also available from the same software facility and identified discrepancies. The attempted strategy of employing a "real γ" in this way seems common-sensible and improved results in some cases but appeared to introduce large errors especially when used for expansions, and the problems with "real γ" will be reviewed in some detail later. This effort predated Barragan et al. [***11***], but is reviewed here last because it is to be the basis for, and lead into, the analogous efforts in this tutorial.

The attempted estimate treated real oxygen as an ideal gas obeying equations (1) to (3) over a sequence of variable pressure intervals. Each was treated as beginning where the

[5]Not to be confused with the thermo program CAP (Coefficients and Properties) that is available from NASA – Cleveland, now NASA-Glenn.

last left off and employed a value of "real γ" obtained by dividing the C_p for the mid-point of the segment by the C_v for the midpoint employing popular spreadsheet software linked to the CAPP thermo software. This incremental integration yielded many useful results, despite the cited discrepancy.

She applied the method to six traditional oxygen compatibility calculations: adiabatic compression, adiabatic expansion, design of distance/volume pieces, total pressure estimation, TNT equivalency estimates, and maximum achievable gas velocities, and she discovered important results that every OSP should become at least qualitatively familiar with, including that the common impression that final temperature predictions made with equations (1-3) are always greater than would be experienced in real oxygen is *not* always correct. She offered a preliminary remote paper [***10***] at the Spring 1999 ASTM G-4 Seminar (Seattle).

Reasonably good correlation was obtained between the calculations and direct end-point isentropic data from the same CAPP software for some of the calculations. Unfortunately the problem of reconciling the results for some of the calculations in particular (adiabatic expansion) sidetracked the effort, and the hard-copy paper was never finalized nor distributed publicly. However, the results of this paper are so worthwhile that the writer will replicate (mimic) them here so that they are not lost. He has been shown the last (1999) drafts and communicated with Koeller prior to preparing this tutorial.

The earlier Leslie [**9**] and later Barragan et al. [***11***] papers suggest different approaches than Koeller as to how such calculations should be performed and reconciliation of the various methods is warranted. Therefore, the Koeller draft paper and its specific data will be referred to often in detail and expanded upon in this effort and then compared to the other approaches.

This effort.

The specific goals of this tutorial in order are as follows.

- Cite primary data resources for this tutorial in detail.
- Provide another round of analysis as to the potential error inherent in use of Equations (1-3) relative to real oxygen.
- Provide detailed, "simplified" derivations on performing adiabatic compression/expansion calculations.
- Critique the presentation of Equations (1-3) in standard texts and ASTM standards and propose alternatives.
- Explore the role of real heat transfer to these calculations.
- Replicate, document, and expand upon the several analyses in the Koeller [***10***] paper for numerous types of calculations.
- Consider methods to provide a simplified PC algorithm for OSP use in making these more precise calculations.
- Consider similar issues for several other oxidants and gases of interest namely: Fluorine, Nitrogen Trifluoride, Nitrous Oxide, Nitrogen, Argon,

Helium, Carbon Dioxide, Carbon Tetrafluoride, and selected mixtures of oxygen with some of the latter gases.

Data Resources for This Tutorial

The principal resources for data in this tutorial[6] in 2005-2007 were software packages available from the U.S. National Institute for Standards and Technology (NIST) available from their NIST Standard Reference Databases web site (http://www.nist.gov). The previously cited Air Products software CAPP and doubtless similar software at perhaps every air separation company is likely similar, and the availability of the NIST software makes this capability available widely for nominal costs.

One is NIST Standard Reference Database 12 *Thermodynamic and Transport Properties of Pure Fluids Reference Database*, Version 5.0 (copyrighted 2000) [***16***]. This database is Windows PC software that enables extraction of a spectrum of properties for a range of fluids including oxygen and other fluids that will be examined later. The database is claimed to be "based on the most accurate pure fluid equations currently available". "For each fluid the recommended thermodynamic surface is represented by an empirical multiparameter classical equation of state based either on a modified Benedict-Webb-Rubin equation of state or a more general type of Helmholtz energy equation of state". Its price was then currently $200.

NIST12 covers the following pure fluids of interest to OSPs (and many others of less interest to OSPs), several of which are addressed by this tutorial using data therefrom: oxygen, fluorine, nitrogen trifluoride, nitrogen, argon, helium, neon, and carbon dioxide. In 2016 the writer could no longer find this database for sale on the NIST web site.

The second database used in preparing this tutorial was NIST Standard Reference Database 23 *NIST Reference Fluid Thermodynamic and Transport Properties Database (REFPROP): Version 7.0* [***17***]. This DB appears to use the same math as DB 12 for those fluids of interest to OSPs, but is more flexible if also more quirky. However it did not contain all of the fluids of DB12, but it contained oxygen, argon, nitrogen, carbon dioxide, carbon tetrafluoride and water, and it allowed for calculation of properties for mixtures of up to twenty components using a "new Helmholtz energy model". The price was then currently $200.

It appears many if not all of the fluids available in NIST 12 have been rolled into NIST 23 which in 2016 was at the Version 9 level, appears to have been significantly expanded and was priced at $250.

NIST also has what it calls a WebBook database available on line, but it is not promised to be a continued free service. NIST referred to this on-line DB as the NIST Standard Reference Database Number 69, June 2005, Eds. P.J. Linstrom and W.G. Mallard [***18***]. In 2007 it ap-

[6]The writer considered numerous resources including Selover [***14***], Wagner and de Reuck [***15***] which is limited to 300K, an Internet web site which as of this writing did not vary C_p and C_v as a function of pressure, NASA *Coefficients and Properties* (*CAP*) software (which apparently compensates C_ps a function of T only), and Outokumpu HSC Software (which apparently also compensates C_p as a function of T only).

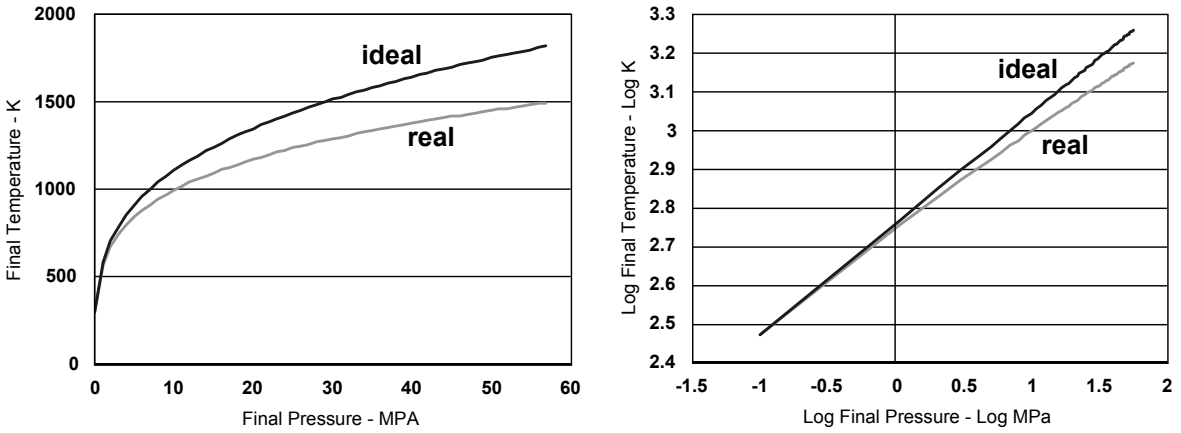

FIG. 2—*Adiabatic compression of ideal oxygen of constant γ = 1.4 (upper) and real oxygen per NIST DB 12 (lower). Above 1500K, NIST extrapolates their equations of state. (Initial pressure = 0.1013 MPa, Initial temperature = 298.15K). Ideal curves are blue and real curves are green in digital versions.*

peared to contain all of the fluids of DBs 12 and 23 and more. Specifically, it also contained dinitrogen monoxide (N_2O) and sulfur hexafluoride (SF_6) that both would be of interest to OSPs. This on-line DB is much less easy to use than the discrete products. It appears all of the fluids that are examined in this tutorial are now included in the current Database 23.

The NIST software appears to have many of the same capabilities as the Air Products' package CAPP. Doubtless there are other systems out there to which comparisons could be made. However the writer does not have access to CAPP or any of the others, but perhaps other OSPs will be willing to publish comparisons and extensions to the results in this tutorial.

Caution! NIST DBs report data in two ways: one is rooted in their equations of state and the other is as extrapolations from it. For oxygen their "best" data are limited to 1500 K and are extracted from their equation of state. This tutorial reports results to the extent of their extrapolations and does not discriminate between them.

Yet Another Analysis of Rapid Compression of Real Oxygen

The procedures for estimating adiabatic compression with the NIST software are straightforward. An insulated system (including any system transitioned so rapidly as to preclude heat transfer, but not so rapidly as to lose equilibria) experiences no change in entropy and so one can specify a constant entropy condition and place ranges on either the temperature or pressure, and the software will produce tables or graphs of the intervening conditions.

Figure 2 Exhibits the output from the program for oxygen for the approximate starting-condition variables in Leslie [***9***] and Barragan et al. [***11***] in comparison to predictions for Equations (1-3). These are fairly consistent with those results and also Koeller's [***10***] estimates.

As has been reported by those previously reviewed references, the real-gas final tem-

TABLE 2—*Comparison of NIST12 and NIST23 DBs with Wilson et al.* [***8***]*, Leslie* [***9***]*, and Barragan et. al* [***11***].

	P_f/P_i									
T_f Method Using:	**2**	**5**	**10**	**20**	**50**	**100**	**200**	**340**	**500**	**1000**
Eq 10 in [*11*][a] (Recalculated)	363	472	576	701	912	1111	1354		1760	2145
Data from [*8*] Table 2[a]	363		572	696		1097	1335			
Leslie [*9*][b]								1365		
Eq 11 in [*11*][a]	362	464	557	666	837	990	1166		1441	1686
Eq 6 in [*11*][a]	362.2	464.8	558.3	667.3	838.8	992.3	1169.2		1444.2	1687.4
NIST12 DB [*16*][a]	362.4	466.4	561.2	671.4	844.1	998.5	1177.2	1332.9	1457.6	—
NIST23 DB [*17*][a]	362.4	466.4	561.2	671.4	844.0	998.5	1177.2	1332.9	1457.6	—

[a] T_i = 298.15 K, P_i = 101.3 kPa
[b] T_i = 300 K, P_i = 100 kPa .

peratures for these starting conditions are lower than the ideal-gas estimates. Table 2 indicates good correlations at those pressures that are addressed. In the case of the NIST DBs, temperatures below 1500K are extracted from their equation of state models, and temperatures above 1500K are their extrapolations of their model.

Primary Implications for OSPs

Clearly anyone with a copy of either NIST DB can extract very precise (and hopefully accurate) estimates of the desired data for a modest cost. While it is available, they can also resort to the complimentary NIST Internet version, also. Although these DBs are not difficult to use, they are not obvious to use nor always convenient either and involve some learning curve. In addition, they do not calculate every parameter of interest nor always converge to an answer.

Barragan [***11***] (as modified here), and Leslie [***9***] found that their real-gas estimates were lower than their ideal gas estimates for the same starting conditions. Barragan found them lower

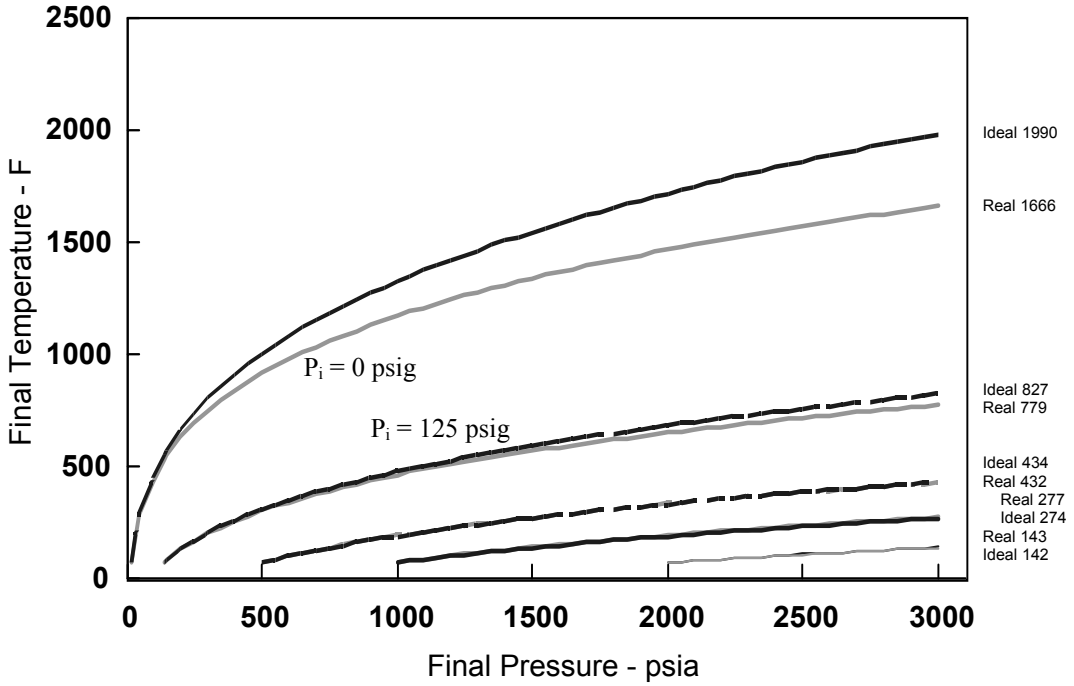

FIG. 3—*Adiabatic compression of ideal oxygen of constant γ = 1.4 and real oxygen per NIST DB 12 .. Above 1000K, the NIST values are NIST extrapolations. (Initial temperature = 76°F). Ideal curves are blue and Real curves are green in digital versions.*

by 8% at $\mathbf{P_f/P_i}$ = 10 (revised here to 3% lower if the suspected error cited here is correct) and 32% lower at $\mathbf{P_f/P_i}$ = 1000 (revised here to 21% lower with a more traditional value for γ), respectively in absolute temperature. Is this significant? Koeller [***10***] performed the calculations (two ways) with similar results (similar to the corrected values) at the same starting conditions. However, at higher-pressure starting conditions, Koeller reported that the accuracy of ideal gas predictions with real γ is initially much better and then actually inverts at some point and becomes worse in the opposite direction. This is an important result. The starting conditions examined by Barragan et al. [***11***] and Leslie [***9***] are not always the real-world starting conditions in some very important systems.

Figure 3, using the NIST23 DB data replicates Koeller's plot and also affirms her result that the ideal-gas estimates are quite close to the DB predictions at higher initial pressures and also invert (though the precise inversion pressure from the NIST12 DB is quite a bit different from her's). Later figures will present data at lower (as well as higher) starting pressures and at a spectrum of starting temperatures, as well. The largest inverse differences are at the lower conditions (at and also below room temperature). Further, the significance of the differentials in these estimates and of the adiabatic compression itself can be viewed in different light than is presented in the earlier treatments.

Are the differences significant to the OSP when using real gas predictions at room tem-

TABLE 3—*Real Versus Ideal Differential Temperature Predictions*

	ΔP = 65.3 psi P_f = 80.0 psia	**ΔP = 69.4 psi P_f = 84.1 psia**	**ΔP = 289.8 psi P_f = 304.5 psia**	**ΔP = 348.3 psi P_f = 363.0 psia**	**ΔP = 2985 psi P_f = 3000 psia**
Ideal gas rise (γ = 1.4)	~330F°	~342F°	~730F°	~795F°	~1892F°
Real gas rise (NIST23)	~318F°	~330F°	~675F°	~730F°	~1576F°

perature and atmospheric pressure yield absolute temperatures perhaps only 3-21% lower? Maybe this is a reasonable built-in safety factor.

Consider that most of the concern that is addressed to adiabatic compression applies to the ignition of polymers. It would also apply equally to high surface-area-to-volume materials (fines such as dusts, and powder and perhaps some sharp or pointed edges) and to volatile liquids, but the latter are scrupulously avoided in oxygen systems. Different polymers ignite at different temperatures (partly due to differing tendencies to vaporize or off-gas). Among the least compatible materials, autogenous ignition typically occurs at roughly 400°F or higher (there are exceptions), and yet many of even the most compatible polymers ignite at roughly 800°F or below (there are also exceptions such as PTFE which is reported to ignite above 800°F at elevated pressure and at roughly 900°F+ at atmospheric pressure). If these polymers are in use at room temperature (70-80°F), then the minimum temperature rise (ΔT) above ambient that might be required to promote ignition would range from a minimum of about 330 F° to a maximum of about 730 F°, a mere difference of approximately 400 F°, about a 2:1 ratio in the differential. Although the more sensitive materials ignite at about a 32% lower *absolute* temperature, they require a larger 45% lower *rise* in temperature (that is, stimulus or jump start). So it is more realistic to make comparisons on the basis of temperature differentials than on absolute temperatures. To this end, the differences between ideal gas and real gas estimates can be more valid on the basis of rise rather than absolute temperature.

Table 3 shows how the most and least compatible polymer autogenous ignition temperatures (AITs) compare to the temperature rises possible from the compression of room temperature atmospheric-pressure oxygen to pressures up to typical full commercial oxygen cylinder pressure (~3000 psig).

This table suggests that when room-temperature, atmospheric-pressure oxygen is compressed to about 80 psia (65 psi rise), the ideal gas model would predict temperatures at the threshold of the autogenous ignition temperatures (400°F, 330F° rise) of easily ignited polymers, while real gas prediction would be about 12F° lower. The real gas model would predict about 84 psia (70 psi rise) to achieve this same condition (at which point the ideal gas model would predict 12F° over the threshold).

Similarly, the table suggests that when room-temperature, atmospheric-pressure oxygen

is compressed to about 304.5 psia (289.8 psi rise), the ideal gas model would predict temperatures at the threshold of the autogenous ignition temperatures (800°F, 730F° rise) of difficultly ignited polymers, while real gas prediction would be about 55F° lower. The real gas model would predict about 363.0 psia (348.3 psi rise) to achieve this same condition (at which the ideal gas model would predict 65F° over the threshold).

When the pressurization has achieved full commercial cylinder-oxygen pressures (as high as 3000 psia, about 2985 psid), the real-gas and ideal gas differential temperatures far exceed the minimum ΔT to ignite even the least easily ignited polymers.

Although high surface-to-volume materials would be more sensitive to ignition, clearly in the real world, both high and low igniters can be exposed to potential transient temperatures well above the minimum to enable ignition. Use of a high AIT material is a desirable and worthwhile goal, but there *must* be other key factors operating. A later section will focus on one of these, the role of heat transfer as an additional major player.

Also clearly real oxygen is only slightly more forgiving than would be ideal oxygen, at least for this parameter and these starting conditions. However, when significantly different starting conditions present (as will be examined later), error in ideal calculations can be much different and must be given more consideration.

Nonetheless, for decades, the conservative ideal-gas approximation for at least the most common adiabatic compression has been used to assess material performance. This could mean there is a statistical validation for its continued use. This additional margin of safety may be a factor in the level of system safety that has been achieved to date. The taking of greater latitude on the basis of the more precise estimates may not be prudent but its context needs to be known. Context will be elaborated upon in the following sections.

Adiabatic Compression Math

Appendix A works in painful detail through what the writer hopes are simplified but very detailed derivations of adiabatic processes for three models: (1) ideal gas with a constant specific heat capacity in two ways, (2) ideal gas with a variable specific heat in two ways, and (3) a real gas based on NIST data. These cover the range of methods in the reviewed literature. Many texts employ the advanced, and in the writer's view highly non-simple, concept of entropy in performing these calculations and/or else are cryptic in developing the equations. And so the entropy parameter is not used herein, and the equations are developed in more detail than is used in most texts.

The first ideal-gas derivation, Appendix A, yields equations (A23-A25) very similar to equations (1-3), but it deliberately stops short of incorporating the traditional constant, γ. This first set is directly analogous to equations (1-3), respectively, and were derived for the case where compression results from vessel volume reduction (as in piston compression).

$$P_i / V_i^{(Cv+R)/Cv} = P_f V_f^{(Cv+R)/Cv} \tag{10}$$

$$T_f/T_i = (P_f/P_i)^{R/(Cv+R)} \quad (11)$$

$$T_f/T_i = (V_f/V_i)^{R/Cv} \quad (12)$$

The second set (A50-A52) are also directly analogous to equations (1-3) respectively, and were derived for the case where compression results from gas addition:

$$P_i/V_i^{Cp/(Cp-R)} = P_f V_f^{(Cp/(Cp-R)} \quad (13)$$

$$T_f/T_i = (P_f/P_i)^{R/Cp} \quad (14)$$

$$T_f/T_i = (V_f/V_i)^{R/(Cp-R)} \quad (15)$$

These two sets of equations represent two different and valid ways to do the calculation. Consequently the two sets should yield the same results, since the predicted behavior of the gas does not depend on the way its behavior is calculated. The respective equations can only yield the same results if the respective exponents are equal., which is to say if :

$(Cv+R)/Cv = (Cp/(Cp-R)$ which implies $Cp - Cv = R$ (from Eqs. 10 and 13)
$R/(Cv+R) = R/Cp$ which implies $Cp - Cv = R$ (from Eqs. 11 and 14)
$R/Cv = R/(Cp-R)$ which implies $Cp - Cv = R$ (from Eqs. 12 and 15)

Hence these equations can predict the behavior of ideal gases having constant Cp and Cv (in which case C_p/C_v is consequently constant and is defined variously as γ), but the two methods of calculation will also yield the same results whenever Cp and Cv are variable functions of pressure and temperature provided the variable heat capacities obey:

$$Cp(P,T) - Cv(P,T) = R.$$

And this allows formulation of a "real" variable $\gamma(P,T)$ which is effectively one of Koeller's approaches.

Hence, Equations (10-15) could be compacted into Equations (1-3) symbolically by taking the relation this applies precisely to for ideal gases of constant heat capacity that:

$$C_p = C_v + R \quad (16)$$

and defining $\gamma = C_p/C_v$ and manipulating the equations (10-15) to yield the equations (1-3).

Many (the writer believes most) textbooks do this and the result has found wide adoption and use including in the writer's consciousness and in ASTM Committee G4 documents. Derivative equations, including several used by OSPs that will be dealt with in this tutorial, contain the γ parameter. This practice now seems both less useful and can even be circumstantially misleading as will soon be elaborated.

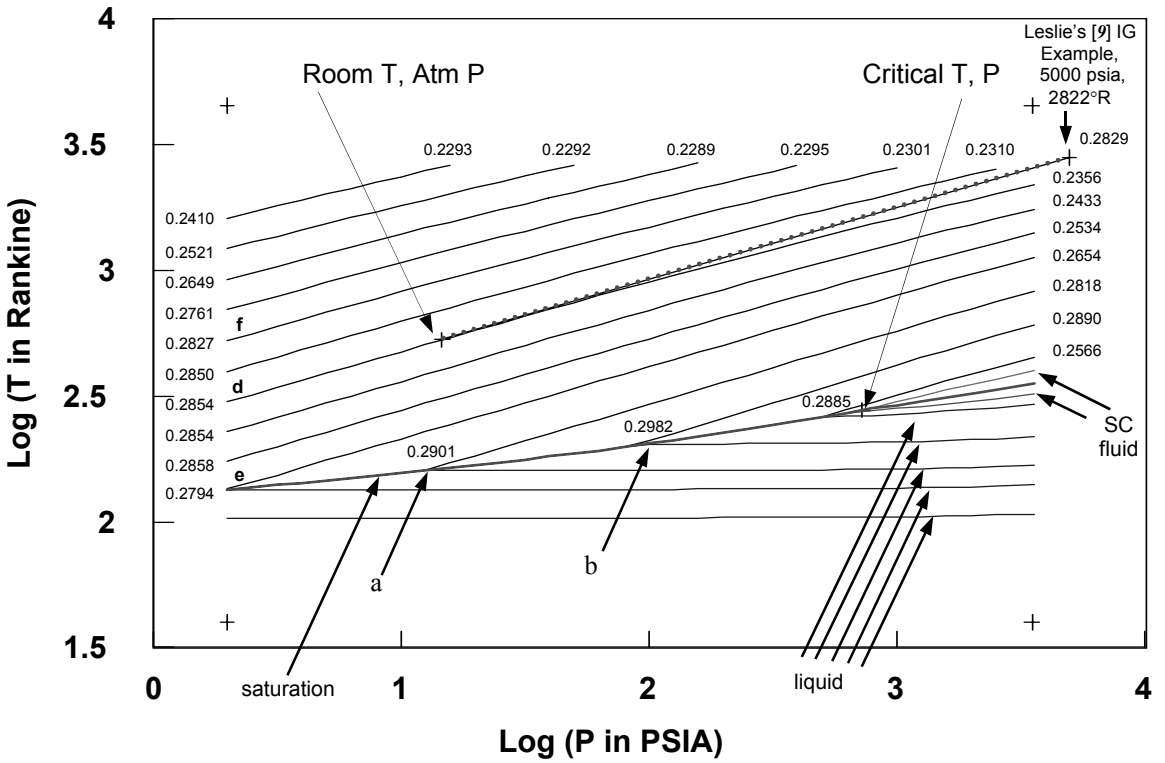

FIG. 4—*Real-Oxygen Adiabatic Temperature Versus Pressure From NIST12 DB. Digital versions have black gas curves, a red saturation curve, blue liquid curves and supercritical fluid curves near saturation are green. Reproduced from Figure A-11 in Appendix A.*

With the availability of NIST databases 12 and 23, the real and presumably most accurate behavioral properties of gases can be extracted. Figures 4 and 5 (reproduced from Figures A-11 and A-12 in Appendix A) exhibit how temperature depends on pressure during the adiabatic pressurization of systems. This is the relationship Leslie [***9***], Barragan et al. [***11***] and Koeller [***10***] explored that may be the most important to OSPs. Figure 4 exhibits the ideal-gas constant heat capacity compression from room temperature and atmospheric pressure example used by Leslie as a beaded curve. Beneath it is the comparable real gas compression.

Figure 4 also exhibits curves for twenty-one different values of constant real-oxygen entropy. If these were ideal-gas curves with constant heat capacities, Equation (2) would define their slopes as $(\gamma-1)/\gamma$, but for cases where $C_p = C_v + R$, the local slopes where heat capacities are constant could also be given as $R/(C_v+R)$ and also R/C_p, and for where heat capacities varied and yet still where $C_p(P,T) = C_v(P,T) + R$ would (at least over local regions) be $R/[C_v(P,T) +R]$ and equally also $R/C_p(P,T)$. Labels at the ends of each gas curve indicate what the local slope of the curve is at each end. The ideal gas curve is labeled with a slope of 0.2829 that is equal to $(\gamma-1)/\gamma$ [by Eq. (2)], for a γ of ~1.4 (apparently Leslie actually used a γ of 1.3945).

Figure 5 exhibits seven curves (five from Figure 4) that form the "supercritical trian-

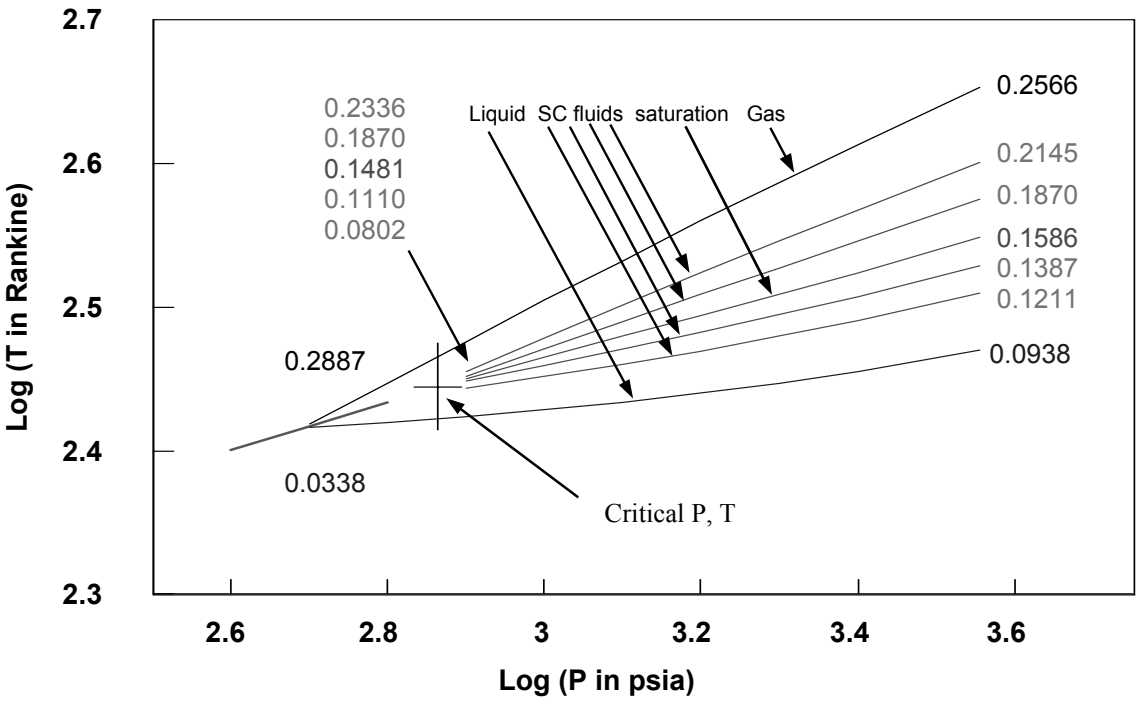

FIG. 5—*Real-Oxygen Adiabatic Temperature Versus Pressure from NIST12 DB*. (In *Region of Supercritical" Triangle*). *Digital versions have black gas curves, a red saturation curve, blue liquid curves and supercritical fluid curves near saturation are green. Reproduced from Figure A-12 in Appendix A.*

gle." Labels at the ends of each line again indicate the local slope of each curve at its end points. These show how the slope decreases substantially as one approaches and produces the liquid condition. However, these Figures 4 and 5 allow us to confirm Leslie's conclusion that the variation in the slope of his example is sufficiently straight to approximate with an empirical polytropic equation, and the same thinking can be extended to cover every curve and every region shown on both figures.

Hence we can now estimate real adiabatic compression temperatures as a function of pressure with the empirical equation patterned after Equation (2):

$$T_f/T_i = (P_f/P_i)^{m_{TP}} \tag{17}$$

Where m_{TP} is the slope of any straight section of any curve on Figures 4 or 5.

Analogs to Figure 4

The state of a gas is specified by three parameters (P,V,T) that yield three two dimensional interrelationships (T vs P, T vs V, and P vs V). The preceding analyses have been ad-

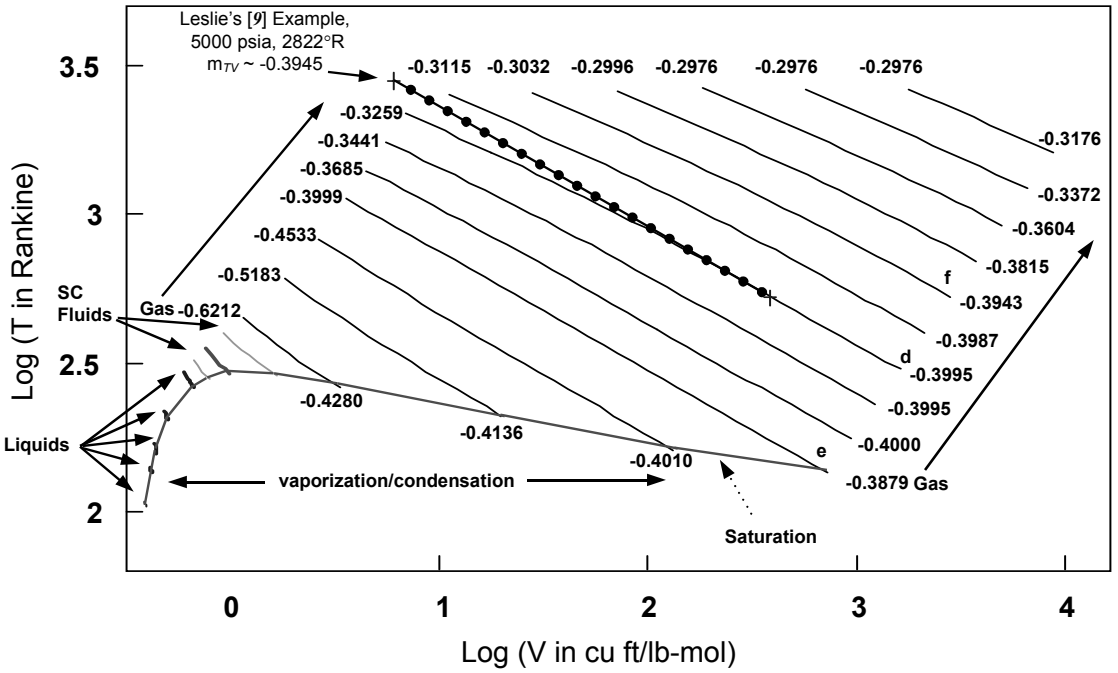

FIG. 6—*Real-Oxygen T vs.V During Adiabatic Processes From NIST12 DB. Digital versions have black gas curves, a red saturation curve, blue liquid curves and supercritical fluid curves near saturation are green. Reproduced from Figure A-14 in Appendix A.*

dressed to the relationship between temperature and pressure, akin to Eq. (2), during adiabatic compression because the abrupt pressurization of a system is considered to be a common and major hazard. But these analyses could have been effected on the basis of temperature and volume, akin to Eq. (3), because compression machinery abruptly reduces the volume of a gas's container), or also on the basis of pressure and volume, akin to Eq. (1). Figures 6 and 7 reproduced from Appendix A (Figures A-14 and A-15), portray the exact same "gas state" conditions of Figure 4 in these other formats using extracts from NIST12 DB. The data points used to produce each analogous segment correspond exactly to those for Figure 4. Similarly to facilitate correlation among the points, the same color-coding of the curves is used on digital copies. Each of these families of curves has its own particular merit in oxidant system analysis and design.

Figure 6 exhibits the temperature versus volume relationship and again, as for Figure 4, the segments are rather straight, supporting the use of an empirical equation to approximate them. Again, twenty-one real-gas curves and one ideal gas curve are shown. If these were ideal-gas curves with constant heat capacities, Equation (3) would define their slopes (m_{TV}) as $(1-\gamma)$, but for cases where $C_p = C_v + R$, the local slopes where heat capacities are constant could also be given as $R/(C_v+R)$ and also R/C_p, and for where heat capacities varied and yet

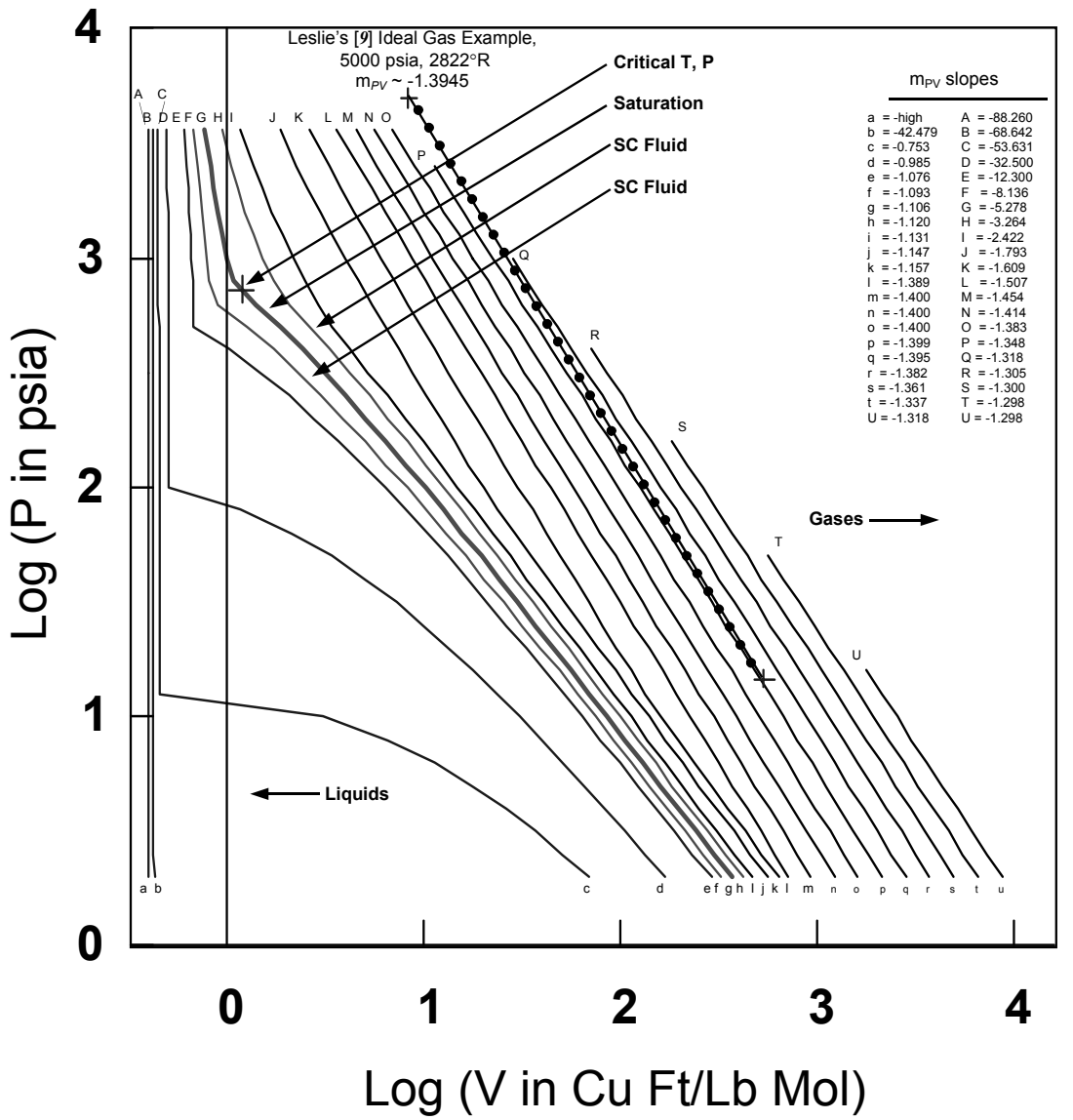

FIG. 7—*Real-Oxygen V vs.P During Adiabatic Processes From NIST12 DB. Digital versions have black gas curves, a red saturation curve, blue liquid curves and supercritical fluid curves near saturation are green. Reproduced from Figure A-15 in Appendix A.*

still where $C_p(P,T) = C_v(P,T) + R$ would (at least over local regions) would be $R/C_v(P,T)$ and equally also $R/[C_p(P,T)-R]$. Labels at the ends of each gas curve indicate what the local slope of the curve is at each end. The ideal-gas curve is labeled with a slope of -0.3945 that is equal to $(1-\gamma)$ [similar to Eq. (3) for Leslie's example], for a γ of ~1.4 (apparently Leslie actually

used a γ of 1.3945).

Hence we can now estimate real adiabatic compression temperatures as a function of volume with the empirical equation patterned after Equation (3):

$$T_f/T_i = (V_f/V_i)^{m_{TV}} \quad (18)$$

Where m_{TP} is the slope of any straight section of any curve on Figures 6.

Figure 7 exhibits the pressure versus volume relationship and again, as for Figures 4 and 6, many of the segments (at least the segments for gaseous oxygen) are rather straight, supporting again the use of an empirical equation to approximate them. Again twenty-one real-gas curves and one ideal gas curve are shown. If these were ideal-gas curves with constant heat capacities, Equation (1) would define their slopes (m_{PV}) as (–γ), but for cases where $C_p = C_v + R$, the local slopes where heat capacities are constant could also be given as $-(Cv+R)/Cv$ and also $-(Cp/(Cp-R)$, and for where heat capacities varied and yet still where $C_p(P,T) = C_v(P,T) + R$ would (at least over local regions) would be $-(C_v(P,T)+R)/C_v(P,T)$ and equally also $-(Cp(P,T)/[Cp(P,T)-R]$. Labels at the ends of each gas curve indicate what the local slope of the curve is at each end. The single ideal gas curve is labeled with a slope of –1.3945 that is equal to (–γ) [similar to Eq. (1) for Leslie's example], for a γ of ~1.4 (apparently Leslie actually used a γ of 1.3945).

Hence we can now estimate real adiabatic compression pressures as a function of volume with the empirical equation patterned after Equation (1):

$$P_f/P_i = (V_f/V_i)^{m_{PV}} \quad (19)$$

Where m_{TV} is the slope of any straight section of any curve on Figures 7.

Table 4, exhibits the local values of the slope (m_{PV}) at the beginning and end of every segment as shown in Figure 7. They are shown for the segments from upper left (high P, low V) to lower right (low P, high V) and on digital copies the color coding is preserved. There are columns of data for the real (actual, best) local m_{PV}, the slope based on $C_P/(C_P-R)$ (per Eq 13), the slope based on $(C_v+R)/C_v$ (per Eq. 10), and the slope based on real γ (that is, C_P/C_V) with all data extracted from the NIST12 DB.

Notice that at higher values of pressure (top entries) all four ways of calculating the slope give similar values differing only in the third or four decimal places. Appendix A explores how this is where the relationships: $C_p = C_v + R$, and $C_p(P,T) = C_v(P,T) + R$ are most closely obeyed. As one examines entries moving down the table, discord appears and when one hits the saturation level and below all of the calculated values exhibit substantial discord with the "best" value. For conditions at the top of the Table (higher pressures and temperatures) gases are reasonably ideal (PV ~ nRT), specific heats are constant and $C_p = C_v+R$). However, as pressures and temperatures decrease, all three of these parameters break down differently.

TABLE 4—*Comparison of* $-m_{TP}$, $(Cv+R)/Cv$, $Cp/(Cp-R)$, Cp/Cv *for Figure 7.*

	Beginning of "Straight" Segment				End of "Straight" Segment				
	$-m_{TP}$	$(Cv+R)/Cv$	$Cp/(Cp-R)$	Cp/Cv[a]	$-m_{TP}$	$(Cv+R)/Cv$	$Cp/(Cp-R)$	Cp/Cv	
Gas	1.318	1.319	1.319	1.319	1.298	1.297	1.297	1.297	**Gas**
Gas	1.337	1.340	1.340	1.340	1.298	1.297	1.297	1.297	**Gas**
Gas	1.361	1.363	1.363	1.363	1.300	1.296	1.296	1.296	**Gas**
Gas	1.382	1.384	1.384	1.384	1.305	1.297	1.297	1.298	**Gas**
Gas	1.395	1.395	1.395	1.396	1.318	1.297	1.297	1.300	**Gas**
Gas	1.399*	1.399	1.399	1.400	1.348*	1.298	1.296	1.304	**Gas**
Gas	1.400	1.400	1.399	1.401	1.383	1.303	1.299	1.315	**Gas**
Gas	1.400	1.399	1.399	1.402	1.414	1.313	1.307	1.334	**Gas**
Gas	1.400	1.400	1.398	1.405	1.454	1.326	1.315	1.362	**Gas**
Gas	1.389	1.371	1.363	1.392	1.507	1.342	1.322	1.404	**Gas**
Gas	1.157	1.262	1.183	1.689	1.609	1.362	1.319	1.500	**Gas**
Gas	1.147	1.262	1.183	1.689	1.793	1.371	1.283	1.685	**Gas**
Gas	1.131	1.262	1.183	1.689	2.422	1.360	1.205	2.116	**Gas**
SC Fluid	1.120	1.262	1.183	1.689	3.264	1.349	1.176	2.337	**SC Fluid**
Saturation	1.106	1.262	1.183	1.690	5.278	1.339	1.164	2.406	**Saturation**
SC fluid	1.093	1.262	1.183	1.689	8.136	1.332	1.167	2.324	**SC fluid**
Liquid	1.076	1.262	1.183	1.689	12.300	1.325	1.173	2.199	**Liquid**
Liquid	0.985	1.265	1.183	1.689	32.500	1.296	1.189	1.858	**Liquid**
Liquid	0.753	1.262	1.183	1.689	53.631	1.270	1.192	1.679	**Liquid**
Liquid	42.479	1.265	1.183	1.689	68.642	1.254	1.190	1.596	**Liquid**
Liquid	high	1.231	1.184	1.486	88.260	1.236	1.190	1.479	**Liquid**

*Segment passes through room temperature and atmospheric pressure.
[a] Cp/Cv = "Real" γ
On digital copies: Black—gas
Red—saturation, Green —supercritical
Blue—liquid
All data derived from NIST12 Database [***16***]

Indeed, at low temperature the use of all three calculations are flawed. But remarkably, *real gas still wants to compress in a nearly linear log/log P/V, T/V and T/P relationships*. Even when the initial temperature of the gas is very near the boiling point of the oxygen, the curves are still remarkably linear. In other words, one is better off relying on use of the NIST databases (or Figures 4, 5, 6, and 7 based on them) to assess real-gas behavior than to do the math.

For gaseous oxygen at the boiling point and 2 psia, a rapid compression to 3600 psia yields an estimated final temperature of about 668°F per the NIST12 DB. However, if there is liquid present, then equilibrium is an issue and things are more complicated.

Figure 4 exhibits adiabatic compression of 2 psia gas at the boiling point (the black curve next to the label for $m_{TP} = 0.2794$), and for 2 psia liquid at the boiling point (the blue curve immediately below point "e", and also for numerous intermediate *equilibrium* mixtures (that initially begin on the red curve and then split off from it as black or blue lines such as at points "a" and "b") on Figure 4. When there are two phases (both gas and liquid) present, *equilibrium* compression (stress on the word equilibrium meaning at uniform pressure and temperature throughout) results in an initial slow warming and slow pressure rise along the red saturation (boiling point) curve. If the mixture is predominately gaseous then more appreciable adiabatic heating of the gas fraction will ultimately convert the liquid into gas and then the resulting gas will warm with a greater slope.

Appendix A elaborates on this process in some detail and tabulates examples in the Table with Figure A-13. For example, a mixture of 89.3% gas with liquid by mass is predominately gas and will vaporize fully at point "a" and further heating during compression will be along a black line to a final temperature of 370°F at point "c". Conversely, an initial mixture of 9.6% gas with liquid by mass is predominately liquid and equilibrium pressurization will result in the liquefaction of the gas which will condense fully at point "a" and heating will then exhibit a very slow pressure and temperature rise slope thereafter along a blue (liquid) line to a final temperature of about minus 292°F (-292°F) at point "d". Further, a mixture of 78.1% gas with liquid by mass is predominately gas and will track the red saturation curve to point "b" where in equilibrium it will be fully gaseous and will then heat during compression to a final temperature of 151°F at point "e". And again similarly, a mixture of 23.5% liquid at the beginning will during equilibrium compression track the red saturation curve to point "b" where it will be fully condensed and will then track the blue (liquid) curve to a final temperature of about minus 242°F (-242°F) at point "f". The appendix gives other examples, as well.

However these are not the only adiabatic processes OSPs should be concerned about! These are for equilibrium (uniform temperature and pressure throughout) adiabatic compression. However, rapid pressurization of segregated liquid/gas mixtures would seldom be in or near equilibrium. OSPs should also analyze these cases from a second perspective.

Figure 8 exhibits a vessel on the left containing quiescent liquid and gas. In normal gravity the liquid usually collects into a pool at the bottom and is not nearly in good heat exchange with the entire gas. As an extreme example, now think of the same vessel baffled as depicted to the right of Figure 8. In this case, rapid pressurization is more nearly like rapid pressurization of the gas alone and the liquid alone much as if they were isolated by a valve between the vessels. In this case, for a vessel containing 2 psia oxygen in any ratio of gas to liquid at the boiling point (about –325°F at 2 psia), this writer would suggest the gas fraction will achieve a local equilibrium within itself at the same final temperature 668°F that a fully gas system would, and the liquid will compress to achieve a local equilibrium within itself at the transient final temperature (about -319F, an increase of only 6F°) that a fully liquid system would achieve. Later, after transferring heat between them, they may come into equilibrium with each other and achieve the equilibrium values predicted by NIST DB 12.

As a result a conservative analysis of an oxygen system's dynamics might assume any gas fraction will compress independently from the liquid unless there is compelling reason why an equilibrium would prevail between the two phases.

Some mixtures lying on the saturation curve (red on digital copies) of Figure 4 (those passing through point "b") will compress when under complete equilibrium to the point where the oxygen achieves the critical point conditions (the point at which only one phase is present at 731.43 psia, -181.4°F per NIST12 DB). This region was presented in greater detail in Figure 5. Equilibrium adiabatic compression of liquid/gas mixtures that pass through the critical point produce curves that fan out to the right from the critical point.

If the oxygen is entirely gaseous at the critical point, then adiabatic compression will

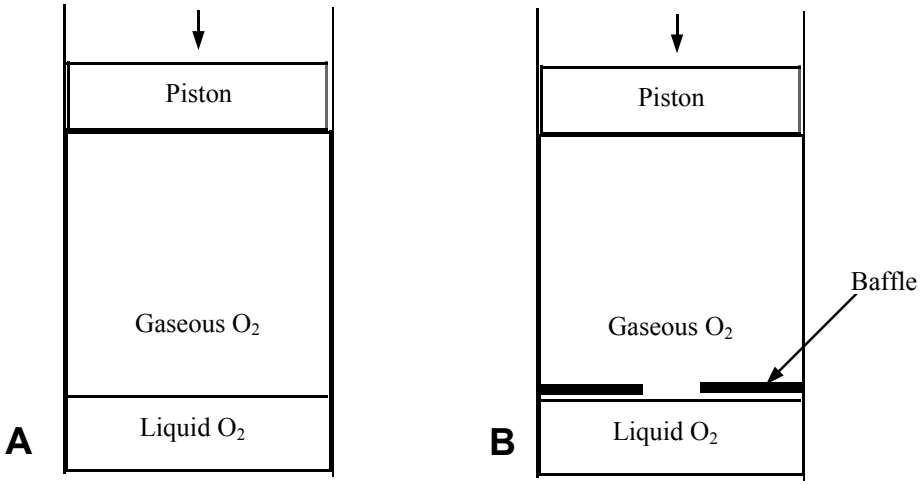

FIG. 8—*Vessels With Little Equilibrium Between Phases During Compression.*

heat and pressurize it along the top curve (black on digital copies) of Figure 5. Actually this "curve" is a rather straight line that is remarkably parallel with the gaseous compression curves above it. Its slope (which is the applicable exponent that one would use in Equation 17 ranges from 0.2387 to 0.2566 which is remarkably close to the 0.2829 for compression of ideal room temperature oxygen gas.

If the oxygen is entirely liquid as it passes through the critical point, then adiabatic compression will heat it to a much smaller extent and pressurize it along the nearly flat bottom curve of Figure 5 (blue on digital copies). Actually this "curve" is another rather straight line that is remarkably parallel with the liquid compression curves below it. Its initial slope is remarkably close to that of the liquid sub-cooled oxygen curve below it.

For conditions of two-phase "mixtures" between these two curves (where the two phases will typically be separate), slower equilibrium compression will produce a supercritical fluid of various slope as shown on Figures 4 and 5 (as the green curves on digital copies). However, even in these cases, one should recognize the possibility for lesser degrees of equilibrium (for example a "mixture" segregated in a vessel to the extreme degree as shown in Figure 7B). In this case, the gas phase which is becoming supercritical and gaining density will still tend to form a lower density supercritical fluid than will the liquid which is becoming supercritical and losing density. This is again a conservative perspective.

Textbooks that were consulted for terminology to use in describing supercritical oxygen like this were of little help and even create an impression that the significance and curious behavior of supercritical fluids extends to all pressures and temperatures greater than those of the critical point. However, we have seen that at least with regard to adiabatic compression, that the fluid along the black curve just above the triangular region behaves very much like gaseous oxygen at any conditions further above it. Similarly, supercritical oxygen along the liquid curve

(blue on digital copies) that is just below the triangular region behaves in adiabatic compression much like liquid oxygen that is further below the critical point. This writer will call the "supercritical triangle" between these two curves (between the lowest black and highest blue curves), the *hybrid transition state* of supercritical oxygen. This word choice is predicated on the following for the fluid depicted therein.

When a liquid/gas oxygen mixture (of roughly 45% gas) passes through the critical point, it behaves differently than the gaseous oxygen at conditions above or the liquid oxygen below. Indeed, it goes through a range of properties. Those mixtures a little higher in liquid exhibit a lower slope. Those mixtures a little higher in gas exhibit a greater slope. But the heating properties exhibit a transient range and the slopes are like a mathematical combination of the gas and liquid slopes. Hence *hybrid transition*.

However, notice that the adiabatic curves for fluid in the hybrid transition state are also remarkably straight. More importantly, the slopes can therefore be used to predict the heating using an equation like that for the thermodynamic properties of the fluids (Table 4 shows how the functions are close to the real m_{TP} values). Table 4 also shows how estimates based on heat capacities in this way would fare, and shows that use of real γ in this hybrid transition region would produce extreme error.

As noted in Appendix A, the highest temperature produced by compression of supercritical oxygen in this hybrid transition region up to the 3600 psia case would yield only a maximum of roughly –60°F, a level that would not concern most OSPs. This is not a great risk to oxygen safety, but this same effect may be more important with other fluids and oxidants.

Limitations of Standards and Texts

The Appendix A derives the equations for ideal adiabatic compression in two ways, one based on use of the specific heat at constant pressure and one based on the specific heat at constant volume. As already noted, neither incorporates, nor does either need to incorporate, the ratio, γ, of specific heat capacities. However, virtually every standard thermodynamics text the writer checked with and recalls expresses adiabatic compression in terms of γ (sometimes the alternative symbols, k or n, are used by engineering texts for this same ratio). This appears to be an unfortunate effort at simplification that ill-serves the OSP, because γ appears to be one of the less useful ways used to approximate real oxygen.

When an ideal gas with either constant specific heats or variable specific heat is assumed, the assumption of ideality compels the two ideal specific heats to differ by the amount R. However this condition does not always apply for real oxygen. And unlike ideal gas which is used to approximate real gas, the use of a real γ does not always produce the best, or even a good, approximation of the desired and necessary polytropic equation exponent. The specific heats of real gas vary in independent ways and in some instances their difference is much different than R.

The empirical variables called: m_{TP}, m_{TV}, and m_{PV} here appear to generally provide a better exponent and allows similar equation structures to be used yet still can be flawed in some regions.

Consequently, one can choose to approximate real oxygen as ideal gas of constant specific heats using Equations (1-3), or even more carefully can choose to approximate real oxygen as ideal gas of variable specific heat using data for the variable specific heat of real oxygen, but if any then seek to approximate real oxygen using "real" γ (as the writer had hitherto considered reasonable), an error mechanism is introduced where $C_P \neq C_V + R$ and the domain of calculation is degraded, and quite significantly in some (albeit lesser used) cases.

The applicable equations in Appendix A for final temperatures (A23-A25, A50-A52) are dependent on *either* C_p *or* C_v but do not require both. The attempt at simplification in standard texts artificially substitutes C_p or C_v for R in these equations (perhaps much as an enterprising individual might find a way to include the speed of light). This approximation is indeed an approximation and lends reasonably good answers over some regions, such as at room temperature and atmospheric pressure, but a more applicable and more rigorous approach is to simply avoid the artificial introduction of γ in this way.

Since, there is no serious simplicity lost in a more rigorous formulation, this writer recommends that future revision of G4 standards (such as G 63, G 94, and G 88), and textbooks as well, avoid use of the PV^{γ} formulation and instead use a similarly compact but more empirical approach based on the formulas: $T_f/T_i = (P_f/P_i)^{m_{TP}}$, $T_f/T_i = (V_f/V_i)^{m_{TV}}$, and $P_f/P_i = (V_f/V_i)^{m_{PV}}$ as are developed herein. And as will be proposed in later sections these standards would also benefit from the introduction and elaboration of the concept of minimum ignition energy and to relate it to the heat transfer properties of adiabatic compression.

The Figures 4, 5, 6, and 7 provide both qualitative and quantitative perspective on real oxygen. And finally, this approach can be supplemented with high definition graphics or a simple PC algorithm that can allow the accuracy and precision needed in such calculations.

Caution! Although improvement derives from substituting empirical variables for γ in the polytropic equations used here, the parameter γ is used extensively in many other calculations (including five types to be examined in a later section of this tutorial), and one must be sure that when seeking better "real-fluid" calculations that the substitution of the empirical variables for γ is still valid for those as well.

Choosing Optimum Exponents

Numerous textbooks that employ γ in their formulae for adiabatic compression approximate it as 1.4. In many, this is described in theory[7] which deduces that γ will take on the following values for ideal gases:

1.67 For monatomic molecules (Ar, He, Ne, etc.)

[7]The classical equipartition theory deduces that KT/2 energy will be absorbed by each degree of freedom in a molecule. See John [***19***] and Kennard [***20***].

1.40 For diatomic molecules (O_2, N_2, H_2, F_2. etc)
~1.2-1.3 For triatomic molecules (CO_2 , N_2O, etc.)

Note that for gas that approximates ideal gas (like oxygen does in many of the calculations here) the calculation of the isothermal work to compress the gas will be similar to those calculated in Appendix A (the area under the region abcde of Figure A-2), but that as the molecule size increases, its heat capacity increases also. Therefore reintroducing the heat into the gas incrementally will produce progressively different temperature rises. This is why the value of γ, and similarly for the magnitude (since the slope is negative) of the related empirical slope, will decrease as the molecule gets larger, and increase as the molecule gets smaller. Indeed, this is reflected in the case of an extremely large molecule for which the heat capacity would be very large and the temperature rise very low. In this case, the values of γ and magnitude of $-m_{PV}$ should fall toward a lower bound of 1.0 (below a value of 1.0, adiabatic compression would cool the gas), and the adiabatic compression Equation (19):

$$P_i V_i^{-m_{PV}} = P_f V_f^{-m_{PV}}$$

would become the ideal gas equation ($P_i V_i = P_f V_f$). Therefore the entire range of values that γ and $-m_{PV}$ can assume for an ideal or near-ideal gas is from only 1.0 to a maximum of about 1.67. In real gas, however, as it becomes very non-ideal (approaches condensation) we have seen (Table 4) the values of approximations to γ and $-m_{PV}$ for oxygen being at least as high as 5-26. The real values of $-m_{PV}$ have gone only slightly above 1.40 in its extremes for oxygen.

In the case of oxygen in the ASTM G4 standards, however, the original thinking in adopting a value of γ of 1.4 was not so elegant. It was merely rounding off the actual value of γ at room temperature and atmospheric pressure from about 1.396 to 1.4. This was adopted by ASTM G4 in its earliest consensus on adiabatic compression. And other texts also seem to make adjustments. For example Wilson et. al. [***8***] publish a table (their page 322) of final temperatures for compression of ideal oxygen and ideal Nitrox (50-50 oxygen and nitrogen mixture which is a mixture of diatomic gases to yield a diatomic mixture). They cite the procedure of ASTM G 88 as their basis, but their calculation for oxygen appears to be based on a "real" γ of 1.395 while their Nitrox calculations appear to be based on a "real" γ of 1.397.

Rounding γ to 1.4 for oxygen appears to yield reasonable and conservative results for the most common STP starting-condition case. Fine-tuning of γ can yield improvements in the results for these same starting conditions. Figure 4 and Table 4 indicate the possibilities.

If one wished an optimum exponent, one could extract it from a database or select it from the Figures 4, 5, 6, and 7, and Table 4, though reading logarithmic data accurately is not easy. And so it would be desirable to have a simple method to obtain approximate values of a suitable adiabatic exponent for other starting conditions or even for other gases, and so later sections will explore the significance of these variables in more detail, and the next section will propose methods to extract logarithmic data.

Quest for a Simple Compression/Expansion Resource

So far, the implications of real versus ideal oxygen have been considered. Estimating the behavior of real oxygen, can be done, to a conservative extent, using the equations reviewed here and in the cited papers. Some larger companies have in-house software and there are several software packages available commercially. All of these have issues and may present availability challenges for many OSPs, especially for knowledgeable technical personnel who are not steeped in mathematics. The OSP and the safety of the oxygen-exposed community would be well served by a robust resource such as a simple algorithm along the lines of the ASTM Committee G4's former utility G4Math or way to read Log/Log plots.

ASTM G-4 provided the highly simplified complimentary algorithm in G4Math that served to do ideal-gas/constant-specific-heat calculations, among other calculations between roughly 1992 and the mid-2000s. A simplified companion algorithm would also be worthwhile. The development of standards is intended to avoid oxygen fires and explosions and thereby avoid injury and fatalities that damage not only the direct victims but the industry and G4 as a whole. Anything that improves G4's standards or expands their use, or facilitates their correct application is of benefit. The writer encourages the adoption of such tools from within ASTM G-4 and offers the examples presented here for consideration and modification, but is aware that some such endeavors are not currently allowed [8]. Nonetheless the proposal is made for whatever benefit it may provide.

Leslie (as reviewed earlier and in Appendix A) has suggested using an approximate values for m_{Pv} fro compression of atmospheric pressure, room-temperature oxygen (and this tutorial argues the same approach can be applied at all common pressures and temperatures) obtained from linear regression fitting of the data. This would be very easy to program in the same language [9] used for G4Math (as reviewed in Appendix C). However, as we have seen, Leslie's paper dealt with only one set of starting conditions. Furthermore, for a curve of constant slight concavity, using a least squares fit, results in estimates that are too low at the lower pressures and too high at the upper pressures. Figure 4 showed how the real gas behaves at all common starting conditions. This one graph presents a rather good capsule overview of real adiabatic

[8] The writer has proposed ASTM G4 consider adoption of a real-gas algorithm even though he is aware that not only is ASTM G4 reticent about pursuing new PC utilities but that the Committee, has backed away from the utilities it has already provided and no longer distributes the existing algorithms. ASTM has withheld permission to ballot further algorithms apparently based on liability concerns (although its Committee E-27 sells the computer facility CHETAH related to fire and explosion behaviors). The writer continues to encourage the existing utilities, including G4Math, and feels that further adjuncts are not only desirable, but necessary to fully serve the missions of G4 and ASTM, often with as much import as do its standards, themselves.

[9] G4Math.exe Version 1.0 through 1.2 were written in Microsoft Visual Basic Versions 1.0 to 3.0. This software offers a number of advantages that are particularly useful for this tool, as discussed in Appendix C. With the advent of 64-bit computing, importation of the code into 32 bit software has been done to allow its continued use.

compression but logarithmic scales are difficult to read with sufficient precision. One could also choose to accept larger percentage errors early in the compression process in exchange for more accurate predictions later in the process where the accuracy of the estimate is more critical. And it would also be straight forward and precise, if more involved, to approximate the slight curvatures present in the curves of Figure 4 with a series of short straight line segments.

At lower temperatures, at and below the saturation curve, the situation is more complex. A more easy alternative would be preferred.

Traditionally, select engineering textbooks have had a thick wad of graphs included between the pages and back cover. Indeed, for Rankine (steam) engine performance determinations, one could open a graph for the adiabatic thermodynamic behavior of steam that was a couple feet long on each side and peppered with grids to improve precise reading of the data. ASTM Standards could do the same. However, today huge graphs in the form of Figures 4, 5, 6, or 7, could be distributed as a high-definition computer graphic, a computer file with enough pixels to allow adequate precision that can be zoomed in on with many software packages (perhaps Photoshop and GIMP being the ultimate).

Figure 4-7, can then be vetted, based on NIST and various corporate facilities, optimized and published in G4's standards in low resolution form with the high-def graphic available separately.

However, the writer, would additionally propose a method to read the graphic similar to that which he employed in his FLLAME (Fire Limits for Linearly Afflicted Minds Everywhere) algorithm (a program that, like G4MATH.exe was originally written in 16-bit Visual Basic 3.0 and has been upgraded to 32-bit Version 4.0). In that case, the previously developed graphical element is present that depicts the fire-limit map of a material (whether empirical or theoretical). The PC mouse is used to place a cross-hair pointer on a region of the fire map that is either inside or outside the fire limit (or passes through or around the limit in accordance with various fluid flow circumstances) and it is then clicked, and a report box lists the spectrum of mixture parameters for the chosen location. To incorporate an approach like this with real-gas adiabatic compression (and the same is true for adiabatic expansion also), one could employ a figure somewhat like that of Figure 4 or Figure 4, itself. This would be the "map" or graphical element. One would first place the cross hair on the starting condition (a continuous readout of the pointer position would assist) and click to establish "starting" conditions, then move it to the final condition *on the same isentropic (adiabatic) line* (to the right of the starting point for a compression, to the left for an expansion) and click a second time. Bold users could do interpolations of both the starting and finishing conditions as well. The report box would cite both the initial and the final conditions, including values of m_{TP}, m_{TV}, and m_{PV} , and changes that took place. OSPs would seldom need more or better data.

This would also allow for simple what-if experimentation. Placing the pointer crosshair location on other potential lines would provide the calculations for those speculative points as well. Placing the crosshair on any point or intermediate would also allow the drawing of a line of any desired slope for comparison purposes, and of estimating empirical values for γ to use in equations for calculating real gas velocities, TNT equivalencies, etc.

The writer has prepared one possible example (proof of concept), currently called adiabat32.exe, of such a utility for a number of different gases. This "draft" has not been thoroughly vetted nor validated and so is provided for evaluation only, and must be taken as an "as is" and "use at your own risk only" effort. It was made available separately on the writer's home site from 2007 to about 2011 as 16-bit software. However, it must be repeated that ASTM Committee G4 has been reluctant of late to pursue additional PC utilities like this for a series of reasons. The prospect that such an effort would find a warm reception and adoption are scant and without the ASTM G4 imprimatur any such effort would be much less valuable, credible and prestigious. Hopefully a way can be found to exploit its potential benefit.

Real-Gas Heat Transfer

In many paradoxical instances, the more one compresses a gas, the higher will be its final temperature, *but the less will be the amount of heat transferred from the final gas slug* and vice versa. This paradox occurs when one is pressurizing gas in a fixed volume (such as a component) from various starting pressures to a constant final pressure, such as that in a commercial cylinder.

In 1992 the writer made his first attempt to relate the risk of exceeding an *in-situ* ignition temperature with the risk of exceeding an *in-situ* minimum ignition energy [***6***]. It was reprised in 2002 [*7*]. This effect derives from the interplay of temperature and heat transfer during adiabatic compression. The lower the initial pressure in a fixed-volume system, the greater will be the final temperature predicted, albeit often with a smaller amount (mass) of hot oxygen. However, the greater the initial pressure, the larger (more massive) will be the final slug of hot gas that is produced (albeit often at a lower final temperature). But as physics would have it, over a significant range that applies to most oxidant systems, the higher will be the temperature achievable, the smaller will be the amount of heat that can be transferred.

Even incredibly high temperature (for example plasma discharge temperature) with negligible heat transfer may not be an effective ignition source. Small sparks and arcs have often failed to ignite even the most vulnerable of polymers. Similarly, high heat transfer at a temperature far below the ignition condition may not be an effective ignition source either. There may be a circumstantial optimal condition somewhere in between these extremes.

Please allow an example to allegorize this aspect. It is not merely the temperature of the oxidant that causes ignition. The temperature the material contacting the fluid achieves is also crucial. One can wave their hand through some oxygen-fuel flames at a speed that will produce negligible injury despite the several thousand degree flame temperature. However, a similar wave through a steam jet might produce a terrible burn, owing to the high heat transfer that condensing steam can produce even at a mere couple hundred degrees temperature. One's hand may actually be heated and injured more in the low temperature stream than in the high temperature stream.

So where does the greatest amount of heat transfer above the ignition temperature occur (without meaning to suggest that this is the exact most vulnerable point)? And in fact, if real

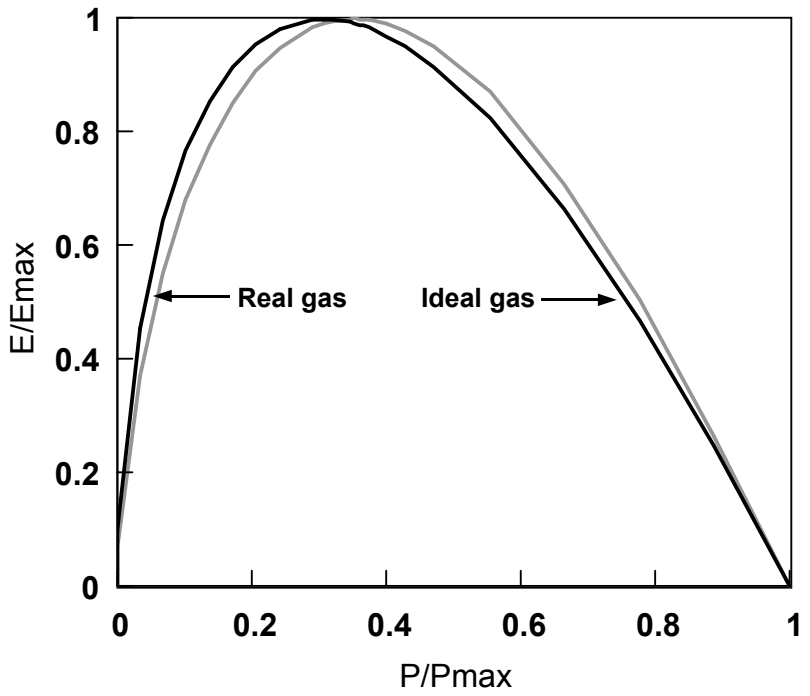

FIG 9—*Maximum Relative Heat Transfer Before Compressed Gas Cools to Room Temperature. Starting 70°F and 15 psia, Final pressure 3600 psia. On digital copies: Black—Ideal gas. Green—Real gas per NIST 12.*

oxygen does not produce a higher temperature, does it perhaps transfer an offsetting increase in the amount of heat transfer possible or does it work oppositely? With the NIST12 DB data, a good, albeit still coarse, perspective can be had.

As a first approximation, Figure 9 repeats the earlier ideal-gas approximation. It indicates a maximum heat transfer when the starting pressure is about 30.8% of the final absolute pressure. What this is saying is that if a starting gas at the optimal pressure is rapidly pressurized to 3600 psia, and then the gas is allowed to cool uniformly (which is not the case) then when the gas has returned to room temperature it will have transferred a maximal heat compared to any other starting pressure. However, when that maximal heat has been transferred, the final gas temperature would be only room temperature and no longer a serious risk.

Figure 9 also presents a curve that is the change in gas enthalpy compared to the maximum enthalpy change of the gas during compression multiplied by the final density as extracted from the NIST12 DB. This is a real-gas version of the previous calculation. For the room temperature starting condition the curves are very similar. The maximum in the real-gas case is at about 35.4% of the final pressure and the maximum transfer (not shown) is about 14% *greater* than the ideal gas case would predict.

As a result, this analysis suggests that oxygen at room temperature and atmospheric

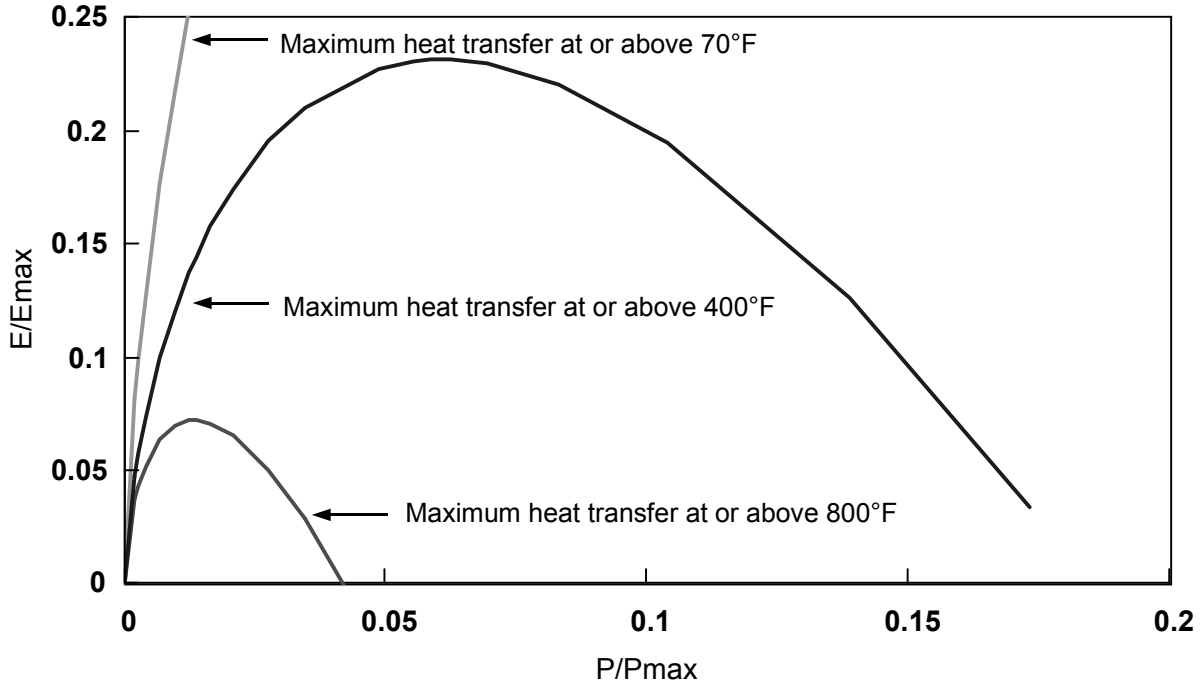

FIG 10—*Maximum Relative Heat Transfer Before Compressed Gas Cools to 400 °F or 800°F. Starting 70°F and 15 psia, Final pressure 3600 psia.*

pressure would compress to 3600 psia to more than 1700°F which is much higher than the autogenous ignition temperature of most polymers and then in cooling back to room temperature would transfer from the gas a heat of about 36 BTU/ft^3 of vessel volume. An initial gas slug compressed from an initial room temperature and extreme-case 1275 psia would compress to 3600 psia to form a slug with about thirty times the mass of the 1700°F slug but at a peak temperature of only 257°F which is less than the autogenous ignition temperature of most polymers but upon cooling back to room temperature would transfer a much larger heat (by a factor of more than ten) of about 397 BTU/ft^3 of vessel volume. Therefore, one might ask what is the maximum heat transfer at the time when the gas has cooled to the transient *in-situ* ignition temperature or even the autogenous ignition temperature (the latter likely to be the lesser).

Little is published about the transient in-situ ignition temperatures of materials but a small further refinement of this analysis is nonetheless still possible based on known autogenous ignition temperatures. Recall that some polymers ignite at temperatures as low as 400°F and most ignite at temperatures below 800°F. A refinement of the analysis is possible by calculating the amount of heat transfer that the gas might provide if cooled from the final peak temperature to either of these benchmarks.

Figure 10 shows both of these for real oxygen. In this case, a final pressure of about 3600 psia is assumed. One curve shows the maximum heat transfer possible before the gas

cools to 800°F and one curve shows the maximum heat transfer relative to cooling to 400°F.

This result is important! Whereas one might argue that there is not so much difference between materials that ignite at 400°F and 800°F when you are exposing them both to the peak 1700°F, but there can in fact be a huge difference. The material that ignites at 400°F will absorb much more heat before the gas cools to its ignition temperature during the transient cool-down and its surface will therefore warm much closer to or above its ignition temperature. This bottom line is even more dramatic than this simplistic analysis suggests. In many cases the compatible polymers (most notably PTFE) will be much more dense than the low igniters (PTFE has a specific gravity of about 2.3 while polyethylene is less than 1.0). This means that even for comparable heat transfers, the temperature rise in the compatible materials will be less. So, yes, the high igniters do indeed deserve the good reputations they have earned.

In the analysis of Figure 10, the first curve (maximum heat transfer at or above 800°F) is maximum for a starting pressure of about 50 psia (P/Pmax = 0.0139), and the maximum heat transfer is about 7-8% of Emax. When pressurized to 3600 psia then allowed to cool to 800°F, side-by-side PTFE and PE would be exposed to this maximum heat transfer, but then the gas temperature would drop below 800°F as it cooled further. By the time it cooled to 400°F, the additional heat transfer possible to the still vulnerable PE component would be twice this amount. This might be the worst case exposure for PTFE, and it should be much worse for PE. However, the likely worst case for PE would be if the starting pressure were to be at the maximum in the blue curve (maximum heat transfer at or above 400°F) at about 225 psia (P/Pmax = 6.25%). At a starting pressure of 225 psia, the final temperature does not achieve 800°F (it only hits 682°F, so PTFE could not heat above the 800°F level. However, the heat transfer to PE might be about 23% E_{max}, which is about twice the heat transfer at or above 400°F that would occur at an initial pressure of 50 psia. Clearly, the more vulnerable materials are more vulnerable across the board and might be especially vulnerable to higher starting pressures.

These latter 400°F and 800°F curves will change a lot depending upon starting temperature. Figure 11 exhibits these same curves for two additional starting conditions. The black curves are for an initial room temperature (70°F). The red curves are for a starting gas temperature of 100°F, and the blue curves are for starting gas temperatures of –30°F. These suggest that warm initial gas temperatures produce higher heat transfers relative to fixed threshold temperatures. The three lower curves are heat transfer upon cooling to 800°F, and the upper three curves are for heat transfer upon cooling to 400°F.

Again, there are few data available for in-situ ignition temperature and in-situ ignition energy during such transient events. Some materials will begin to melt (which can shield against high temperatures), some will begin to vaporize and other effects are important also. But today, only autogenous temperature is routinely reported.

However, the concept of ignition energy is well established. Papers on the minimum ignition energy (MIE) are few in most relevant contexts. However, to borrow words from an earlier paper [*7*], "The LOX mechanical impact test is, indeed, a minimum ignition energy test but

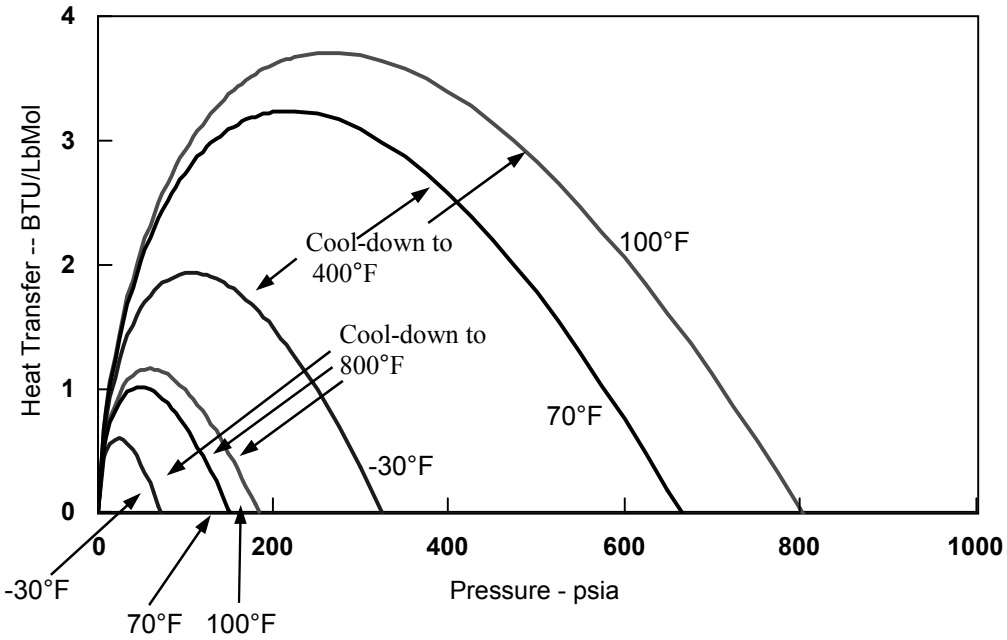

FIG. 11—*Maximum Relative Heat Transfer Before Compressed Gas Cools to 400 °F or 800°F. Starting 70°F , -30°F and 100°F , (black, blue and red on digital copies). Final pressure 3600 psia.*

is difficult to relate to gas impact. However, the MIE concept is reviewed in many texts of common study by oxygen compatibility practitioners, such as Lewis and von Elbe [***21***], and the auto industry has extensively explored the MIE of air/fuel mixtures in internal combustion engines, for example: Steiner and Mirsky [***22***]. Indeed, Steiner and Mirsky address the particular importance of MIE dependence upon the rate of energy input, a factor which is also crucially important in heat of compression exposure in oxygen."

To experimentally assess transient ignition one might mount a gas cylinder-operated arm on an ignition "bomb" (like that in G 72) with a ram that could push a cool instrumented specimen into, or through, a heated oxygen and then retract it or push it all the way through into a cool region. This would give insight into how quickly materials ignite and how much higher are their *in-situ* ignition temperatures. Such work is not likely any time soon. However a couple of pertinent examples can be gleaned from the literature and follow.

A Bizarre Scenario?

Janoff et al. [***23***] reported that in early rapid-compression tests at NASA, PTFE ignited only at 3000 psia final pressures in an original configuration, but as low as 1000 psia final pressures in a second configuration (these tests were conducted in New Mexico where atmospheric pressure is several psi lower than 14.7. The second system had twice the internal diameter and five times the initial length of oxygen slug (ten times the initial volume). PTFE is reported to

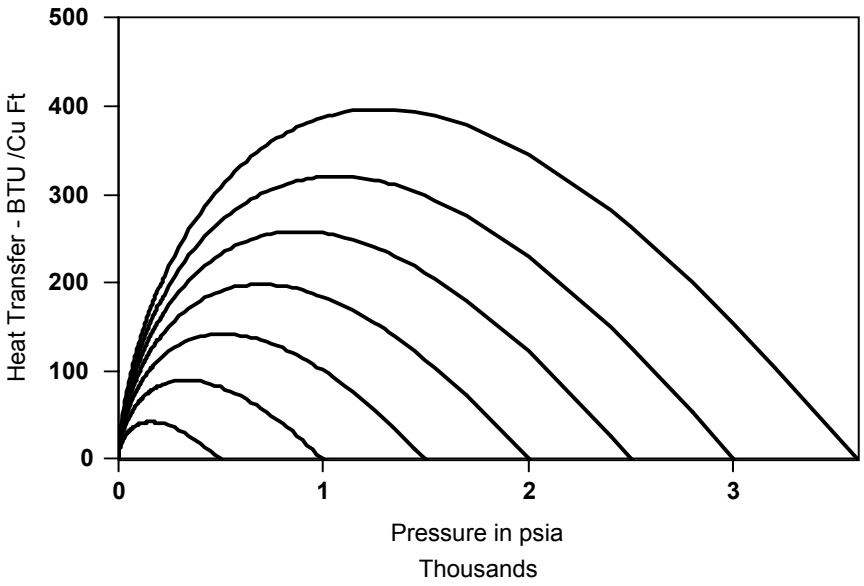

FIG. 12—*Heat Transfer in Compression of Real Oxygen to Various Final Pressures.*

have an autogenous ignition temperature of 950-980°F when soaked in hot oxygen at atmospheric pressure and this figure should decrease in elevated pressures but increase when a transient exposure to hot oxygen obtains.

In increasing the volume of the system, these workers were increasing the size and mass of the final hot oxygen slug, exposing the polymer to a larger heat transfer from the hot compressed oxygen. The result was ignition at lower final pressures, which equates to lower final temperatures, despite the potentially greater heat transfer. This indirectly demonstrates the anticipated result of varying the starting pressure as a means to provide a similar larger mass of hot oxygen albeit at a slightly lower final temperature. It also indicates that larger systems with larger volumes and inherently larger masses of hot final compressed oxygen which also implies a lower surface-area-to-volume (meaning slower cool-down rates) represents a worse (but not necessarily worst) case scenario to have in practical systems.

Figure 12 exhibits curves from NIST databases in the manner of Figure 9-11, but for which various final pressures are presumed for a constant starting pressure. The previously observed trend persists with the maximum in each curve about 30-35% of the final value. The maximum transfer appears roughly linear with final pressure, but heat transfers at 400°F and 800°F might be more complex and warrant further study.

More Sophisticated Analysis

The previous analyses indicate that in some cases a higher starting pressure during adia-

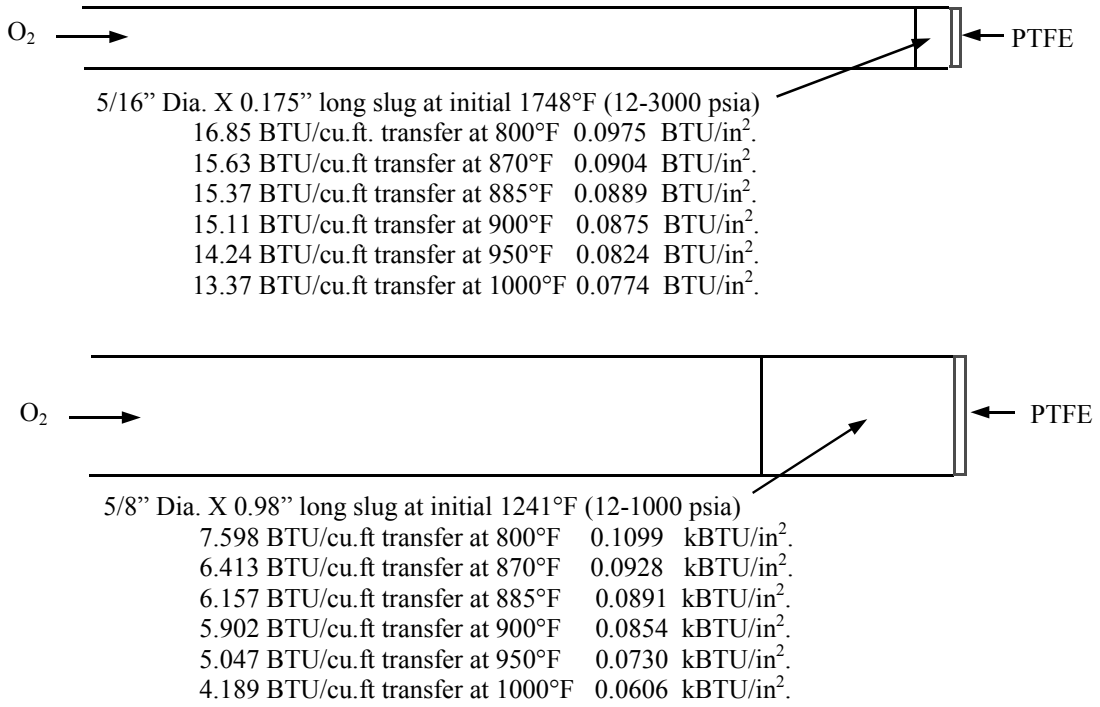

FIG. 13—*Final Slugs in Two NASA Apparatuses* [***19***].

batic compression might yield a more severe ignition climate than would a lower starting pressure. These analyses considered the heat transfer that would occur from a final compressed gas slug representing the oxygen that was initially present in a system.

This analysis is not intended to assert that the lower pressure starting condition is never the more severe. In some cases lower starting pressure ***is*** more severe. Figure 13 exhibits real-gas estimates for two pertinent examples that are to approximate scale and should print on paper to approximate actual size.

In the upper case, the example is roughly that of the early NASA adiabatic compression testing that is the basis for the original example system in ASTM G 74-82 *Standard Test Method for Ignition Sensitivity of Materials to Gaseous Oxygen Impact*. That original system employed an internal volume of about 20 ml from a roughly 10 inch (254 mm) length of tubing of inside diameter of 5/16 inch (7.9 mm). This volume and these dimensions are not too untypical of much oxygen hardware. Often regulators and the like are located several inches from their pressure source and have similar piping dimension and internal volumes.

In the lower case, the system is as revised in later work reported by Janoff et al. [***23***]. This is a doubling of inside diameter and an increase in the length of the initial piping by about 2.5. These dimensions may be somewhat flawed because Janoff et al talk of doubling the inside diameter from 6 mm but the ASTM standard indicated the inside diameter should be 7.9 mm.

Small systems are the kind that are the most likely to be less sensitive to lower starting pressures. When abruptly compressed, the initial oxygen in these volumes will result in small final volumes. In the case of the NASA configuration used in G 74, the final volume would only be a slug that is about 0.18-inch long and 0.31-inch in diameter. The revised system would have produced a slug about one-inch long of about 0.62-inch diameter. Clearly the lateral surface-to-volume ratio of the slug from G 74 would be larger than that of the revised system and in combination with the much shorter length would lead to more rapid cool-down. This is simply a pretty small slug of gas.

The revised system has both the lower lateral surface-area-to-volume ratio and a much greater length likely to greatly reduce end-effect heat losses such as radiation, percolation and buoyancy. For systems that are still larger, the heat loss becomes even smaller as surface-area-to-volume continues to shrink and so if one were to be pressurizing a 12-inch diameter pipeline, then the more severe case might well be the one starting at the lower pressures (within reason). This would clearly be more severe for a long run of piping.

In Figure 13, the real-heat transfer *from* the final slugs is indicated for cool-down to various temperatures. It may be a leap too far to suggest that the heat transferred *from* the slug is linearly or uniformly related to the heat transferred *to* the PTFE target, *but* it is very impressive that as the slug cools, the heat transferred from the slugs differs greatly but the heat transfers per unit area of the target approach each other as the approximate autogenous ignition temperature of PTFE is approached. The transfers per area are equal in this case at a level of approximately 0.0890 BTU/in^2. At this point, the heat transfer has reduced the oxygen slug temperature in both cases to about 885°F. This is written with great ginger, because the in-situ ignition temperature is not known but is assumed to be somewhat greater than the autogenous ignition temperature (known to be about 950-980°F at atmospheric pressure but perhaps significantly lower by a hundred F° or more at the elevated pressures and perhaps even different for the two cases shown). Despite the potential errors that may be present for these two threshold-ignition conditions in these two test apparatuses, clearly this correlation is much closer and more meaningful at understanding the ignition thresholds in the two NASA tests, than is any correlation between peak adiabatic temperature and autogenous ignition temperatures. Further study would be worthwhile both in theory and in the lab.

Figure 14 plots the real-gas cooldown curves listed in Figure 13 for these two systems. The two red curves intersect at about 885°F and at about 0.0890 BTU/in^2. These cool-down curves are for a 12 psia starting condition consistent with the atmospheric pressure in New Mexico. It also shows four curves which compare how these might compare if the starting pressures were higher (relative to a more common 14.7 psia starting atmospheric pressure condition) for the same of final pressures (1000 psia for the larger system, 3000 psia for the smaller system). The two curves which start at 14.7 psia and finish at either 1000 or 3000 psia are shifted from the earlier curves, and their intersection is now at a cooldown temperature of about 850°F, a significant difference. In case the 885°F temperature is significant (and much more study might be needed to validate this surmise), a third set of curves exhibits a starting pressure

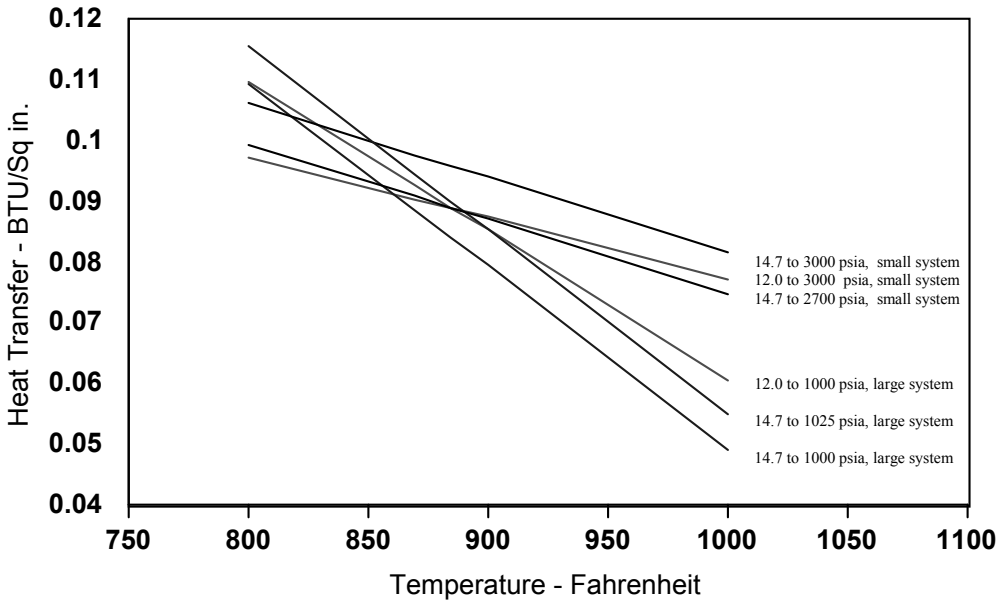

FIG. 14—*Final-Slug Cool-Down Curves in Figure 14 with Variants.*

of 14.7 psia, but shows differing final pressures that will produce an intersect again at 885°F. Perhaps counter-intuitively, the small system might be more sensitive to higher starting pressures and the ignition threshold might shift down to 2700 psia. The larger system might be "over the hump" of sensitivity and might require a higher starting pressure to maintain sensitivity at higher starting pressure. This is reasonable. However, remember the WSTF data are coarse and were not collected for this purpose, and so until someone actually tests and confirms this pattern, it is merely a plausible theoretical surmise.

A Final Fickle Scenario?

Heat transfer discussions such as these have appeared in both of the writer's previous papers [***6,7***] on adiabatic compression assume an incident has occurred. A system, say a regulator, that had been operated without problem for many years suddenly experiences a fire. Was this merely a random, low-probability event that could have happened at any time, or was it predictable? A typical tack is to search for changes to explain the event. The period just before the incident is usually a primary focus. What changed just before the event? Did something break? Was the oxygen different? Purer? Was pressurization faster? Did someone add a contaminant? Did they lubricate the inlet fitting? Indeed, this last question would always be explored very carefully. In this and the earlier prospects, the regulator may have been experiencing conditions it had never seen before that might explain its fire.

The analysis of this section explains a fickle scenario that is easy to overlook. Assume

there is some contamination present that has been present for a long time, maybe years. Maybe it was not added in the sense of someone adding grease or oil (or maybe it was) and maybe it migrated in gradually. Assume that standard practice was always to bleed down pressure in the regulator fully after each use, but that the "change" that occurred just before the fire was that a residual pressure was inadvertently left in.

Maybe the pressure in the regulator was a few psi above atmospheric. Or a few tens of psi. Or even more than a hundred psi above atmospheric pressure. A previous analysis of this case [*7*] discussed how easily this could happen and yet not be obvious to any operator.

In this case, when pressurized to a high level, a lower final temperature than normal would result, surely to be less likely to exceed any component or contaminant ignition temperature than in previous pressurizations. But a higher available heat transfer might result that might be much more likely to exceed minimum ignition energy thresholds than had ever happened previously.

Figures 10 and 11 haves shown how much energy might have transferred before the gas cooled below an 800°F temperature. They also show how much heat might transfer before the gas cooled below a 400°F temperature. If the normal initial pressure during pressurization had been low on these curves, ignition may not have resulted previously because, even though the final temperatures were high, the heat transfers may have been too low, below the level required to transfer the minimum ignition energy of the materials of construction *and* possibly even below that of any contaminant.

A single cycle in which the initial pressure was higher would lessen the final temperature while increasing the heat transfer to any materials/contaminants present. This might possibly exceed the minimum ignition energy for the polymer or contaminant for the very first time in the device's service life, ergo might serve as the reason (as the erratic changeableness, the fickleness) to cause the incident at that particular moment.

Wilson et al. [***8***] perform a rather complex modeling of this issue to assess the temperatures that oil films and damaged polymers might achieve when oxygen is compressed non-adiabatically (non-isentropically) with heat transfer from the oxygen to the oil film or polymer damage and the substrate below during compression. The model qualitatively fits and confirms the anticipated behavior but again, lacking data for in-situ ignition temperatures, in-situ minimum ignition energies, it allows for better understanding but OSPs must still apply much judgment in engineering oxidant systems.

The Koeller Calculations (and Beyond)

Koeller's preliminary effort [***10***] performed a series of six different calculations for both ideal, real, and quasi-real oxygen, the latter predicated on "real γ" values: (1) adiabatic compression, (2) adiabatic expansion, (3) distance/volume piece design, (4) TNT equivalencies, (5) total pressure, and (6) maximum achievable velocities. However in previous sections and Appendix A we have seen that approximating real oxygen using real γ can be flawed. Each increment in the calculation employed the term γ in its formulation and so each may suffer from the

same potential error mechanism. These six topics will be reviewed or replicated using both ideal gas and alternative calculations with NIST12 or NIST23 data plus a wider range of starting conditions, as previously reviewed. Appendix B provides more detailed analysis of the methods and derivations involved in making these remaining calculations.

Adiabatic Compression/Expansion

As reviewed in Appendices A and B, real adiabatic expansion uses the same math as for real adiabatic compression except that the initial stage is taken at a higher pressure. Figures 4, 5, 6 and 7 still apply. Figure 15 compares several ideal-fluid calculations for compression and expansion based on Equation (2) drawn upon the real-oxygen data in Figure 4 .

In Part A the ideal-gas adiabatic-compression data begin at the left (lower pressure) ends (~ 2psia) of the Figure 4 isentropic curves and in every case the ideal gas curves appear comparable to those cited by Leslie and suggest all of the real gas curves can be approximated by polytropic equations with empirically assigned adiabatic exponents. In most (but not all) cases the ideal gas curve diverges and is above the real-gas curve.

In Part B of Figure 15, ideal-gas adiabatic-expansion is shown as straight curves that begin at the higher pressures (right ends of the real gas curves). Here the case is more complicated. In many cases the ideal gas curve (straight line) does not depart greatly from the real-gas curves, but in several cases the ideal-gas curves pass through the saturation curve and data below the saturation curve are sure to be in great error. While empirical approximation as cited by Leslie above the saturation curve would be adequate, predicting where the saturation curve will be intersected requires the use of the data like those on Figure 4.

In expansion, the assumption that the gas and any liquid that forms are separated and will not share equilibrium is much less valid. As a gas expands to achieve the boiling point temperature, fine droplets of liquid of high surface area to volume would form and they would be distributed throughout the fluid. The heat exchange properties between them should be excellent, and so during expansion, near-equilibrium might obtain. Hence when an expansion curve intercepts the saturation curve, it should "bend" and follow the saturation curve.

Distance/Volume Piece Sizes

As reviewed in Appendix B, ideal-gas distance/volume piece design equations were proposed in Santay et al. [***24***] and incorporated into Version 1.2 of ASTM G4Math12.exe for use with an ideal-gas $\gamma = 1.4$. The derivations manipulated Equations (1-3), and so the substitution of $(1\text{-}m_{TV})$ or $-m_{PV}$ for γ is circumstantially valid. The appendix also considers when a segmented (pipeline) calculation is valid. Santay et al. discourage use of FSC designs and focus on temperature controlling (TC) designs. These equations merely calculate a specific compressed gas slug size at various conditions and add a safety factor. Figure 16, page 46, compares several variants of the equations and similar calculations using assorted maximal and minimal values of the controlling exponent and NIST12 DB data for both single-ended and double ended cases.

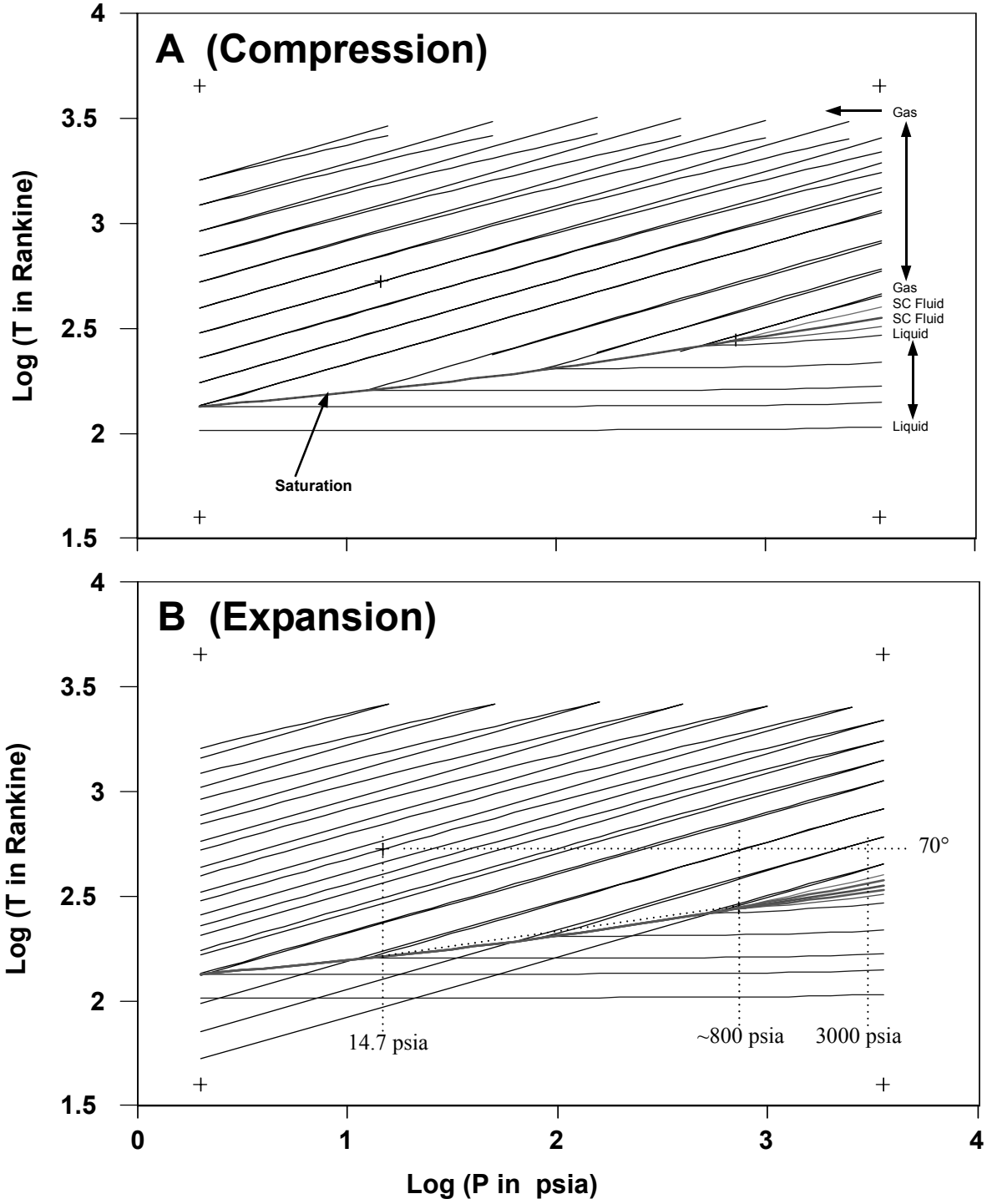

FIG. 15—*Real– and Ideal Oxygen Adiabatic Temperature Vs. Pressure From NIST12 DB.*

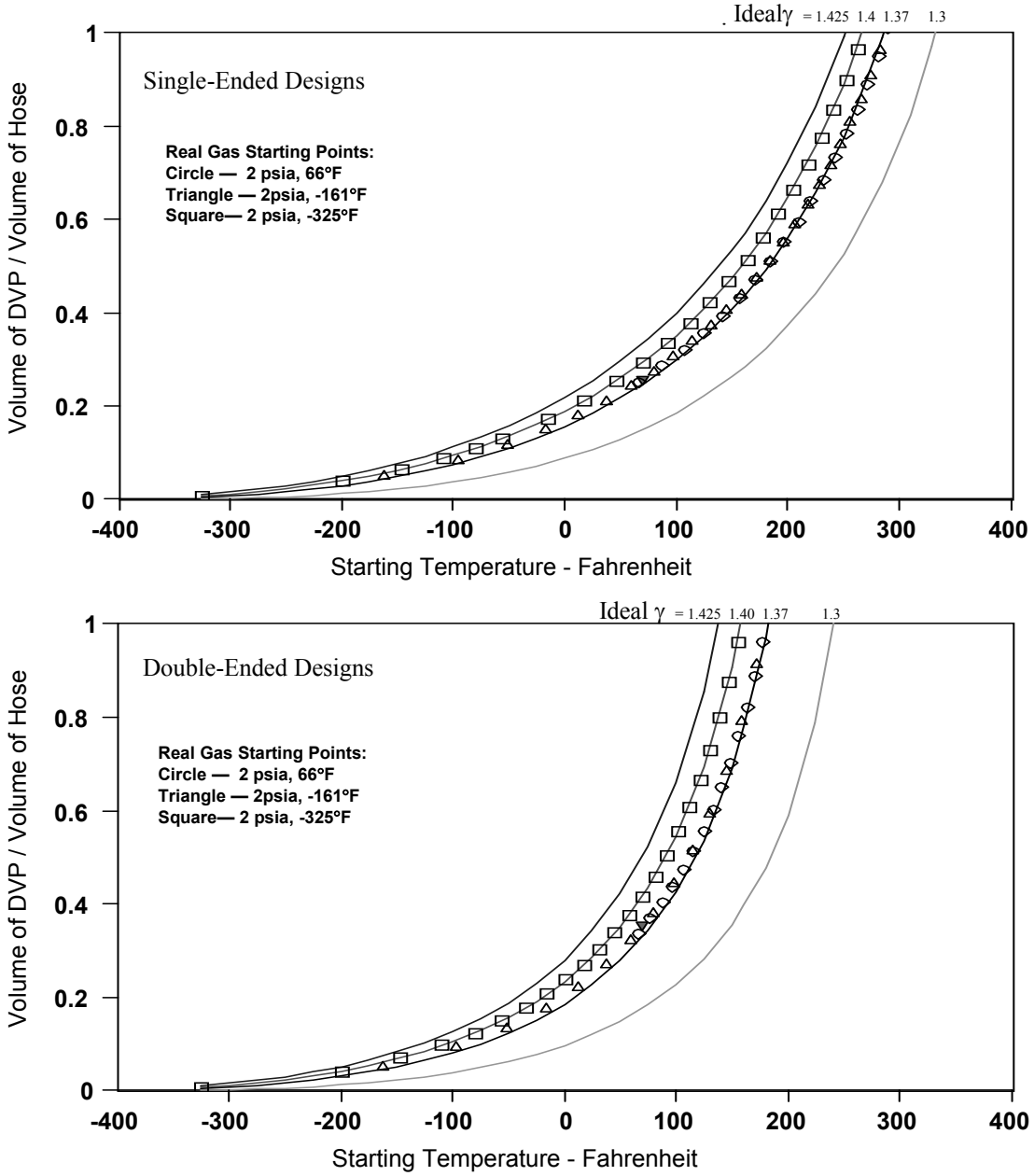

FIG. 16—*Real and Ideal Distance/Volume Piece Designs*

These results all incorporate a twenty percent safety factor (k = 1.2). Each is shown in terms of DVP volume compared to the volume of the flexible hose it is protecting (for single ended DVPs, any significant upstream volume is treated as hose volume).

The four curves (blue, red, black and green on digital copies) are DVP calculations

based on ideal gas of adiabatic exponent, γ , of 1.425, 1.4, 1.37 and 1.3, respectively equivalent to ideal gas m_{TV} values of (1-γ) or -0.425, -0.4, -0.37, and -0.3. These span many of the real m_{TV} values labeled on the ends of isentropes on Figure 6 for real oxygen gas. Finally, both sets of curves exhibit symbols plotted for DVPs calculated from real-oxygen gas data for three adiabatic compression conditions (three isentropic curves) that are represented by selected curves on Figure 4. The symbols exhibit real adiabatic compression for the Figures 4 and 6 curves that pass though the room temperature (~70°F), atmospheric pressure point (triangle symbols) labeled "d" at the low temperature end on Figures 4 and 6, the third curve below that curve which is the curve that just touches the saturation curve at its lowest point (square symbols) labeled "e" at the low temperature ends on Figures 4 and 6, and the second curve above the room-temperature point (circle symbols) labeled "f" at its low temperature end on Figures 4 and 6.

These real curves span most of the practical cases OSPs will encounter. For most conditions below these, the final temperatures do not achieve the 572°F condition that calls for a DVP. Above these curves, most conditions are already above the 572°F temperature and can not be protected with DVPs.

Most of the symbols lie on or between the curves representing the ideal-gas γ exponents between 1.37 and 1.4.

The difference in design sizes are fairly small and so using the more conservative traditional exponent of 1.4 (as is used in G4Math12.exe) in designing these devices is practical, and should be acceptable in most cases.

Indeed, the difference in sizes between the single and double ended designs is often not large, and especially when dealing with small hoses, when one is in doubt as to the future of a system, one might wish to specify a double-ended design DVP dimension even for a single-ended DVP system. If in the future, the need should then come to pressure the system in reverse, the one existing DVP could be supplemented with a second instead of replacing them both. However, for some cases, a single-ended DVP can be installed when it would not be possible to install a double-ended design.

TNT Equivalency Calculations

So far in this tutorial, real-oxygen calculations have often predicted behavior only marginally different from ideal oxygen in most instances of interest to OSPs. But the situation is much different when it comes to mechanical TNT equivalencies, and this will require much more extensive discussion. And if these calculations prove correct and if they reflect reality, then OSPs will need to become familiar with them in some detail.

As reviewed in Appendix B, traditional equations were presented by the writer and associates [***25***] previously (numbers 14, 16, 17 in that paper) to estimate the mechanical (PV) energy in an expanding adiabatic ideal fluid. The derivations begin with Equation (1) and integrate the work differential PdV. As a result, these equations, respectively, would presumably be more appropriate with the empirical adiabatic exponent, $-m_{PV,}$ substituted for γ as follows:

$$E = [-1/(m_{PV}+1)\ ]\ [(P_i V_i) - (P_f V_f)] \tag{20}$$

$$E = [-1/(m_{PV}+1)]\ [(P_i V_i) - (P_f^{([m_{PV}+1]/m_{PV})}\ V_i P_i^{-1/m_{PV}})] \tag{21}$$

$$E = \{[-1/(m_{PV}+1)]\ [(P_i V_i) - (P_f^{([m_{PV}+1]/m_{PV})}\ V_i P_i^{-1/m_{PV}})]\} - \{P_a V_i[(P_i/P_f)^{-1/m_{PV}} - 1]\} \tag{22}$$

The first two equations address an expansion to a final pressure and volume in vacuum. The third addresses expansion in an ambient atmosphere (because a vessel that bursts in an ambient atmosphere that is at the same pressure yields no explosive consequence).

The appendix also describes using a spread sheet for performing mechanical TNT equivalency estimates with quasi-real oxygen in which the specific heat capacities are adjusted for variations due to temperature or for which the adiabatic exponent is extracted from the NIST databases or Figure 7. Finally it describes estimating the mechanical TNT equivalency as the change in internal energy reported by NIST databases in a real gas during an adiabatic expansion, and it compensates that expansion for work done on an ambient atmosphere.

Notice that Equations (22) is for an initial volume of ideal gas, such as a filled cylinder at an initial pressure and in an ambient atmospheric pressure, and it *does not specify an initial temperature*. This equations may be used in assorted ways. Among them, the equation might be used for estimating the explosive energy in a cylinder of gas at a fixed temperature for a series of pressures. It might be used for estimating the energy in a cylinder of gas at a fixed pressure but at various temperatures. It might also be used for estimating the energy in a series of cylinders of differing volume at the same initial pressure and temperature. And it might be used for estimating the energy remaining in a cylinder of gas that is venting or in a slug of gas that is expanding, such that the remaining mass of gas is at a different pressure, volume and temperature at each step.

When used for the first purpose, (single size of vessel at fixed initial temperature varying initial pressure) each calculation produced with Equation (22) is for a complete expansion to atmospheric pressure). Figure 17 shows TNT equivalency curves generated with Equation (22) in this way for the same four levels of γ or real -m_{PV}, that were examined in the previous section on distance/volume pieces (namely, 1.425, 1.4 and 1.37 and 1.3). These values span a large portion of the range of values that are displayed for oxygen gas in Figure 7. Notice that *the lower values of the exponent yield the higher TNT equivalencies*. Also, it is interesting that these curves appear so nearly linear. Note that the upper point of each curve represents a complete expansion that begins on a horizontal line that might be drawn on Figure 18, and each point represents an expansion downward and to the left till it intersects a vertical line that is drawn at the atmospheric-pressure point. Figure 18, duplicates Figure 15 (Part B) and exhibits horizontal dotted lines at 1739°F, 70°F and –10°F (there is an optical illusion that makes these dotted lines appear to be sloped). For use of Equation (22) in this way, each point of the line represents the expansion of the fluid from that point on the line down along a different adiabat

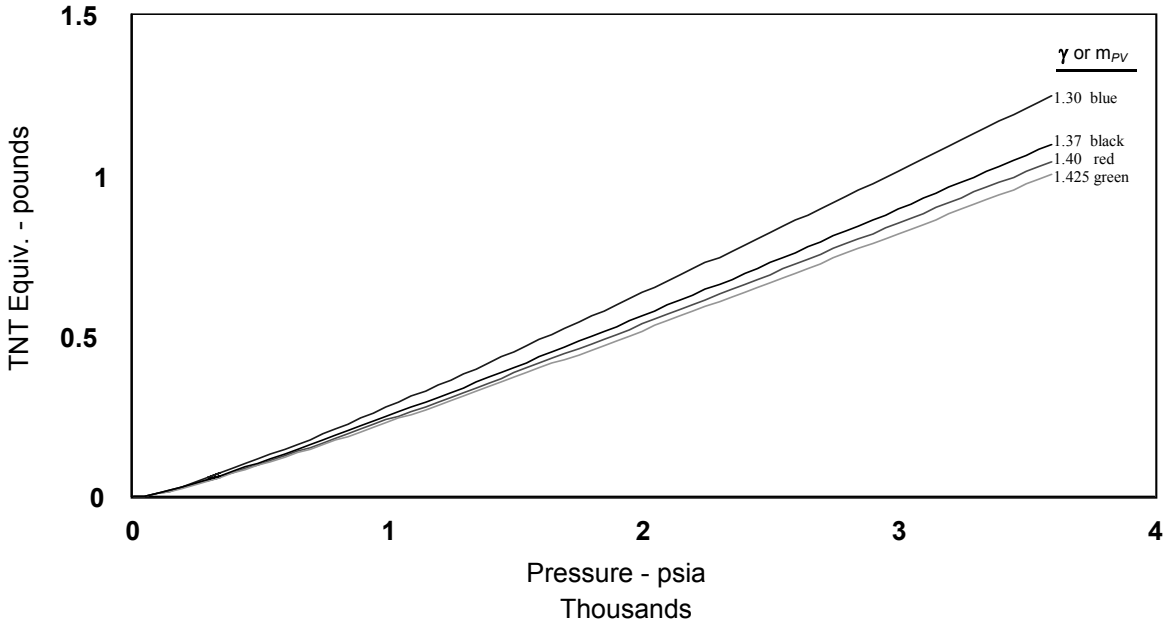

FIG. 17—*TNT Equivalency of Ideal Oxygen for Differing* γ or -m_{PV}. *(For a Vessel of 1.75 Cubic Foot Volume)*

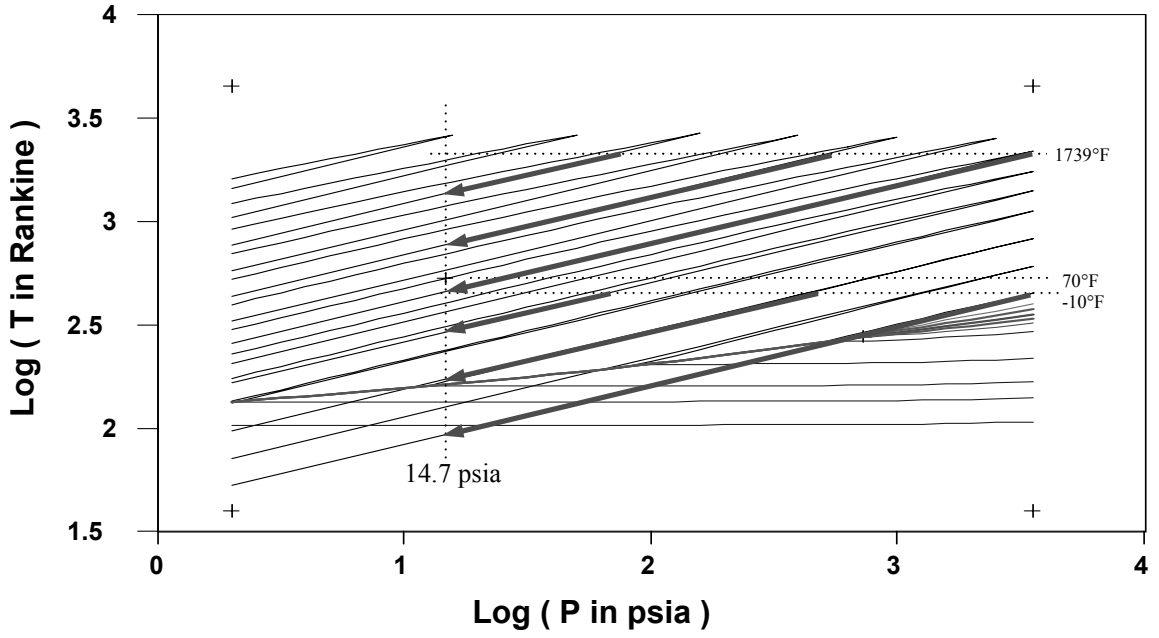

FIG. 18—*Ideal-Oxygen Adiabatic Expansions at two Initial Temperatures*.

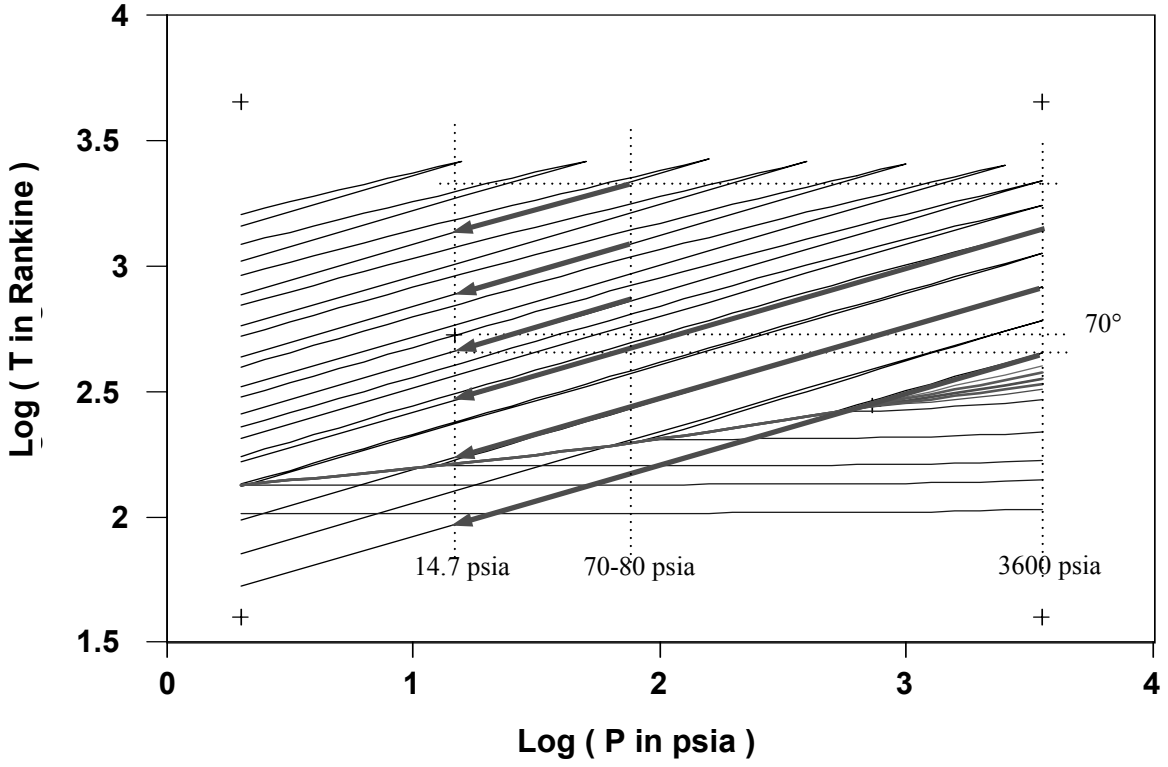

FIG. 19—*Real-Oxygen Adiabatic Temperature Versus Pressure From NIST12 DB.*

(along the portion of the line representing ideal gas) to the atmospheric pressure point shown as a vertical line. Six expansions (six points) are shown as with arrows (red on digital copies), three at 1739°F and three at an initial –10°F. Notice that these six arrows have no fluid states in common. Also notice that for the lowest arrow, the ideal expansion continues below the known saturation curve for real oxygen. Since the ideal gas curve portions of Figure 18 were drawn for an exponent of 1.4, all six of the TNT equivalencies for these six expansions lie on the same curve (red on digital copies) for the exponent 1.4 on Figure 17.

When Equation (22) is used for the second purpose (single size of vessel at fixed initial pressure and varying initial temperature), then the points represent a series of complete expansion to atmospheric pressure that begin on a vertical line on Figure 19. Figure 19 exhibits six ideal expansions like this, three at 3600 psia and three at about 70-80 psia. Here again, these six arrows have no fluid states in common. Again notice that for the lowest arrow, the ideal expansion continues in error below the known saturation curve for real oxygen. Since the ideal gas curve portions of Figure 19 were drawn for an exponent of 1.4, all six of the TNT equivalencies for these six expansions also lie on the curve (red on digital copies) for the exponent 1.4 on Figure 17.

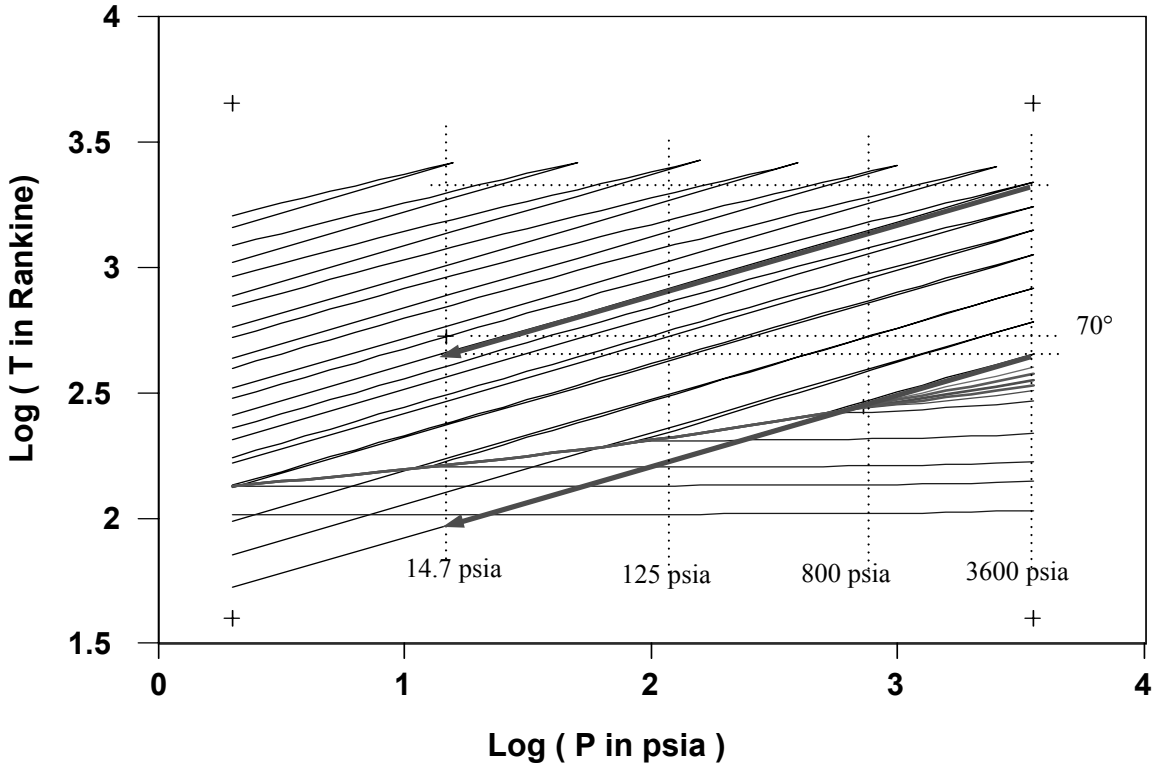

FIG. 20—*Real-Oxygen Adiabatic Temperature Versus Pressure From NIST12 DB.*
(*Constant initial volumes of varying initial pressure and temperature*)

When Equation (22) is used the third way (single size vessel at the variable pressure and temperature that would remain in it after venting any portion), then the stages represent a series of expansions, each laying on top of each other but each being of shorter length. Figure 20 exhibits six expansions like this. The upper red arrow represents three expansions, one beginning at 3600 psia and expanding to 14.7 psia. A second beginning on the curve at the 800 psia point and expanding to 14.7 psia. And a third beginning on the curve at about 125 psia and expanding to 14.7 psia. The lower arrow (red on digital copies) represents three similar overlaying expansions beginning at lower temperatures. In this case all of the fluid states are in common with portions of the expansion states for the initial conditions. Again notice that for the lower arrow, the ideal expansion continues in error below the known saturation curve for real oxygen. Since the ideal gas curve portions of Figure 20 were drawn for an exponent of 1.4, all six of the TNT equivalencies for these six expansions also lie on the curve (red on digital copies) for the exponent 1.4 on Figure 17.

Indeed, one could select any complex interrelationship between pressure and temperature and draw a straight line or even a curve on Figure 20, and use Equation (22) to estimate the TNT equivalency of each point in similar fashion. And all the points would lie on the same

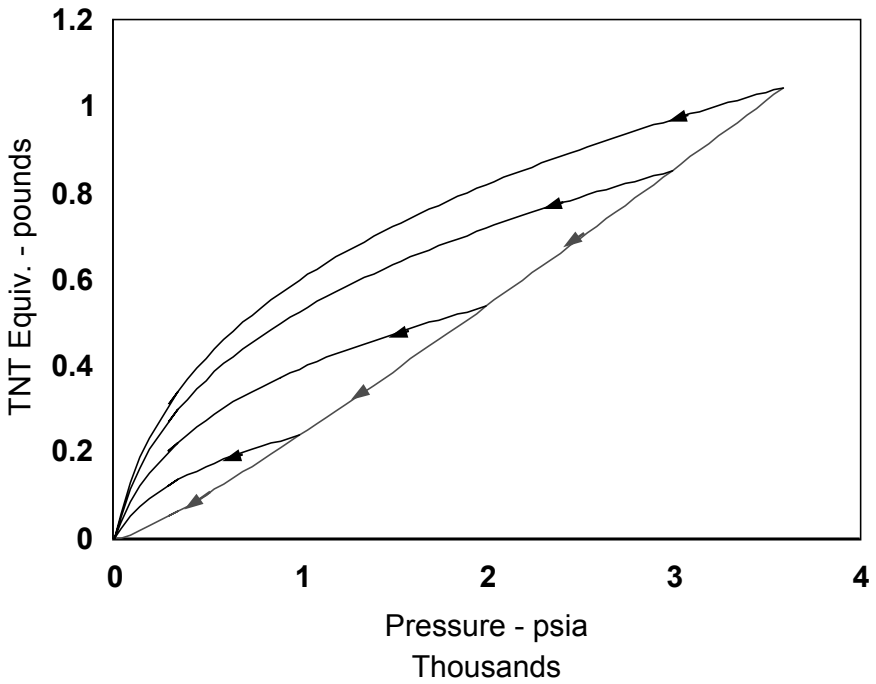

FIG. 21—*Ideal-Oxygen TNT Equivalency Versus Pressure for γ =1.4.*

curve for the exponent 1.4 of Figure 17.

It is perhaps a stunning result for ideal gases in that *the computed TNT equivalencies for all four of these types of calculations lie on the same curve, the same nearly straight line, of Figure 17.*

Yet another TNT equivalency calculation is of interest. That is the TNT equivalency remaining within a single released slug of fluid as the fluid pressure drops. In this case the initial volume, pressure and temperature at each stage are different. Figure 21 exhibits the curve for an exponent of 1.4 generated with Equation (22) and adds to it dashed curves for the energy remaining in single slugs of adiabatically expanding ideal gas for initial conditions beginning at various points along the curve. Note this is equivalent to applying Equation (22) to a series of points for which the volume, pressure and temperature are all simultaneously changing but the total mass of oxygen for each is constant. This exhibits how TNT equivalency is added to a blast as a single slug of gas expands. This is the only analysis so far that tracks the expansion.

A very interesting result of this last ideal analysis, is that although slugs of ideal oxygen of the same volume have nearly linear TNT equivalencies, any individual ideal slug of oxygen releases its energy to a variable extent as it expands. More of the work energy it releases is released at the lower pressures. In other words, when a gas slug at the initial 3600 psia point of Figure 21 expands to 14.7 psia it releases energy equivalent to a little more than one pound of TNT. However, during the progression of the expansion of that slug (the top black curve of Fig-

ure 21), the energy is released variably, and when the slug has expanded to half of its starting pressure (1800 psia), it still has about 80 percent of its initial one pound TNT equivalency yet to be released (still in the form of potential energy). At 25% of its initial pressure (900 psia) there is still more than 50 percent of its ultimate release remaining. The lower pressure portions of the expansion have more "bang for the buck", albeit at a lower pressure. This discussion presumes equilibrium throughout the slug of gas, but in reality, during an explosion, pressure is not nearly constant throughout the slug, and will often form a shock wave of maximum pressure.

When the preceding four types of calculations are performed for real oxygen fluid, the results are dramatically different. As described in Appendix B in this tutorial, the TNT equivalency will be taken as the change in the real-fluid internal energy which incorporates the work done on atmospheric pressure. This again requires a series of analogous curves to illustrate.

The top graph, "A", of Figure 22, "A", is analogous to Figure 18 showing horizontal dotted lines at 1739°F and –10°F. Arrows indicate expansion to atmospheric pressure from three pressures along each line to stress the TNT equivalencies of interest are for complete expansion at each point along the horizontal lines. By analogy, the arrows on this figure are shown laying on the real gas expansions (the upper curves near the top, and on the lowest arrow, the real expansion is shown in two segments where the first arrow terminates at the saturation curve and then its second portion is shown dotted and laying along the saturation curve. In addition, dotted lines are shown at 949°F, 70°F, -106°F, -165°F, and –241°F for scale.

The lower graph, "B", of Figure 22 is analogous to Figure 17 and shows a solid curve (red on digital copies) for an ideal-gas with γ of 1.40 as on Figure 17. Dashed real-fluid curves extracted from NIST12 DB based on internal energy that factors in work against the atmosphere are shown for the seven starting temperature conditions indicated on the upper graph, "A", of Figure 22.

If all seven of the real expansion curves were for ideal gas with a γ of 1.4, their points would all lie on the solid curve indicated for $\gamma = 1.4$, but they are relatively spread out when they are treated as real gas. Those at the higher temperature are more like the ideal gas equivalents, but as temperature decreases, the curves become very different. Notice that the curves at –165°F and –241°F are near or below the saturation curve, yielding the most curious results that will be reviewed in more detail later.

The top graph, "A", of Figure 23, page 55, is analogous to Figure 19 showing vertical dotted lines at 14.7, ~80, 100, 500, 1000, 2000, 3000, and 3600 psia. Arrows (red on digital copies) indicate expansion to atmospheric pressure at three temperatures along each of the 80 and 3600 psia dotted lines to stress the TNT equivalencies of interest are for complete expansion at each point along the dotted vertical lines. By analogy, the arrows on this figure are shown laying on the real gas expansions (the upper curves near the top, and on the lowest arrow, the real expansions at 3600 psia, –10°F is shown in two segments where the first arrow terminates at the saturation curve and then its second portion is shown dotted and laying along the saturation curve.

The lower graph of Figure 23 is curiously analogous to Figure 17, even though it is plot-

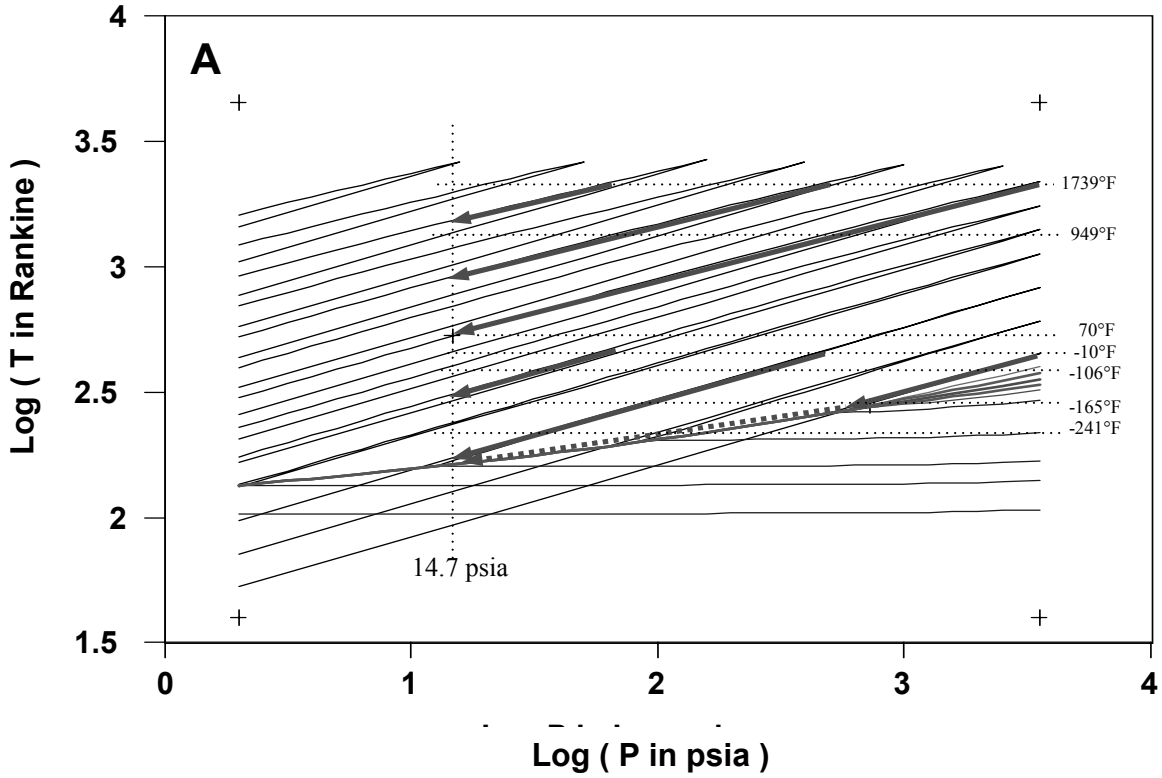

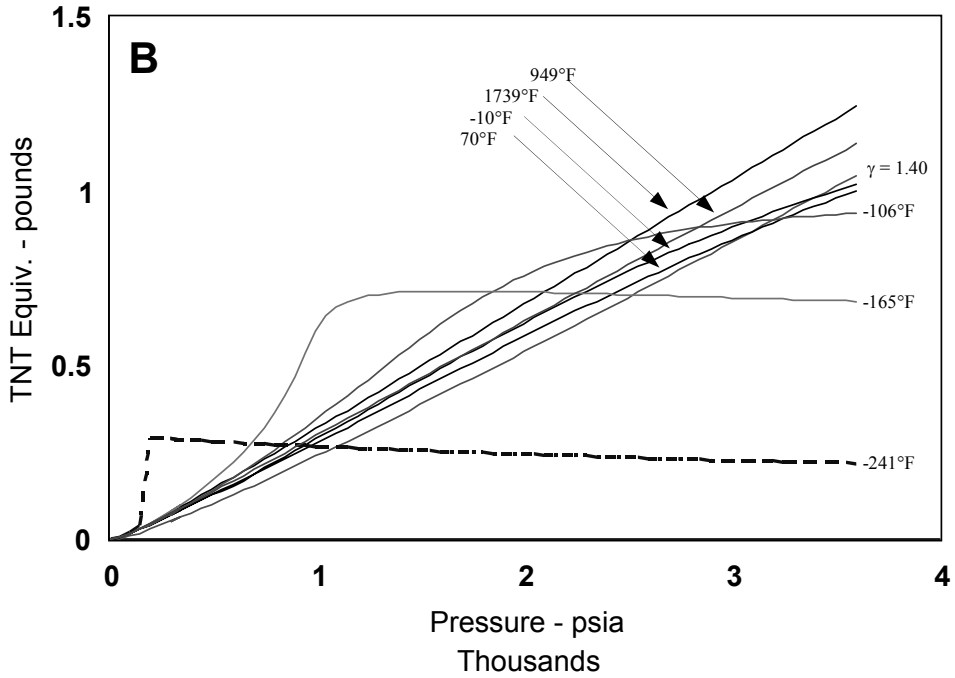

FIG. 22—*Real-Oxygen TNT Equivalency Versus Pressure From NIST12 DB.*

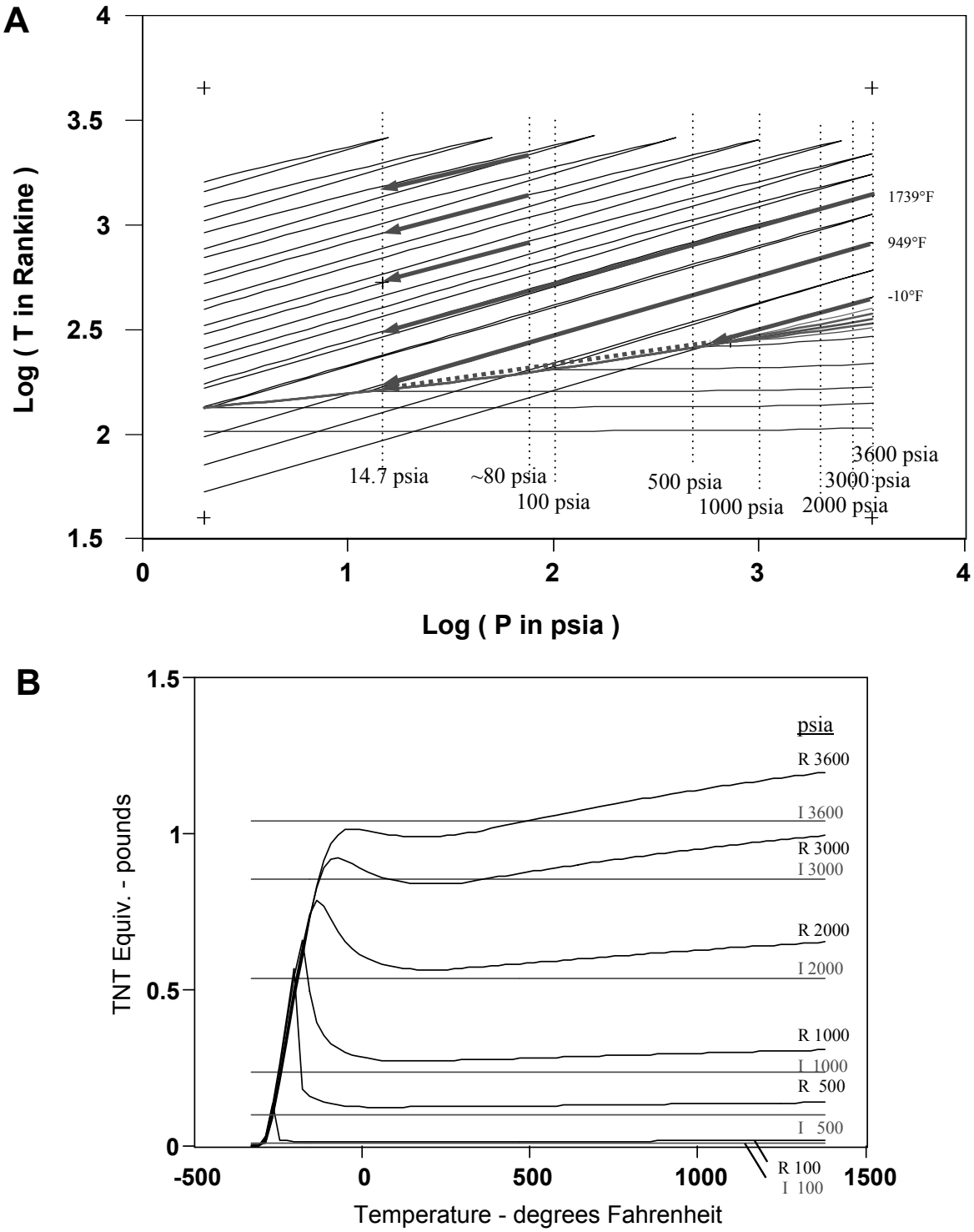

FIG. 23—*Real-Oxygen TNT Equivalency Versus Temperature From NIST12 DB.*

ted with temperature as the abscissa. The horizontal lines (marked "I", red on digital copies) actually represent ideal gas behavior. For example, every point on the top 3600 psia (red) line plots on Figure 17 at the tip of the red curve for the line of exponent 1.4. This is because for an ideal gas, Equation (26) is dependent only on pressure and initial volume and so every point on this curve has the same internal energy.

For the dotted lines marked "R" that reflect real fluid behavior extracted from the NIST12 DB, the curves vary greatly in some regions. In some cases, real fluid has significantly more TNT equivalency (based on internal energy estimates) than does ideal fluid. In some cases it has significantly less TNT equivalency.

Very significantly, here again, the TNT equivalency is especially interesting when the fluid is near or at the saturation (boiling point curve) condition. For some of these curves, the TNT equivalency spikes upward sharply to a maximum that is much greater than the ideal gas prediction. In the case of a constant volume vessel containing real oxygen at various conditions, these curves suggest a vessel containing 500 psia oxygen at high temperature contains far less TNT equivalency (by a factor of about four) than does a vessel near the saturation condition (which admittedly contains a greater mass of fluid).

The top graph, "A", of Figure 24, is analogous to Figure 20 showing a series of arrows (red on digital copies) to illustrate expansions to atmospheric pressure at seven initial temperatures each starting at 3600 psia. In this case the expansions all begin at the 3600 psia side and proceed towards 14.7 psia. This is equivalent to considering what the TNT equivalency is for full expansion of the fluid in a vessel. Each starting point is at a different temperature but starting pressure for each is the same 3600 psia. As in the previous real fluid examples, a lower arrow intersects the saturation curve and bends to follow it (as indicated by the dotted section). The lowest arrow is for liquid.

The lower graph, "B", of Figure 24 is another that is curiously analogous to Figure 17 and shows the same curve (red on digital copies) that applies to ideal gas of $\gamma = 1.4$. Seven real-gas curves are also shown extracted from NIST12 DB based on internal energy minus work against the atmosphere for six starting conditions at 3600 psia and the various initial temperatures. At higher temperatures, real gas behaves like ideal gas, but at low temperatures is much different and can exhibit higher TNT equivalencies than at high temperatures (due to the greater mass present).

If all seven of the real expansion curves were for ideal gas with a γ of 1.4, their points would all lie on the curve marked $\gamma = 1.4$ (red on digital copies), but they are relatively spread out when they are treated as real gas calculations and are reminiscent of the real-fluid curves in Figure 22. Notice that the curves at –165 and –241°F are chosen to intersect and follow the saturation curve, yielding interesting results that will be reviewed later.

Finally, the upper and lower graphs of Figure 25, page 58, are analogous to Figure 21 and are based on the expansion arrows shown the top portion of Figure 24. Here again, the dotted curves reflect the TNT equivalency of the portion of the real fluid remaining in a venting vessel. The solid curves track the TNT equivalency remaining in the vessel's whole

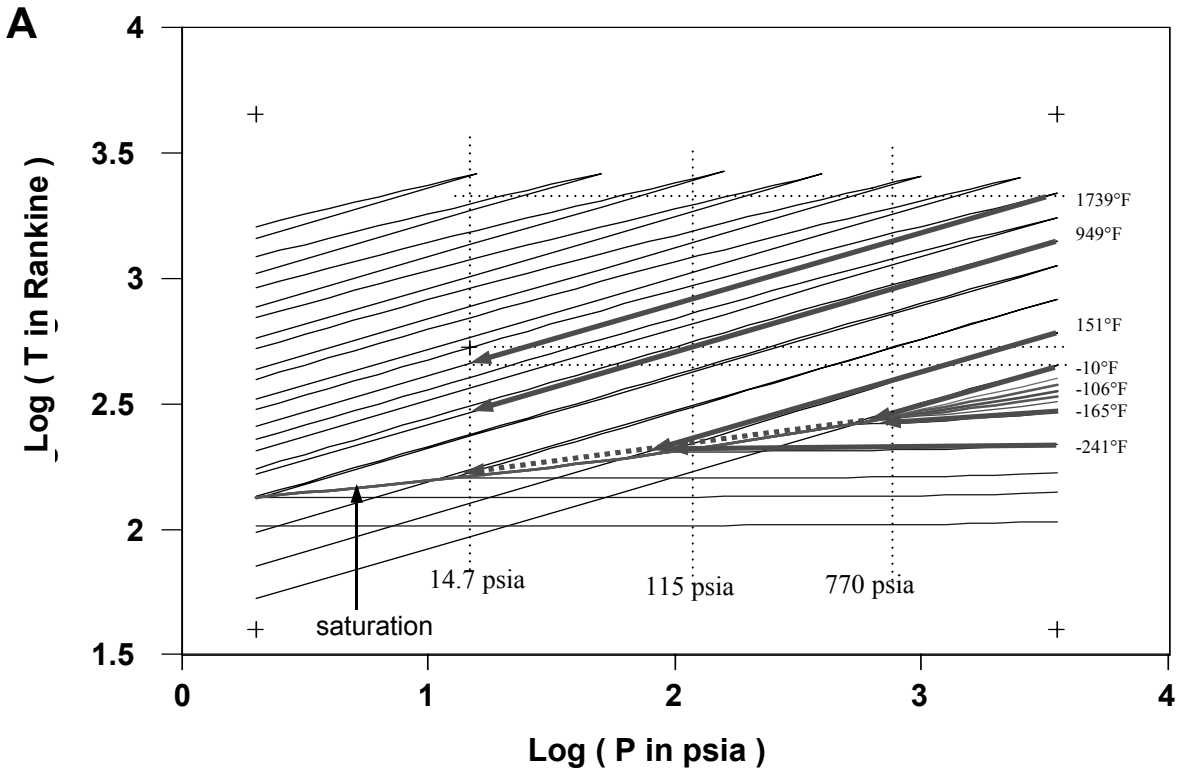

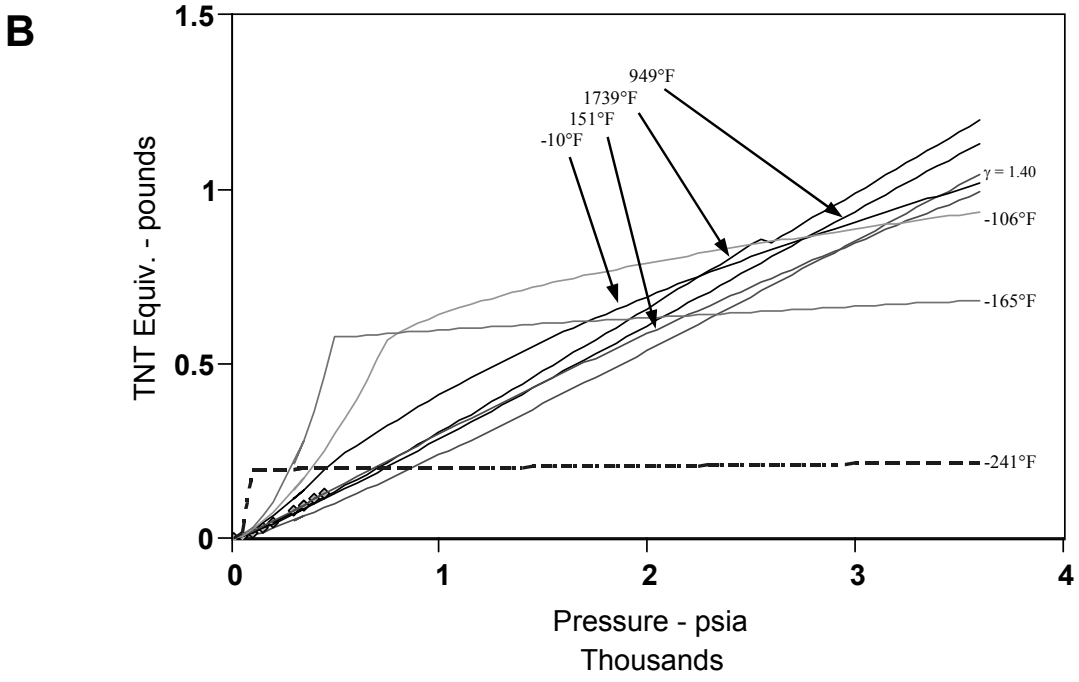

FIG. 24—*Real-Oxygen TNT Equivalency Versus Pressure From NIST12 DB.*

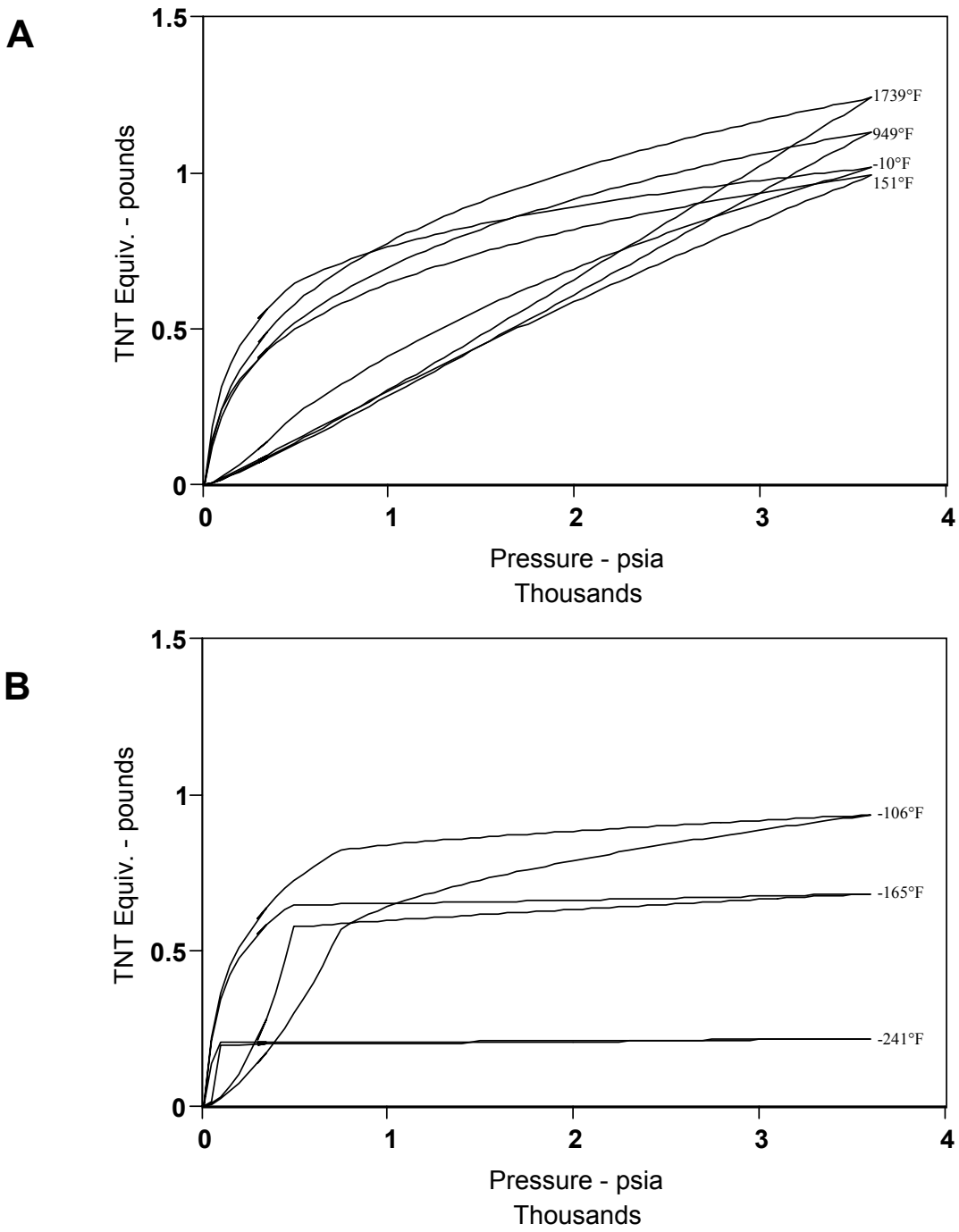

FIG. 25—*Real-Oxygen TNT Equivalency Versus Pressure From NIST12 DB.*

initial charge of adiabatically expanding fluid. Therefore each point reflects a different decreasing pressure, decreasing temperature and increasing volume of a constant mass.

The upper graph, "A", of Figure 25 depicts four of the real oxygen curves from Figure 24 for the energy in the fluid remaining in a vessel and presents the energy remaining in the initial 3600 psia slug of gas as in Figure 21. As in Figure 21, we see that at the higher temperatures and pressures, the TNT equivalency yet to be released at each pressure is highly variable and again this calculation suggests the greatest fraction of energy is released at the later stages of expansion and at the lower pressures. The lower graph, "B", of Figure 25 depicts the remaining three lowest temperature curves at or below saturation from Figure 24 along with the calculation for the fluid remaining in the initial high pressure slug for each. The –106°F starting condition is in the supercritical hybrid transition triangle and ultimately passes through the critical temperature at a little under a thousand psia. The two lower curves start as liquids and intersect the saturation curve from below and then follow it. Here again, a major portion of the internal energy change, which is treated conservatively as being part of the TNT equivalency results from expansion of the flashing liquid.

Is Saturated Fluid Wimpy?

Some may be tempted to terminate a TNT equivalency calculation when the gas has expanded to the point where it intersects the saturation curve on the basis that the gas and its pressure is collapsing into liquid (assuming a collapsing PdV). These calculations would oppose that method.

We have seen that when the initial temperature is high, the real gas curves are not too dissimilar to the ideal gas curves. However when the initial temperature is near or below room temperature and the pressure is high, there is a bend that occurs in the equivalency when the pressure is high enough to produce condensation of the fluid during its expansion. Very significantly, notice that even when the initial temperature is low, (Lo! Even to the point of beginning to expand, to "flash", as a saturated fluid), there is still an appreciable amount, in some cases relatively large amount, of expansion and expansion-energy and heat release remaining.

Indeed, throughout industry, there is a common safety practice, the hydrostatic pressure testing of vessels, in which a vessel is filled with water which is then pressurized. This is considered much safer than pressurizing with a gas because the water is presumed incompressible and therefore contains very little PV energy (little TNT equivalency). If the vessel bursts, the water expands only slightly, there is no great explosion nor fast flying fragments that follow.

Saturated liquid (liquid near the boiling point), however, is much more different than room temperature water. It is less energetic, and perhaps less "angry" than gas in some ways, but if these calculations are correct, it is by no means wimpy in terms of its energy content. Indeed, in industry, vessels that have failed while containing saturated fluids have exhibited significant energy releases.

The writer has always noticed an extreme respect for the explosions produced by steam

boilers. Perhaps so much so that there is a separate vessel code just for them. Indeed, several decades ago, when there was a flurry of interest in steam powered automobiles (to cope with many of the same global issues still being debated today), the danger of an angry boiler explosion was often cited as a major fear.

The writer has heard of several incidents where vessels containing pressurized liquids or (near or fully) saturated fluids produced surprising energy releases. Two involved cryogenic fluids at relatively low pressures that failed. One involved a large vessel under hydro test. In each case, it was surprising how the fragments and systems that failed were was sent flying. Details are too scant to attempt elaboration.

However there is a class of saturated-fluid vessel rupture that is sufficiently common to have produced research and to have been assigned an acronym—BLEVE. It bears consideration even in this withering section. The BLEVE (Boiling Liquid Expanding Vapor Explosion) has been a common event, thanks to the wide use of liquid-filled saturated propane vessels. But BLEVEs are possible with many other fluids also, whether the fluids are flammable or not.

In the most spectacular, even awesome, cases propane-filled railway cars have been damaged and leaked and fires have heated them, elevating the saturated fluid even possibly to the critical point and beyond, to where the vessels burst, yielding a blast wave and a stunning mushroom-cloud fireball.[10] Perhaps the best known case of this mechanism is the famous video taken during the Waco, Texas massacre of 1993, in which the burning building apparently contained a tank of propane for home heating and it burst producing a blast and massive mushroom fireball.

The writer is inadequately knowledgeable at present to surmise and describe how the PV energy in a vessel (whether it is a gas or liquid or saturated fluid) is converted into a shock wave (a potential subject of value to OSPs). Does all of the energy in the style of Becker [***26, 27***] run up to the shock front. If so, would the energy from flashing and expanding saturated fluid do the same? This is a primary concern in abrupt adiabatic fluid expansion. Nor can the writer analyze here how PV energy launches fragments, a secondary but

[10] The root of the acronym BLEVE is unknown to the writer. Prior to the vessel's rupture the liquid within it may be marginally boiling, but the vapor is not expanding, (it is more likely compressing and forming elevated pressure) nor is such *a-priori* boiling necessary to produce the final result which could just as easily come from simple mechanical vessel failure During the rupture, the vapor is expanding, but the liquid is no longer being heated and boiled in the most common sense (boiling taken here as a slow heat transfer process), and it is in fact cooling (absent combustion). The later mushroom cloud may contain liquid and any combustion may be boiling it, but the explosion aspect is then greatly diminished. However the writer would suggest that during the actual burst, when the blast wave is formed, the liquid is experiencing adiabatic cooling and what industry refers to as "Flash"—the liquid is converting suddenly and violently into gas and vapor as a result of adiabatic expansion and cooling and pressure decay, and as analyzed here, is adding the heat lost in cooling to sustain and protract pressure and enhance blast intensity and disperse the remaining fluid as a result. Therefore the writer would be inclined to adopt the acronym FLEVE (Flashing Liquid, Expanding Vapor Explosion) as a perhaps more precisely descriptive term for these events.

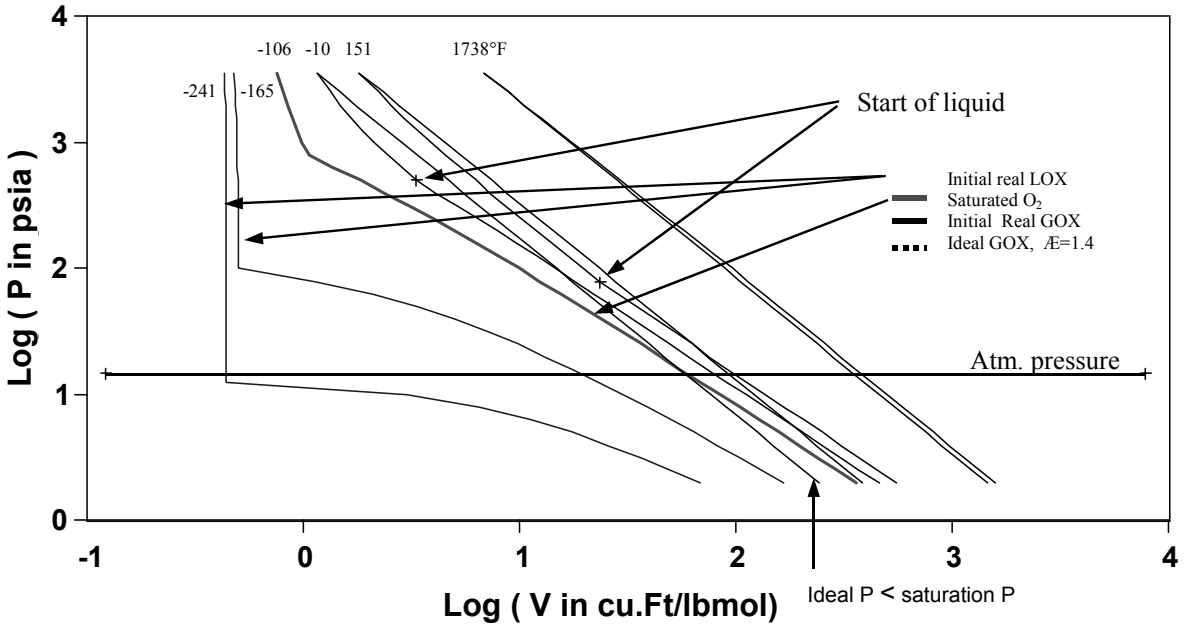

FIG. 26—*Real-Oxygen Adiabatic Temperature Versus Pressure From NIST12 DB.*

still very important safety concern, but is aware from experience that even pressurized water can provide an impressive launch. However, in the spirit of caution, he would tend to assign all of the energy considered in this section to the TNT equivalency. He would not terminate TNT equivalency calculations, including ideal gas calculations, at the saturation curve on the basis of collapsing pressure at that point. Indeed, the calculations here indicate that the PV energy release and release rate does not collapse at that point, —— perhaps counter-intuitively, *they may often increase*.

This point can be illustrated with a convenient observation. Recall from the earlier review that the PV energy in an expanding fluid is inverse to it adiabatic exponent (see page 49, Figure 17). Pressure-for-pressure, argon (γ~1.6) has less TNT equivalency than oxygen (γ~1.4), which has less TNT equivalency than nitrogen trifluoride (γ~1.16). If one examines the two ideal-gas expansion arrows for the upper graph, "A", of Figure 24 (initial 151°F and –10°F), one can see where ideal gas would intersect and pass into the saturation (boiling point) curve. Notice that at this point a bend occurs in the arrow to follow the saturation curve and represents a *decrease* in m_{TP} slope, corresponding to a *increase* in the m_{PV} and $-\gamma$, slopes for Figure 7 (becoming less negative). This indicates the rate of $\int$PdV energy release is *increasing*. Since the ideal gas extension passes through and projects below the saturation curve as in Figure 24, the PV area under it will be less than is under the corresponding portion of the real saturation curve. This point may be so significant that the region of lower pressure for ideal gas (lowest dashed curve) for the initial –10°F gas are illustrated on a PV diagram in Figure 26 and at

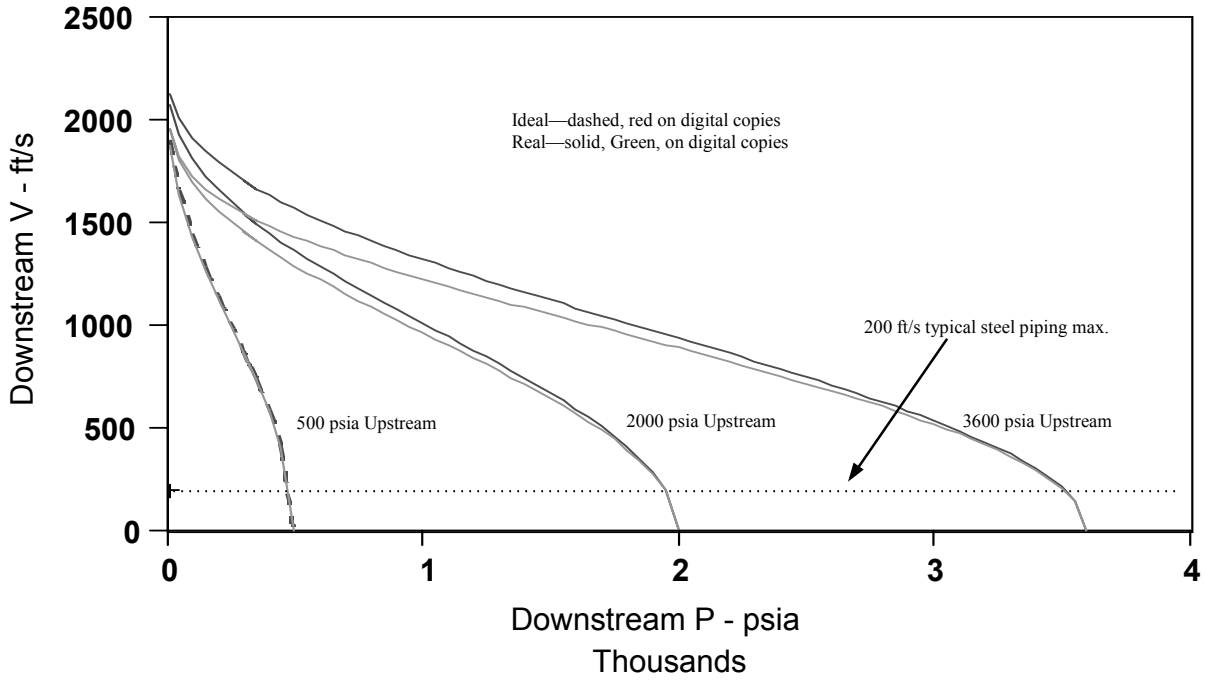

FIG. 27—*Maximum Velocities from Ideal Oxygen and Real Oxygen from NIST12 DB*.
(Upstream stagnant at 70°F.)

higher expansions (larger volumes) lie under the saturation curve which implies that ∫PdV for the ideal gas is less than for the saturated fluid..

Figure 26 is selected curves from Figure 7. One can see how after liquid starts forming the real-fluid curves ultimately intersect the ideal gas curves after which the PV integral contribution for further expansion will be larger than for those ideal gas expansions.

Other astute analysis may fine-tune this analysis or find outright flaws in it, but it was presented here in this painful detail because the writer is not aware of its review in any other oxidant, or other, safety reference.

Maximum Achievable Velocities

Maximum achievable velocity calculations take the static potential energy as pressure in a fluid and convert it into kinetic energy in a fluid stream. Appendix B presents the details of making such estimates.

Figure 27 exhibits the maximum velocities possible from several starting pressures of oxygen as both ideal gas (dashed lines based upon Equations B8 and B9 in Appendix B) and real gas (solid lines) based upon data from NIST databases. In most systems velocities greater than sonic will not actually occur, but they are possible when all the conditions are correct.

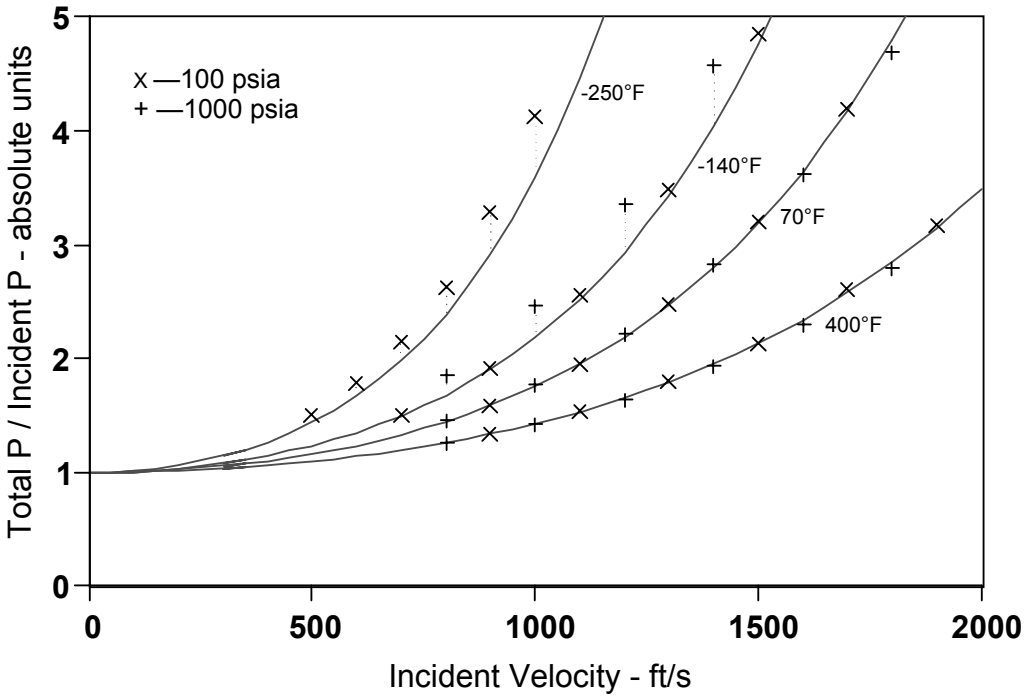

FIG. 28—*Total (Stagnation) Pressures from Ideal and Real Oxygen from 2007 NIST12 DB.*

In most cases, oxygen systems operate with allowed velocities up to 200 ft/sec. When very specific fire-resistant materials are used, velocities at and even above sonic may obtain. For all of these curves up to the 200 ft/sec velocity, the difference between real and ideal gas is negligible. Even in those cases where sonic or greater velocities might obtain and where highly fire-resistant material would normally be used, the difference indicated between real and ideal gases is fairly small.

Total Pressure Calculations

Total pressure calculations consider a moving gas stream and convert the kinetic energy into static potential energy as pressure. Maximum achievable velocity calculations are the inverse of total pressure calculations which take the static potential energy present as pressure in a stagnant gas and convert it into equivalent gas velocity. Appendix B presents the details of such estimates.

Figure 28 exhibits the total or stagnation pressures possible from several starting incident velocities up to several thousand feet per second of oxygen as both ideal gas (dashed lines) and real gas (shown as "x" and "+" symbols) per the NIST12 DB. Ideal-gas curves are shown for four initial, incident gas stream temperatures (400°F, 70°F, -140°F, and –250°F). The ordinate portrays the ratio of total (stagnation) pressure to the initial incident pressure. All four of

these curves cover incident velocities at levels up to and beyond the initial speed of sound.

Remember! The real speed of sound at atmospheric pressure for these four temperatures per the NIST12 DB is 1352.624 ft/s (at 400°F), 1071.534 ft/s (at 70°F), 832.0652 ft/s (at -140° F) and only 669.7030 ft/s (at –250°F).

In these cases, we see that the real-oxygen data at 100 and 1000 psia fit the ideal curves nicely for the ideal gas model at 400°F and 70°F . The real-oxygen data at 100 psia fit the ideal gas model curve nicely at –140°F but at 1000 psia, the data are close to what this tutorial has called the supercritical hybrid transition region ("supercritical triangle") and show some divergence. The real-oxygen data at 100 psia are starting to diverge from the ideal gas model curve at –250°F which at 1000 psia is very close to the saturation (boiling point) condition, and yet the error even here is not large. There are no data points shown for 1000 psia incident pressure at –250°F, because the fluid is a liquid at this condition.

By and large these estimates indicate the ideal gas model is adequate for approximating oxygen at the traditional piping conditions (near room temperature and at pressure to about 1000 psia) and in fact would be adequate for temperature ranges much larger than are usually used.

Oxidants Other than Oxygen

Oxygen is not the only oxidant nor even fluid that is of interest. ASTM Committee G-4 has frequently[11] expressed a desire, nay a earnest intent, to address other similarly oxidizing chemicals such as fluorine, nitrogen trifluoride, nitrous oxide, ozone, and others. A small sampling of papers addressing these other oxidants in various degrees has infiltrated the G-4 symposia [***28-31***], but to the writer's knowledge, none has addressed adiabatic processes.

Three of these oxidants (fluorine, nitrogen trifluoride and nitrous oxide) are also covered in the NIST12 DB, NIST23 DB and/or NIST Internet "WebBook" DB. These are all heavier and larger molecules than oxygen and that makes them interesting in an academic fashion as well as a practical regard, because their specific heats and, therefore γ and M_{TP} values, should be much different from those of oxygen. However, there are far fewer data available with regard to minimum ignition temperature and, even more so, ignition energy for these other materials. Therefore, only a quick overview of them, as an intended beginning, is also included here, and it focuses specifically on compression/expansion and related heat transfer behavior rather than TNT equivalencies, total pressures, distance/volume pieces, and gas velocities. All of these may prove good material for future review. These compression/expansion data are also present in the related PC algorithm.

[11] The writer is a charter member of ASTM G4. In its thirty-plus year history he recalls perhaps a half dozen efforts to branch out into other oxidants. Each effort was usually transient. A few papers resulted or some language was made more generic in some standards. A re-commitment in the mid-2000s to this noble goal was accompanied by some industry-sponsored experimental work on NF_3, but has again proven to be slow-going..

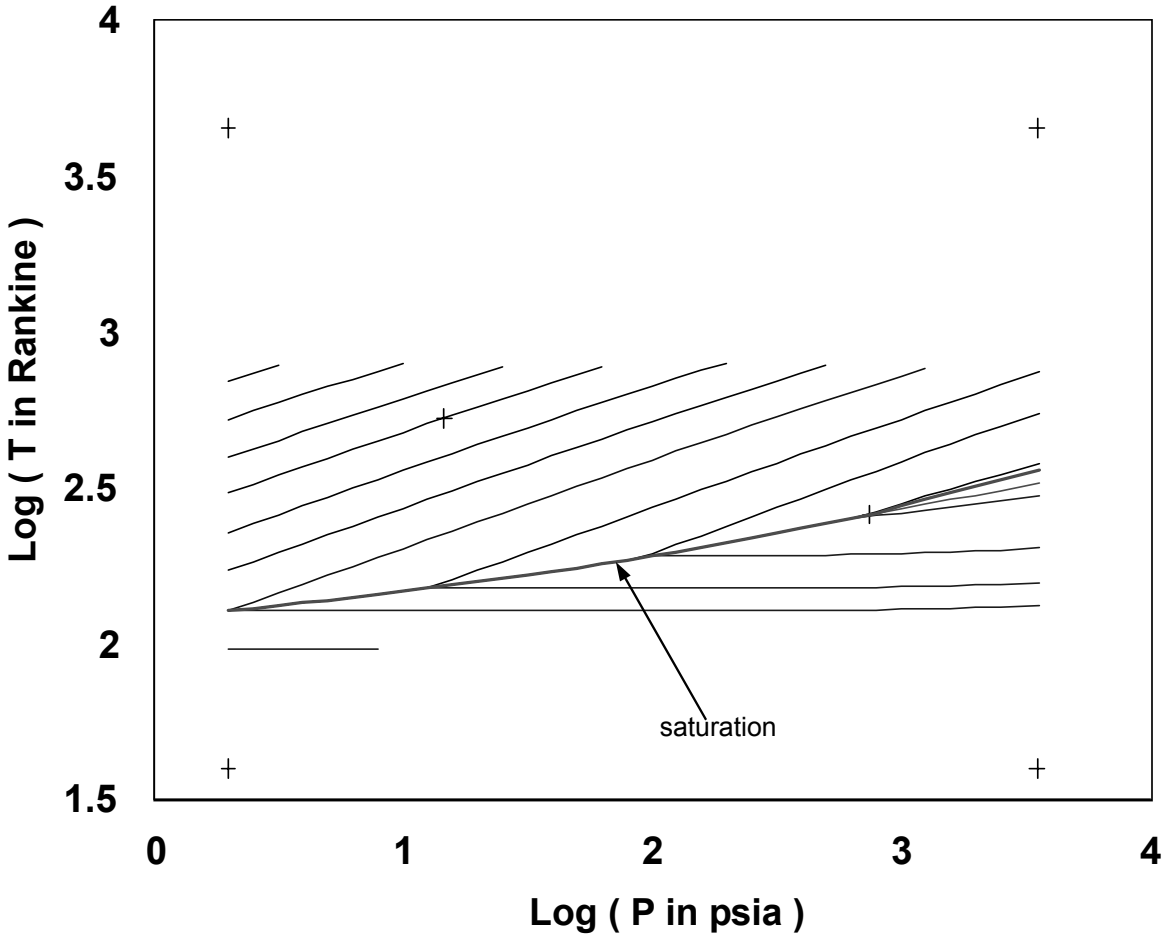

FIG. 29—*Real-Fluorine Adiabatic Temperature Versus Pressure From 2007 NIST12 DB.*

Fluorine

Fluorine (F_2) is a more oxidizing oxidant than is oxygen itself. F_2 is known for reacting with some materials even at room temperature and the heat release is greater [***29***] than for oxygen. Little is published about heat of compression of fluorine and this may in part be due to fluorine being commercially shipped at pressures only to 400 psig in the U.S. Although 400 psig in a large-molecule gas like fluorine having high specific heat will produce much lower final temperatures than were seen with oxygen, the much lower ignition energies validate continued concern for adiabatic compression ignition.

A log/log plot of temperature and pressure is shown in Figure 29 as predicted by NIST12 DB. A copy of this graphic is included in the Adiabat.exe and adiabat32.exe algo-

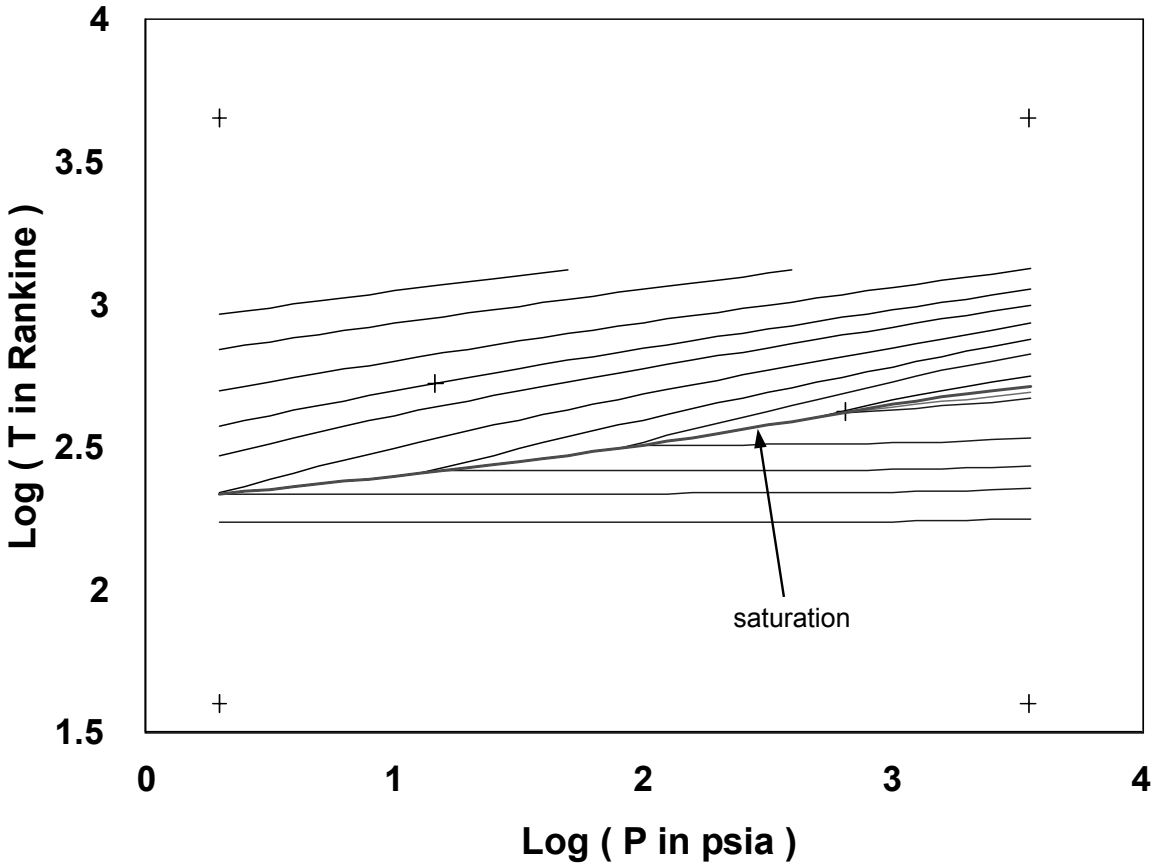

FIG. 30—*Real-Nitrogen Trifluoride Adiabatic Temperature Versus Pressure From 2007 NIST12 DB.*

rithms. It exhibits the straight-segment character and other features of Figure 4 and can therefore be treated similarly.

Nitrogen Trifluoride

Nitrogen trifluoride (NF_3) is more difficult to describe than fluorine [***29***]. It is very oxidizing in terms of reaction heat release, but has for a long time enjoyed a reputation for being more easy to work with (less angry) than fluorine, a perspective that is becoming less persuasive in more recent years.

Although NF_3 is less much aggressive than fluorine on first contact, it is more interesting in an adiabatic compression regard because it is available in higher pressure cylinders at pressures up to at least 1450 psia. It is also a still larger molecule than fluorine (triatomic versus diatomic) with a larger heat capacity. Again there is not a large body of ignition temperature data and especially ignition energy data to consult. NF_3 is depicted for isentropic compression

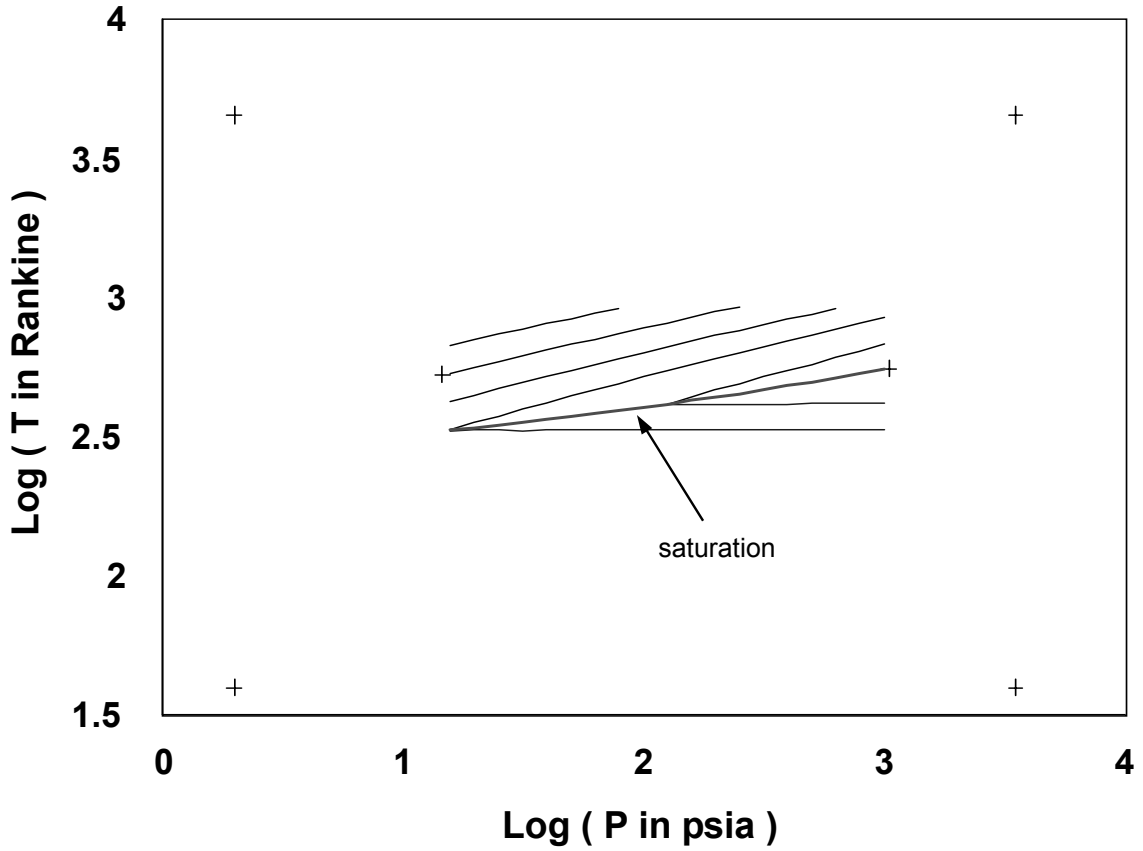

FIG. 31—*Real-Dinitrogen Oxide (N_2O) Adiabatic Temperature Versus Pressure From 2007 NIST WebBook.*

as predicted by NIST12 DB in Figure 30. Again, as for fluorine, it exhibits the straight-segment character and other features of Figure 4 and can therefore be treated similarly.

Nitrous Oxide:

Nitrous oxide data were not included in the NIST12 DB nor NIST23 DB (in 2007), but data were available for a narrow range of conditions (as dinitrogen oxide) on the NIST Webbook (http://webbook.nist.gov/chemistry/fluid/). The webbook was not as full featured as NIST12 and NIST 23 DBs and approximate isentropic values were manually extracted to prepare Figure 31. It appears that in 2016 the current NIST 23 DB does include nitrous oxide.

Like nitrogen trifluoride, nitrous oxide is triatomic and its room temperature atmospheric pressure values of γ and m_{TP} are smaller than for oxygen. Being triatomic, its heat capacity is larger than for oxygen and so it does not achieve as high a temperature for any corresponding compression. However, because of its potential exothermic decomposition, adiabatic

compression can ignite and even detonate N_2O (even in the absence of polymers and contaminates) at relatively low temperatures (below 1000°F) [***32***]. And when ignited its heat of decomposition is large (TNT equivalency of about 0.4 [***25***]). This produces a second hazard mechanism that the designer must cope with.

Again, as for F_2 and NF_3, it exhibits the straight-segment character and other features of Figure 4 and can therefore be treated similarly.

Diluents

Diluent gases are not well defined. The writer has struggled recently to produce an overview of diluents (including proposing a definition) for a future paper/tutorial. However, in the writer's view diluents are not synonymous with inerts (though they include inerts). Nor are they necessarily synonymous with situationally nonreactive chemicals (though they include situationally nonreactive chemicals, too). In comparison to oxygen and the oxidants cited here, argon, helium, nitrogen, carbon dioxide, and carbon tetrafluoride would all be considered diluents in at least most circumstances, even though they are not all inert nor nonreactive.

Argon

Although argon (Figure 32) is commonly thought of as a rather innocuous (inert) diluent in a fire regard (it, like many diluents, has an insidious asphyxiation hazard), it is in fact a seriously important gas with some of the most subtle of fire hazards. Indeed, this writer used the fire-aggravating nature of argon as the punch line for a presentation on fire limits in the early 2000s[12]. As a result of that subtlety, the fire hazard of argon, like its asphyxiation hazard, is similarly insidious. Argon can cause fires when and where one might least expect them.

Argon is not significantly oxidizing, it can be considered nonreactive under most circumstances (but not every last one). Argon is as well studied as oxygen and its data (Fig. 32) are in both the 2007 NIST 12 and NIST 23 DBs. It is available at extremely high commercial pressures.

Argon is a monatomic molecule with a low specific heat, hence its values of γ and m_{TP} are larger than for oxygen, and this makes it atypical (along with helium and a few others gases). Argon is a large atom and that lends a low thermal conductivity to it that distinguishes it from the other monatomic molecule, helium, that is reviewed here.

Adiabatic compression/expansion of argon is depicted in Figure 32 for isentropic processes as predicted by the NIST12 DB. A copy of this graphic is included in the Adiabat.exe and adiabat32.exe algorithms. Once again,, as before, it exhibits the straight-segment character and other features of Figure 4 and can therefore be treated similarly.

Most of the importance of argon, as with most of the diluents here, is in mixture with

[12] In the early 2000s the writer proposed his FLLAME (Fire Limits for Linearly Afflicted Minds, Everywhere) approach to analyzing fire limits, in which he argues that argon exhibits "fire limit" behavior (both lower and upper limits) in some situations even though it is inert.

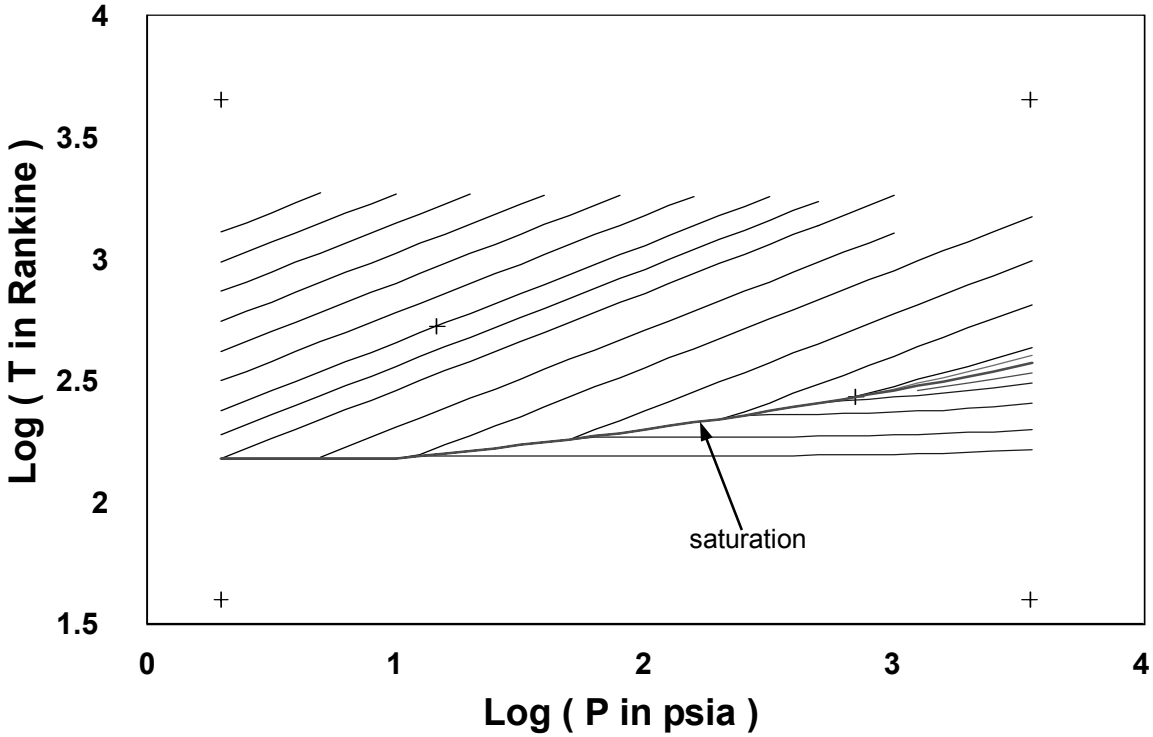

FIG. 32—*Real-Argon Adiabatic Temperature Versus Pressure From 2007 NIST12 DB.*

oxidants. In the writer's world view, the serious OSP does not appreciate the adiabatic compression hazard sufficiently until that OSP appreciates the adiabatic subtleties of argon.

Helium

Helium (Fig. 33) is similar to argon in important ways and differs in important ways. Like argon, helium is also often thought of as innocuous but can circumstantially exacerbate some fires. It is also a monatomic molecule but is a small molecule of low heat capacity and high thermal conductivity. The high thermal conductivity apparently causes the rate of combustion after ignition to accelerate in many polymers. It has low heat capacity and consequently higher values of m_{TP} and γ than for oxygen but very similar to those for argon and lead to similar large adiabatic heating and cooling.

Figure 33 exhibits adiabatic process data for helium. These data proved somewhat challenging for the writer to tease from the NIST databases, frequently failing to converge to values over portions of several curves and leaving gaps (that are easy to extrapolate) in them. A copy of this graphic is present in the associated PC algorithm. Once again,, as before, it exhibits the

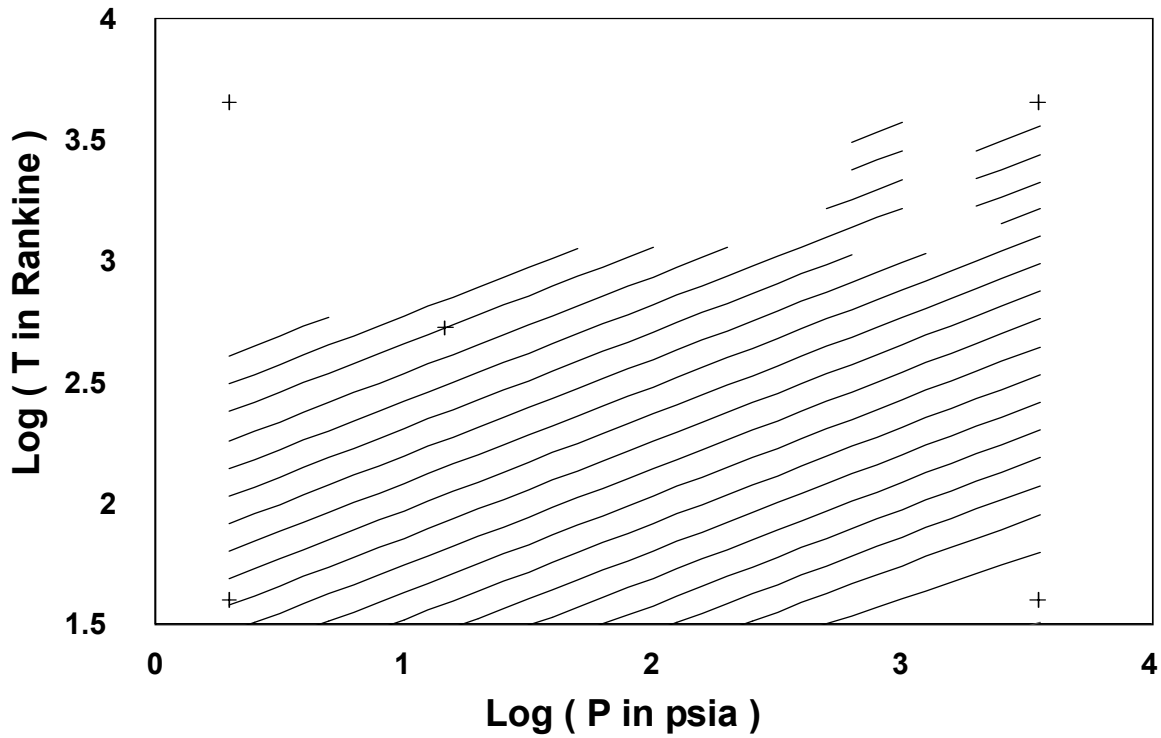

FIG. 33—*Real-Helium Adiabatic Temperature Versus Pressure From 2007 NIST12 DB.*

straight-segment character and other features of Figure 4 and can therefore be treated similarly.

Nitrogen

Nitrogen (Fig. 34) can be a reactive factor in the combustion of some metals, and routinely reacts in the combustion of gases (to produce often toxic products like NO, And NO_2) but to a large extent is not very reactive in many instances, especially where combustion with polymers is concerned.

Figure 34 exhibits adiabatic process data for nitrogen. Nitrogen properties are very similar to oxygen (both are diatomic and have similar mass and heat capacity) and so its adiabatic processes are very similar. Its saturation curve is close to that of oxygen over the range depicted. But its high temperature adiabatic exponent is slightly larger. Therefore compression of atmospheric-pressure room-temperature fluid to 3600 psia yields 1738.5°F for oxygen but 1885.5°F for nitrogen. Curiously the NIST 12 DB projects compression processes for nitrogen to higher temperatures than for oxygen, and so the nitrogen data that are shown here are extended to higher temperatures. A copy of this graphic is included in the adiabat.exe and adiabat32.exe algorithms. Once again, as before, it exhibits the straight-segment character and other

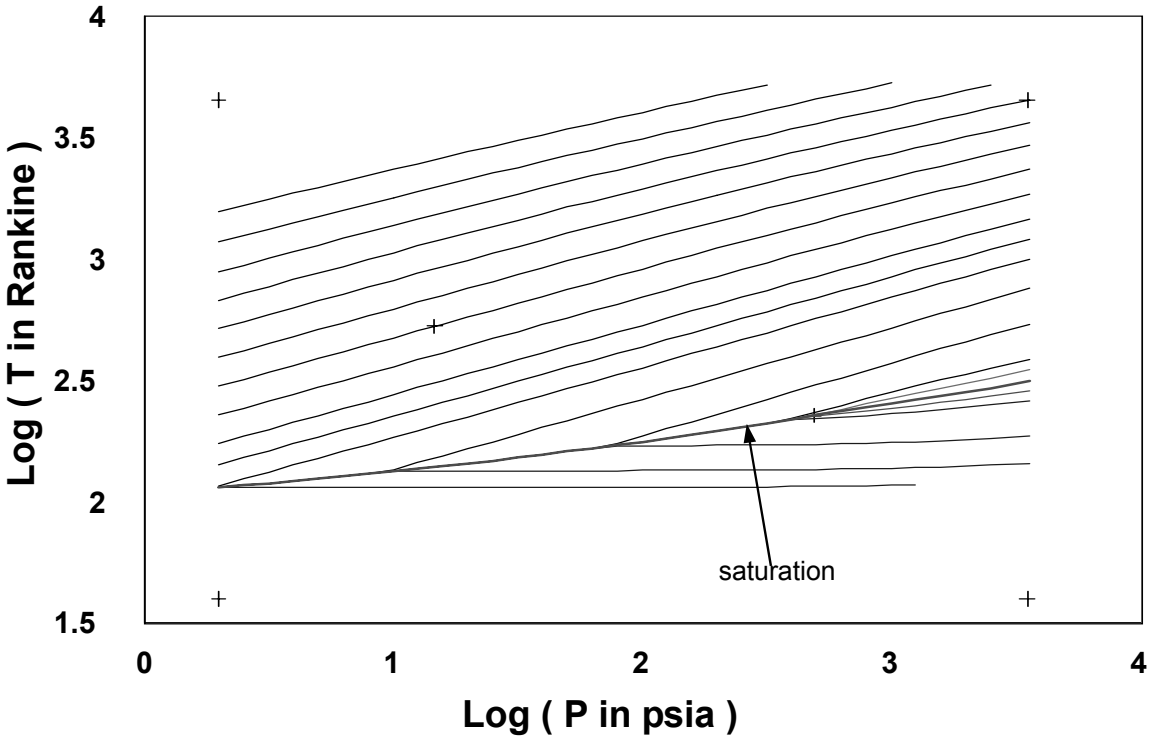

FIG. 34—*Real-Nitrogen Adiabatic Temperature Versus Pressure From 2007 NIST12 DB.*

features of Figure 4 and can therefore be treated similarly.

Carbon dioxide

Carbon Dioxide (CO_2), Fig.35, is a triatomic molecule, meaning higher mass and larger heat capacity, therefore smaller $-m_{PV}$ and γ. It is saturated with oxygen and so is non reactive in combination with many materials (excluding some metals). This means smaller slope to the adiabatic curves. It also means that carbon dioxide in mixture with oxygen would tend to reduce flammability and to be less likely to produce temperatures likely to lead to ignition.

Adiabatic processes for carbon dioxide are shown in Figure 35. The curves have the low expected slope and low peak temperatures. The mapped region from the NIST 12 DB is small, because carbon dioxide has a fairly high boiling point (-109°F) at atmospheric pressure and indeed a portion of its triple point curve appears on the plot and is indicated. A copy of this graphic is included in the adiabat.exe and adiabat32.exe algorithms. Once again, as before, it exhibits the straight-segment character and other features of Figure 4 and can therefore be

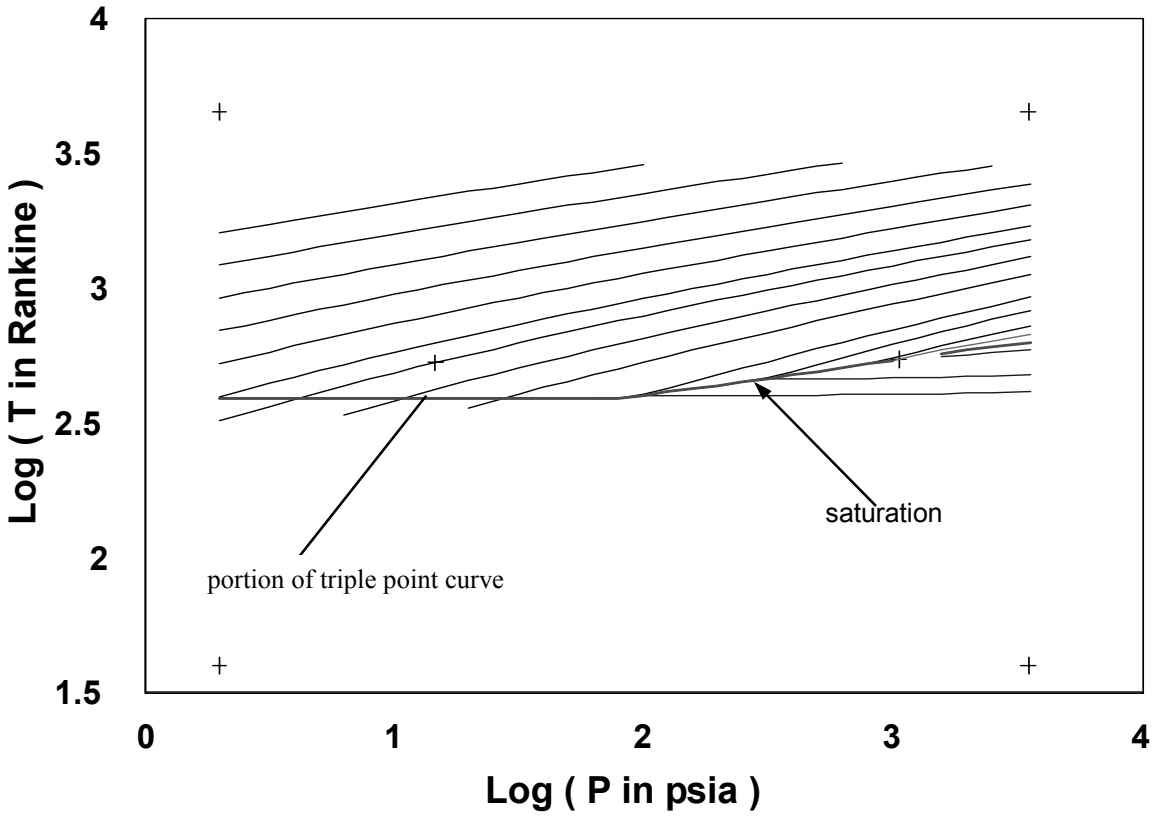

FIG. 35—*Real-Carbon Dioxide (CO_2) Adiabatic Temperature Versus Pressure From NIST12*

treated similarly.

CF_4

Carbon tetrafluoride (tetrafluoromethane, CF_4), Fig. 36, is the largest diluent molecule shown here. It has five atoms in its molecule that yield a high heat capacity and mass and therefore less adiabatic heating and smaller slopes to it m_{TP} curves. As for all the fluids shown here, its adiabatic curves are rather straight, allowing for the use of local m_{TP} or γ parameters.

Adiabatic process curves for CF_4 are exhibited from 2007 NIST 23 DB as Figure 36. It has a normal boiling point mid-way between carbon dioxide and oxygen (-198.5°F). A copy of this graphic is included in the adiabat.exe and adiabat32.exe algorithms. Once again,, as before, it exhibits the straight-segment character and other features of Figure 4 and can therefore be treated similarly.

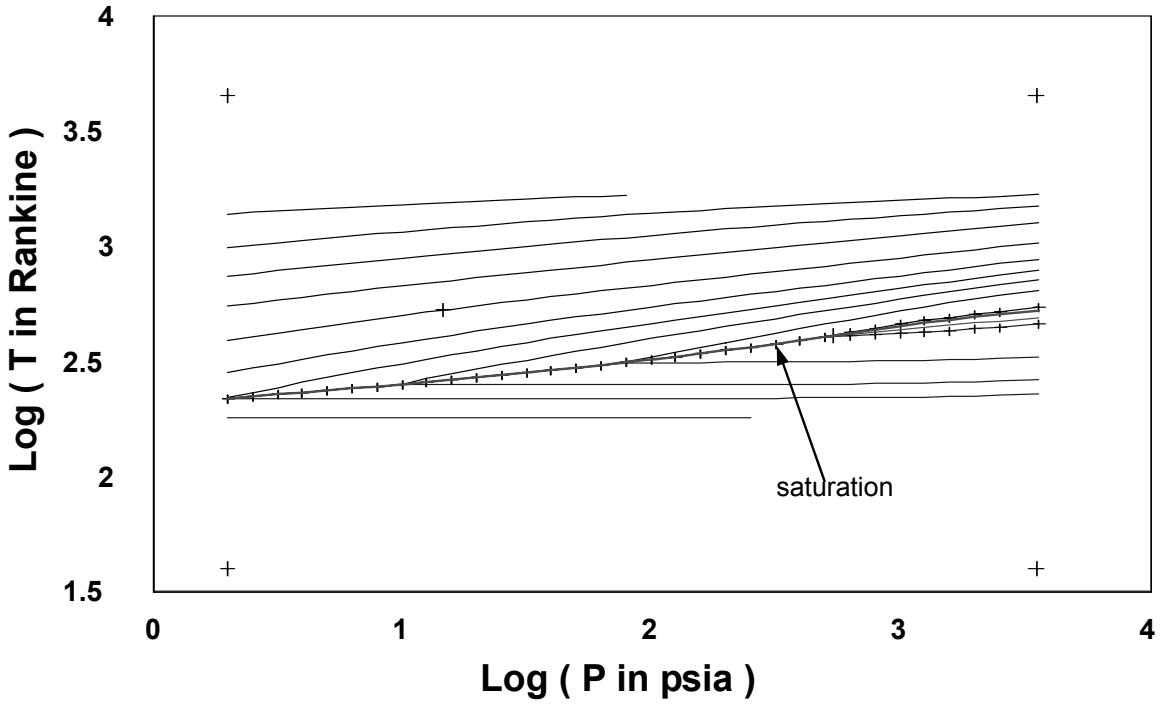

FIG. 36—*Real-Tetrafluoromethane (CF_4) Adiabatic Temperature Versus Pressure (From 2007 NIST23 DB).*

Mixtures of Gases

Oxidants are frequently used in mixtures, and often the reason for the mixtures is to moderate their reactivity. Sufficient diluent may shift the mixture across a fire limit (the oxidant index) into nonflammability, But it may also shift it the other way into flammability. It may slow (but may also accelerate) combustion rates when fire is possible, and it may reduce (but may also sometimes increase) the ability to ignite and/or burn. This section will focus exclusively on adiabatic processes related to mixtures.

Systems employing air or oxygen-enriched air are in widespread use. Oxygen in mixture with helium is widely used for breathing gas systems. Some bulk fluorine is delivered in mixture with diluents. And in general, whenever an inert gas or nitrogen is mixed with an oxidant, it is usually taken as reducing the demands on the system for compatible materials. *But this is not necessarily always the case*. NASA treats high pressure air in some cases as equivalent to oxygen in fire risk, and one could reasonably argue (and some have) that air at some high pressure situations might be a greater hazard than are some lower pressure oxygen systems.

The writer has made a campaign (unsuccessfully to date) out of promoting the analysis of fire limits as a project within ASTM G-4, (and to lesser extent, a few other places, too), and as noted earlier in this tutorial, the punch line for that earlier campaign is the way that argon can increase the hazard and fire potential of certain gas mixtures. There are scenarios in which the

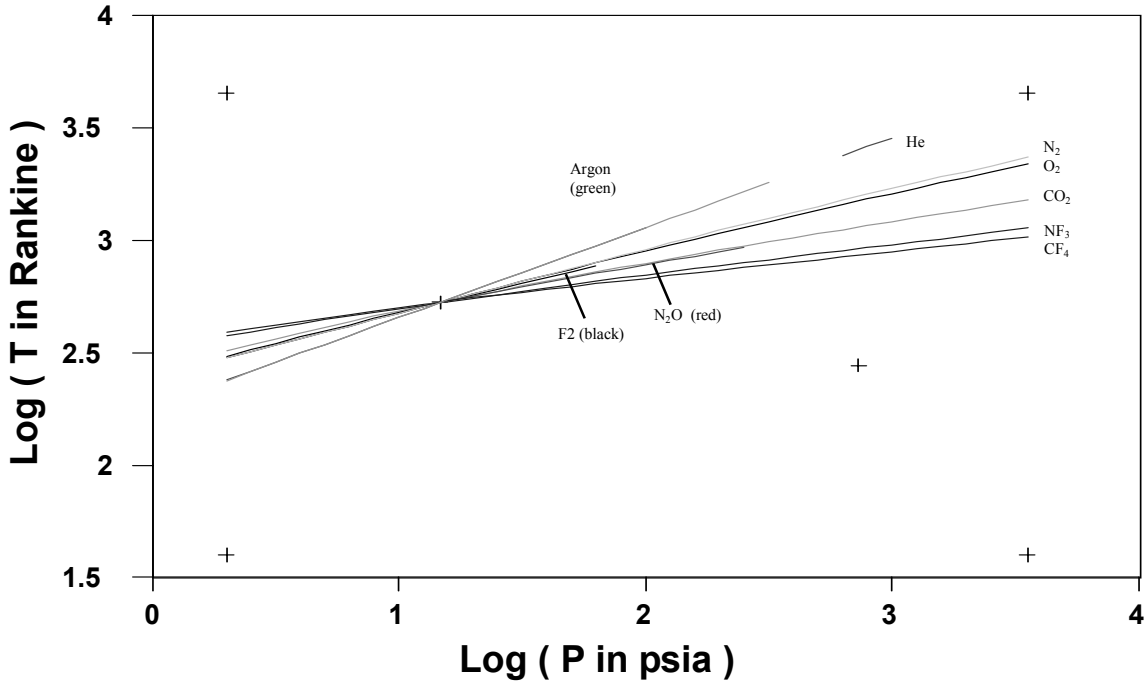

FIG. 37—*Real Adiabatic Temperature Versus Pressure for Several Fluids Starting at Room Temperature, Atm. Pressure (From NIST12 DB, NIST 23 DB and NIST WebBook).*

addition of argon to a constituent gas stream in some processes can shift the mixtures from being safely *outside* a fire limit to being dangerously *inside* a fire limit.

It is also this same way with adiabatic processes as well, and it is for related reasons. The NIST23 Database allows for replicating several of the adiabatic-process calculations performed so far for mixtures of oxygen (and only oxygen) with several nonoxidant gases. Several gas mixture combinations will be examined starting with perhaps the most interesting case: oxygen/argon. However, NIST 23 allows for the analysis of only a few combinations, and some of the possible combinations can be queried to only limited final pressures in some cases.

Figure 37 recapitulates a capsule of how the pure diluent gases behave in adiabatic processes compared to oxidants using data from both NIST 23 and NIST 12. Note that monatomic gases such as argon and helium in particular heat much more quickly and to higher levels than any of the oxidants shown, but the data do not extend to similarly high final pressures. However, if one assumes that a law similar to Dalton's Law of Partial Pressures applies, one then could form linear combinations of the behaviors of real fractions independently and combine them. Would such an approach be valid as an approximation? One could also extrapolate the fairly straight lines, and because the noble gases are the most nearly ideal in behavior, the extrapolations would probably be fairly valid for them in particular. A copy of this graphic is in-

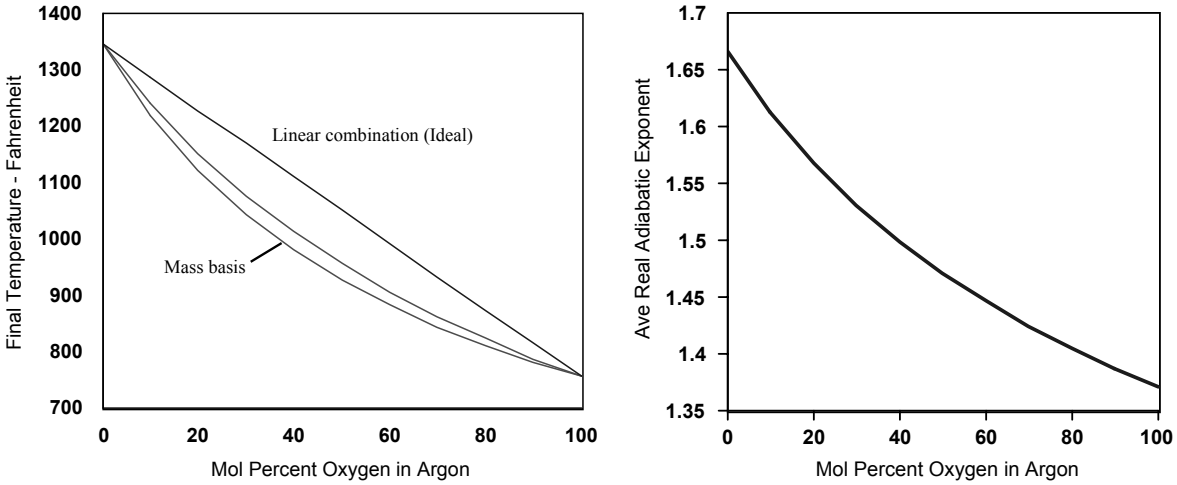

FIG. 38—*Real-Oxygen/Argon Mixtures Adiabatic Temperature Versus Composition From NIST23 DB*. (Initial Atmospheric pressure, 70°F, to 316 psia Final Pressure).

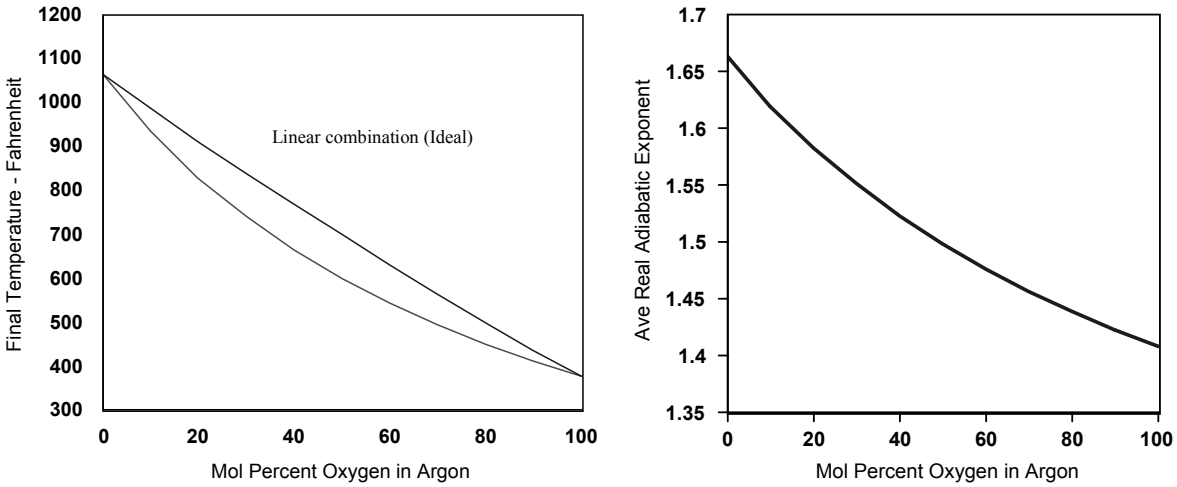

FIG. 39—*Real-Oxygen/Argon Mixtures Adiabatic Temperature Versus Composition From NIST23 DB*. (Initial Atmospheric pressure, -290°F, to 3600 psia Final Pressure).

cluded in the adiabat.exe and adiabat32.exe algorithms.

Oxygen/Argon Mixtures

Figure 38 exhibits data from the NIST 23 database for peak temperatures that result from compression of mixtures of oxygen with argon. This figure portrays oxygen/argon mixtures compressed from room-temperature atmospheric-pressure conditions to 316 psia, because 316 psia is approximately the highest pressure for which the database calculates a final

argon temperature relative to these starting conditions. Figure 39 depicts a corresponding compression from –290°F, 14.7 psia to a final pressure of 3600 psia, because NIST 23 estimates final temperatures for both pure oxygen and argon to 3600 psia for this starting condition and as is seen on Figures 4 and 32, both of the pure-gas compression properties are fairly ideal for this compression (that is, both "adiabats" are rather straight). Also shown on the curves are "ideal" analogs for which an adiabatic exponent was estimated as a linear combination of the argon and oxygen average adiabatic exponents, $-m_{PV}$, in proportion to the mole fraction present.

To the right of the curves are the approximate average adiabatic, $-m_{PV}$, exponents that apply. These curves exhibit a curvature similar to that in the temperature curves and to each other.

Using either the NIST real-oxygen/real-argon data or the "ideal gas" estimates, both show that adding argon to oxygen increases the final temperatures produced during compression. The more diluent argon added, the higher the temperature, and in some cases, the greater the risk of ignition. If the argon fraction is sufficiently high, it may thwart propagation, or it may slow resulting combustion. However, for those cases where the final compressed mixture is above the *in-situ* oxidant index for an exposed material, an incident might result (might be *caused*) by the presence of argon.

Figure 40 shows how the full adiabats would look in comparison to the 25, 50 and 75 percent mixtures. One can surmise how much error would result in these two cases by assuming linearity in the estimates. Such rough estimates are fairly easy to accomplish with the related PC utility algorithm, for those comfortable enough with this material to infer the potential error in any such estimates.

Oxygen/Nitrogen Mixtures

Figure 41, page 78, exhibits data from the NIST 23 database for peak temperatures that result from mixtures of oxygen with nitrogen. This figure portrays oxygen/nitrogen mixtures compressed from room-temperature atmospheric-pressure conditions to 3600 psia, because 3600 psia can be calculated for a final nitrogen temperature relative to these starting conditions. Also shown on the curve are "ideal" analogs for which an adiabatic exponent was estimated as a linear combination of the nitrogen and oxygen average adiabatic exponents in proportion to the mole fraction present. Notice that the endpoint adiabatic exponents differ by much less than in the oxygen/argon example and the curvature present is less.

To the right of the temperature curve are the approximate average adiabatic exponents that apply. These curves again exhibit a curvature similar to that in the temperature curve.

Using either the NIST real-oxygen/real-nitrogen data or the "ideal gas" estimate, both again show that adding diluent nitrogen to oxygen increases the final temperatures produced during compression (albeit much less than for argon). The more diluent nitrogen added, the higher the temperature, and in some cases, the greater the risk of ignition. If the nitrogen

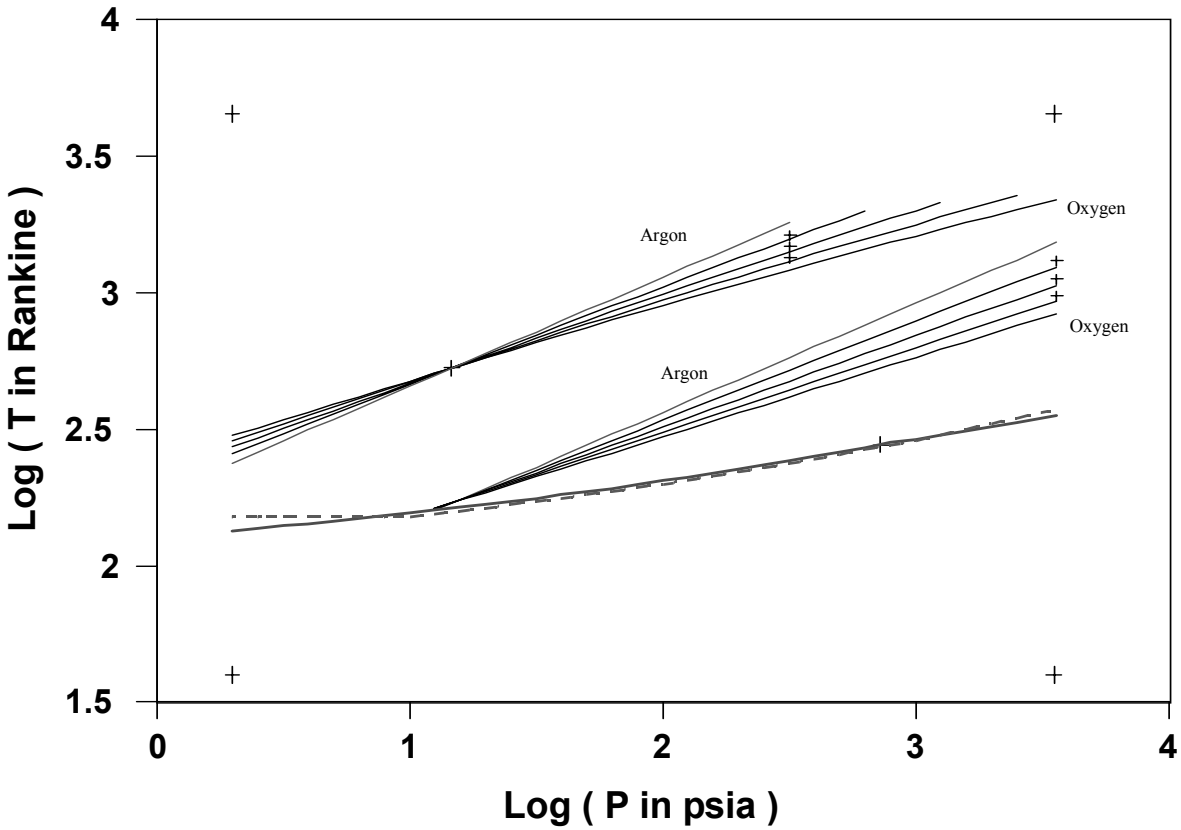

FIG. 40—*Real-Oxygen/Argon Mixtures Adiabatic Temperature Versus Composition From 2007 NIST23 DB*. (Initial Atmospheric pressure, -290°F or 70°F , to Max. Reported Final Pressure).

fraction is sufficiently high, it may thwart propagation, or it may slow resulting combustion. However, if the mixture is above the *in-situ* oxidant index for an exposed material, an incident might result (might be *caused*) from the presence of nitrogen .

Oxygen/Carbon Dioxide Mixtures

Figure 42 exhibits data from the 2007 NIST 23 database for peak temperatures that result from mixtures of oxygen with carbon dioxide. This figure portrays oxygen/CO_2 mixtures compressed from room-temperature atmospheric-pressure conditions to 3600 psia, because 3600 psia can be calculated for a final nitrogen temperature relative to these starting conditions. Also shown on the curve are "ideal" analogs for which an adiabatic exponent was estimated as a linear combination of the carbon dioxide and oxygen average adiabatic exponents in proportion to the mole fraction present. Notice that the endpoint adiabatic exponents differ by much less than in the oxygen/argon example, the curvature present is less, and the slope of the line is positive in the direction of diluent addition rather than negative.

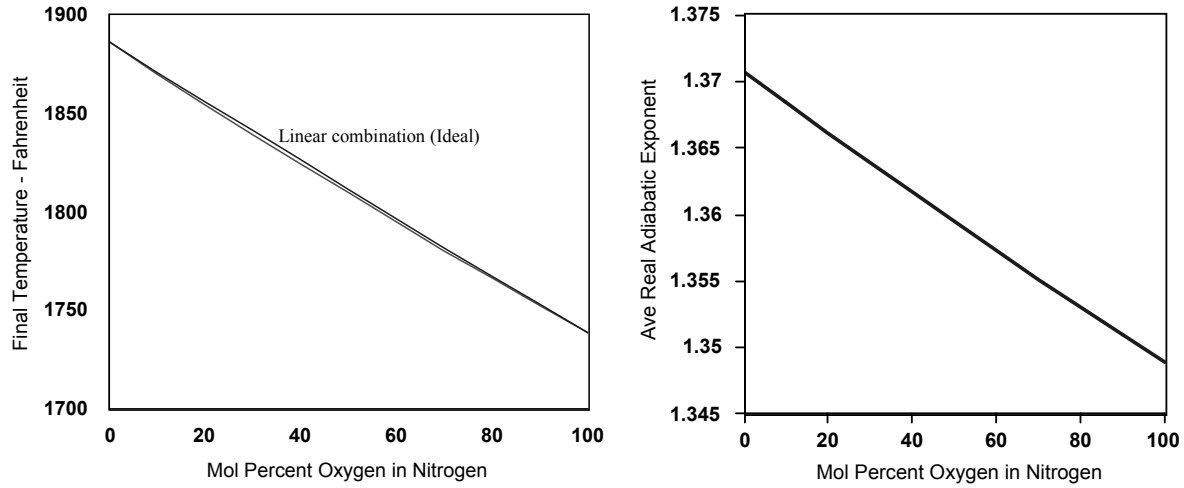

FIG. 41—*Real-Oxygen/Nitrogen Mixtures Adiabatic Temperature Versus Composition From NIST23 DB*. (Initial Atmospheric pressure to 3600 psia Final Pressure).

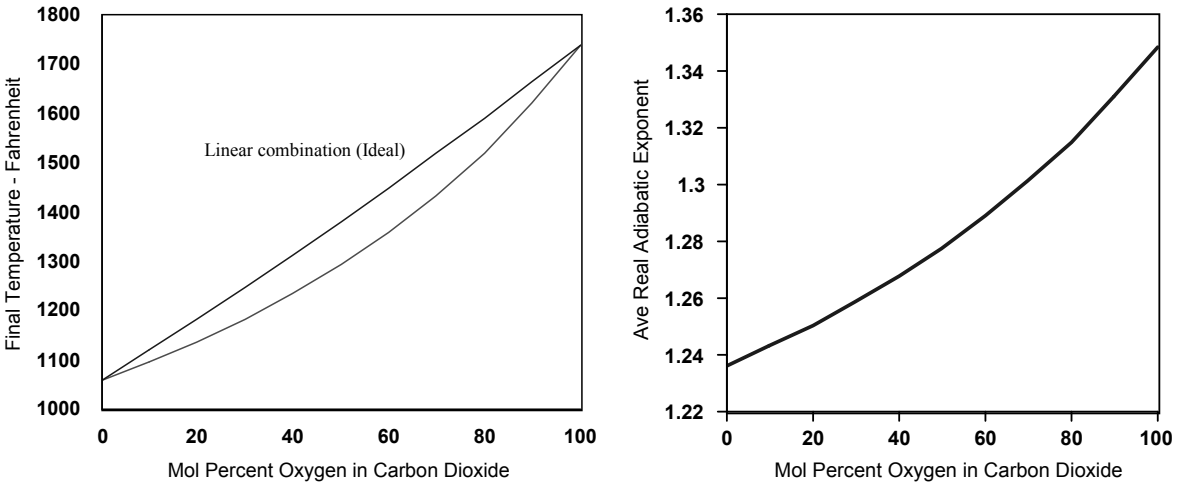

FIG. 42—*Real-Oxygen/CO_2 Mixtures Adiabatic Temperature Versus Composition From NIST23 DB*. (Initial Atmospheric pressure to 3600 psia Final Pressure).

To the right of the temperature curve are the approximate average adiabatic exponents that apply. These curves again exhibit a curvature similar to that in the temperature curve.

Using either the NIST real-oxygen/real-CO_2 data or the "ideal gas" estimate, both again show that adding diluent carbon dioxide to oxygen decreases the final temperatures produced during compression. The more diluent CO_2 added, the lower the final temperature, and in some cases, the lesser the risk of ignition. If the CO_2 fraction is sufficiently high, it may thwart propa-

gation even in the presence of ignition, or it may slow resulting combustion. However, if the presence of CO_2 in the mixture shifts the fire-limit outside the *in-situ* oxidant index of any exposed material, then an ignition and incident might be prevented by the presence of CO_2.

Heat Transfer Revisited

The immediately prior section explored adiabatic compression of a range of gases and focused on final temperature. A critical part of the overall story however, is heat transfer. We have seen that other oxidants and diluents compress differently than does oxygen. This leads to differing final predicted temperatures during adiabatic compression, and in some cases mixtures with oxygen lead to higher final predicted temperatures than would obtain for pure oxygen. By this time, the reader should be champing to know what happens to heat transfer with these other gases and even more importantly what happens when they are in mixture with oxygen.

When a gas slug is compressed into a dead end, it may fill the dead end to overflow such that heat losses to the compressing gas upstream can be ignored. In this case, it is possible that the lowest initial pressure, which usually (but maybe not always) yields the highest final temperature can be the worst case scenario. However, when the slug is on the order of the dead end volume, loses to the compressing gas and upstream can affect the cooldown rate. In this case a higher initial pressure with its greater mass in the final slug can be a more severe case despite a lower final temperature, because it can transfer more heat to a target material.

In the earlier case when the hotter slug cools, its will ultimately pass through the same pressure and temperature as is present in the cooler more massive slug.

When one is varying the gas composition, it is not only the final temperature and pressure but the thermodynamic properties (heat capacity, thermal conductivity) of the fluid itself that are important. One's interest is in the heat transfer that will occur for the same initial and final pressures as concentration is varied but also in how the initial pressure affects the result.

Figure 43, exhibits, the maximum heat transfer that will be possible from several real fluids adiabatically compressed to 2300 psia from varying initial pressure. The data are from the 2007 NIST 12 database. The gases shown are oxygen, helium, carbon dioxide and nitrogen trifluoride. The heat transfers are in the same order for maximum heat transfer at or above 400° F and at or above 800°F. Helium provides the greatest, followed by the larger oxygen molecule, then the still larger carbon dioxide molecule and finally the largest nitrogen trifluoride molecule. For compression from atmospheric pressure, helium transfers about 20% more heat at 400°F as at 800°F (about 42 versus about 35 BTU/cu ft). Oxygen transfers a little less than twice as much heat (about 25 versus 15 BTU/cu ft). Carbon dioxide transfers about three times as much heat (about 18 versus about 5 BTU/cu ft). And nitrogen trifluoride transfers no heat at or above 800°F but transfers about 10 BTU/cu ft at or above 400°F

Helium exhibits its greatest heat transfer at or above 400°F at about a 200 psia initial pressure (about 95 BTU/cu ft) and at or above 800°F at about a 75 psia initial pressure (about 55 BTU/cu ft). Oxygen is less effective at heat transfer and exhibits its greatest heat transfer at or above 400°F at about a 125 psia initial pressure (about 50 btu/cu ft) and at or above 800°F at

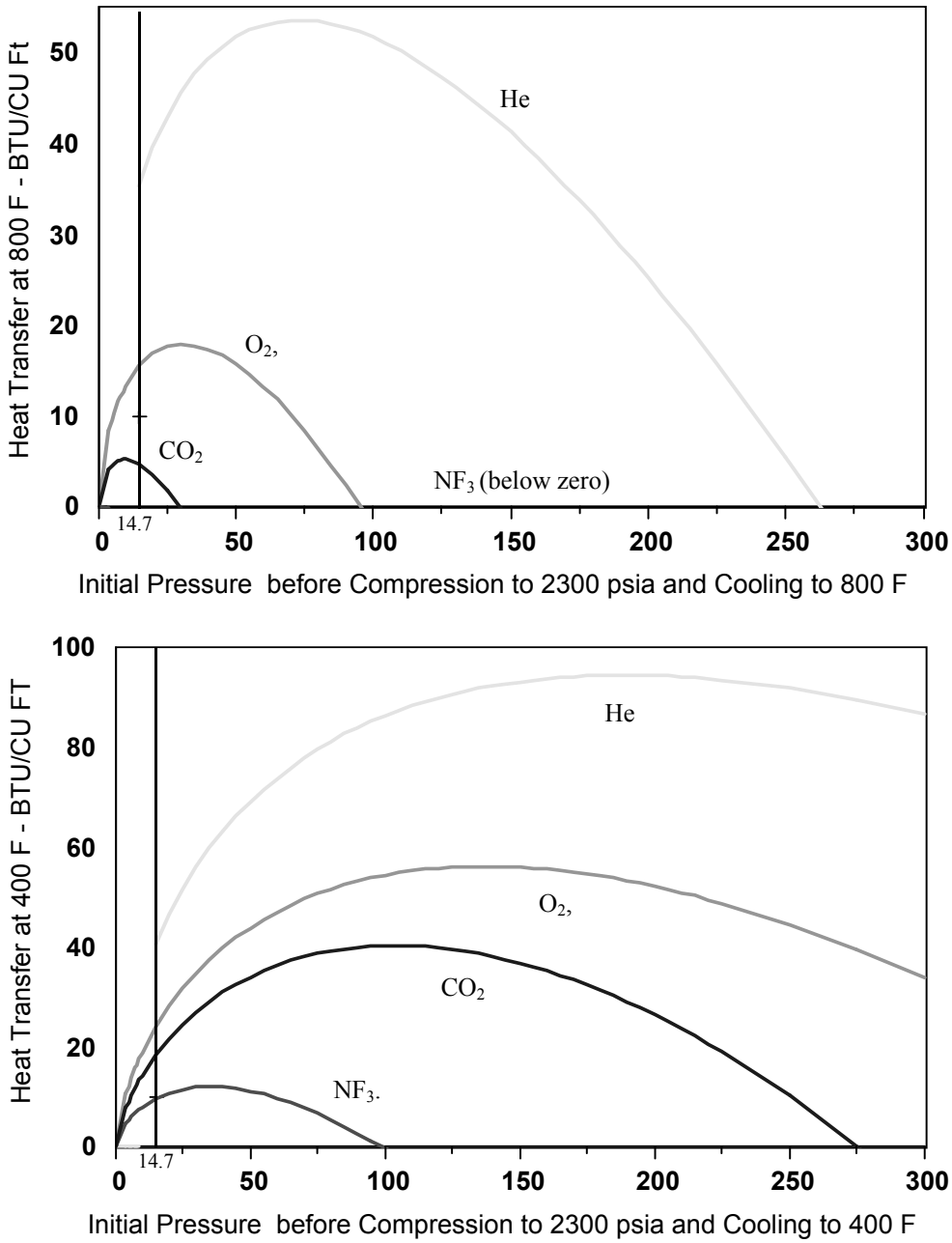

FIG. 43—*Real Transfer Revisited for Four Fluids: O_2, He, CO_2, and NF_3.*

about a 30 psia initial pressure (about 17 BTU/cu ft). Carbon dioxide is still less effective at heat transfer and exhibits its greatest heat transfer at or above 400°F at about a 110 psia initial pressure (about 35 BTU/cu ft) and at or above 800°F at about a 10 psia initial pressure (about 5

BTU/cu ft). Notice that this last maximum is below normal atmospheric pressure, and in this case *a lower initial pressure produces a curious higher heat transfer*. The maximum for nitrogen trifluoride at or above 400°F at about a 30 psia initial pressure (about 10 BTU/cu ft).

Previously we saw that mixtures of oxygen with diluents produced peak temperatures intermediate to the temperature rises for the individual pure gases. Therefore not only do mixtures affect the final temperatures possible but they affect the heat transfer possible, and as noted before, this influence begs for further study.

Additional and Exotic Issues

Shock waves

This tutorial, as for two earlier incarnations [***6,7***], ducks the issue of shock waves and to a lesser extent supersonic flow. Among the fastest pressurizations possible are those that occur upon exposure to a shock wave (which may literally happen in microseconds and micro-inches). Their speed should certainly serve to minimize heat loss, but there are other things happening that may also be important. Unfortunately, shock waves are not a routine topic in past ASTM Committee G4 publications, but there are valid reasons for that.

Among the few mentions of shock waves is that of Janoff et al. [***33***]. In it, adiabatic compression tests of PTFE-lined hoses are reported. The interior of the hoses was videoed during the compression and a flash was observed that is attributed to shock ionization, but the authors report that the hose lengths were too short to have experienced fully developed shock waves. They always noticed the flash dissipated before any evidence of flame was seen.

In another report, Ducrocq et al [***34***] examine how shock waves and shock-tube effects may affect ASTM adiabatic compression tests.

Shock waves are possible but rare occurrences in most oxygen systems. They are scrupulously avoided and tend to occur only during upsets, failures, or incidents. Nor does there appear to be a simplified reference that addresses key shock wave properties from the perspective of the OSP. Alas, the writer has found none to date that simplify the issues sufficiently for his own intellect.

If the writer has time, an attempt to produce a simplified tutorial on shock wave and supersonic pressurization would be a favorite goal of some priority. Perhaps an older reference can be found (before the theory became heavily mathematical) that would provide better insight. Perhaps examining them from a kinetic theory perspective would help. At present he is skeptical that their significance is as great as one would be inclined to fear, but he has little beyond macro-opinion to base that upon. However, he is greatly troubled that laboratory test systems go to extremes to produce the fastest pressurization possible (understandably to produce the most adiabatic, therefore worst case, temperature conditions), when in the real world most oxidant system fires result from simple and even fairly slow manual opening of valves.

Two examples to support the cited macro opinion will be cited. The previously mentioned tests of PTFE hose [***33***] reported at NASA's White Sands Test Facility produced ignitions and video records exhibited a significant delay (difficult to estimate with high speed pho-

tography) to the writer's recollection. The pressurization produced some system trauma but then the system settled down and after the delay, numerous spots of illumination (fires) followed. This (if conveyed correctly) might be more consistent with a soaking ignition at temperature than a flash ignition in a shock wave. In this case one would long to see how the system might behave under a slightly slower pressurization that was still fast enough to approach adiabatic conditions. Indeed, in this old series of work, the tendency to ignite increased when the downstream tube diameter was increased which would lead to a greater "classical" likelihood of ignition and perhaps a less likely stress by shock waves.

A horrible complication would exist if some materials were more shock sensitive and other were more "slow" sensitive, but the writer can not rule this prospect out.

Scanning a short series of references [***19, 35-37***], it appears that shock waves exhibit a number of interesting behaviors:

- Shock waves are possibly the most extreme form of nonequilibrium system that could be experienced. Local temperature and pressure can vary widely, indeed "local" may mean over the previously cited microinches and microseconds.
- Shockwaves "sharpen". When a large fluid pressure wave propagates, the leading portion will tend to become an "edge" and will tend to exhibit an extremely abrupt increase in differential pressure. The "sharpness" of the edge, its abruptness in differential pressure, initially increases with time and travel.
- They can impact surfaces (and perhaps other shock waves) and reflect and deflect producing primary shock waves and secondary reversion waves, the latter of much reduced pressure and seriously different behavior.
- During impact they can sweep away the present fluids in something called expansion waves. A previous effort [***5***] likens them to tidal waves.
- They can be focused to interact with each other (apparently leading to increased pressure due to multiplied density but perhaps not nearly as greatly increased temperature).

The G 4 collegium would benefit from a series of simplified analyses of shock wave and supersonic flow to simplify and debunk any errors in this summary. However there is a bottomline of sorts that can be proposed for consideration. If shockwaves (as is the case for supersonic flows) are important, then the OSP community approach should perhaps not be to test and select materials to resist it, but rather should be to thwart it. Shock waves (like supersonic flows) are unique and special. They form only under the most favorable conditions or when truly brute force is applied. Instead of designing to endure them, perhaps a series of design thwarts should be formulated and should seek to figuratively and literally "cut" shock waves down to size.

Computational Fluid Dynamics

Computational Fluid Dynamics (CFD) Software has been applied to several analyses published in the ASTM G4 collegium [***9,34,38***]. More are sure to follow. It has been used in industry for perhaps a couple decades and is coming into wider use as software competition and more economic pricing evolves. However, as of today it is still expensive and specialized and not easy to do. Many OSPs will not be in a position to employ CFD software for some time. The writer is nearly perfectly unfamiliar with this software, but will attempt to comment and pose questions anyhow.

CFD software offers great promise and challenge. In actual adiabatic compression heat transfer can play a significant role. Formation and reflections of shock waves and supersonic flows are another key variable not addressed by the analyses in this tutorial, and factoring them into CFD analysis would be a boon if indeed that is not the case today.

But, just as the treatment of adiabatic compression through the years has employed generalizations that were not precise (and which this tutorial has sought to put some of them into a better perspective), the limits and capabilities of CFD software also needs a perspective.

So many textbooks on fluid mechanics consider the ideal gas, constant heat capacity model that the writer would first ask if CFD software does the same. This tutorial argues there is a great benefit to using the same equation form as for ideal gas, constant specific heat (IGCSH) analysis but of employing the variables m_{TP}, m_{TV}, and m_{PV}. If CFD software employs the IGCSH model, can different values of gamma be specified? There can be important differences between ideal and real gas. Do CFD software packages address real gas in any of their analyses?

This tutorial focuses on whether a low starting pressure is more severe than the higher starting pressure depending on system dimensions. Can CFD software address this issue?

Fines (particles) should be very sensitive to shockwaves and may be produced by them. Can CFD software predict when contamination will be mechanically removed from a surface and dispersed in the hot final oxygen slug (something that would make them very sensitive to ignition and may have been present in one series of rapid pressurization tests of contaminated systems [***39***]).

So What? — Proposed Wisdom and Judgment

As noted in the introduction: "The book on rapid compression and expansion is not closed." Much analysis has been presented here and the way has been pointed for much more. Today, the prudent design of an oxidant system is more in the realm of wisdom and judgment than in precise engineering calculations. If one were to read this tutorial, what key items might be worth retaining for future use (should these analyses survive scrutiny)? In this same spirit, the writer will propose a number of "insights" that one might wish to keep in back of mind when considering oxidant hazards.

- Ideal gas calculations with an assumed adiabatic exponent, γ, of 1.4, have been and remain sufficiently accurate for the many common oxygen system evaluation including:
    - Predictions of final temperature from the adiabatic compression of room-temperature, atmospheric-pressure oxygen.
    - Predictions of required temperature controlling DVP volumes for any practical conditions
    - Predictions of gas velocities at low differential pressures.
    - Predictions of stagnation pressures from normal gas velocities.
- The use algorithms such as the withdrawn G4Math Version 1.2 still appears valid and slightly conservative for each of its common uses with oxygen gas.
- When the above calculations are needed for oxygen at uncommon or extreme pressures and temperatures, or when the behavior of other fluids at common or uncommon conditions is of interest, calculations based on software such as the NIST12 and NIST23 databases may provide the necessary real-fluid predictions but at the price of some degree of complexity.
- For uncommon or extreme conditions, a coarse perspective on the behavior of real fluids (oxidants and diluents) and mixtures can be had with high-definition log-log plots extracted from databases, and a simple algorithm (such as adiabat.exe and adiabat32.exe) can help with the reading of such plots. Such diagrams give a empirical perspective on the behavior of the fluid that would be difficult to achieve with the use of ideal gas models, with or without compensating corrections, and can be learned and employed without an advanced theoretical underpinning.
- At common, uncommon or extreme conditions for a wide range of oxidants and diluents, empirical variables, m_{TP}, m_{TV}, and m_{PV}, may be most preferred for real fluid calculations, short of using actual database queries. Plots and databases are sources for the use of m_{TP}, m_{TV}, and m_{PV} . In general, however, they are preferable to γ , and their use can maintains much of the simple equation structure that is present in ideal gas, with less manipulation than compensating of specific heats, or solution of complex equations of state (which even in the case of the NIST databases may sometimes fail to converge to a numerical answer).
- Inert gases (inherently inert or situationally inert) as well as similar diluents are not always innocuous as is often assumed. Especially in the case of argon, diluting oxidants can lead to a rare but important increased risk. In some cases a lot of argon may be good while a little argon may be bad.
    - As for most low γ fluids, Argon diluent increases the final compression temperature and may also increase the heat transfer to a target material.
    - For most large γ fluids, dilution of oxygen decreases the final compression temperature and may also decrease or increase the heat transfer to a target material

- Low initial pressures lead to relatively higher final compressed temperatures.
- Higher final pressures lead to relatively higher final compressed temperatures.
- Final compression temperatures are rather well behaved (following an approximately exponential equation) even for low initial pressures and even at low initial temperatures as low as the boiling point (saturation) condition.
- High final temperature may lead to material ignition if in excess of the *in-situ* ignition temperature *and if sufficient heat transfer (above the in-situ min energy for ignition) also occurs* for the oxidant concentration present.
- Higher initial pressures can lead to higher heat transfers up to an optimum pressure above which higher pressure leads to lower heat transfers.
- High heat transfers can lead to material ignition if in excess of the *in-situ* minimum ignition energy, *and if sufficient temperature is also present* for the oxidant concentration present
- Ideal fluid approximations of heat transfer during adiabatic compression are good estimates of real gas behavior at most common conditions, and would lend themselves to a simple algorithm. At extreme conditions further study is indicated.
- Heat transfer subtleties may account for "fickleness" in some kinds of oxidant incidents and should always be evaluated.
- When TNT equivalency is equated to the fluid internal energy change, ideal gas estimates are practical for only a few mechanical TNT equivalency calculations, notably those for very elevated temperatures. Real gas calculations are probably preferable in many cases where final temepratures occur at or below room temperature, especially where any degree of approach to the fluid's saturation condition or actual condensation of the fluid may occur.
- Fluids at the boiling point or saturated condition can contain significant amounts of internal energy that may be released in a depressurization, through the process of "flash."

Future Effort

Fine tuning and correcting errors (if necessary) of this tutorial are an obvious future need. Hopefully a dialog on this material will develop and any flaws will be identified (and they could prove to be many and important). Clearly, additional algorithms devoted to heat transfer issues, TNT equivalencies might be desirable as would expansion of adiabat.exe and/or adiabat32.exe to address not only the T vs. P event, but the T vs. V and P vs.V events as well as TNT equivalencies and others.

Summary

OSPs can often benefit from a range of calculations. Among them are adiabatic compression, expansion, velocity and total pressure estimates, and energy-release estimates. But

some OSPs are not comfortable with both the thermodynamic and mathematics functions. As a result questions arise as to how much error might the ordinary range of material evaluations suffer.

In some cases the error can be significant and even those who do not do such calculations, relying instead on judgment, need to know where extra care is needed and an attempt to flag these cases has been made.

Some of this math has been reviewed in painful detail and hopefully simplified. Much more detail than usual has been presented to allow these methods to be understood and used more widely and to be channeled into the most appropriate form for OSP use. Further, overview calculations have been performed to give a qualitative perspective. That perspective has been extended to compare a series of oxidants, diluents and mixtures not yet extensively debated in the ASTM forum.

A simply PC utility algorithm has been proposed and prototyped that can provide much help with appreciating adiabatic processes and getting to approximate answers.

And the continuing need for work in this area has been examined. Only time will tell if this particular material and approach is fatally flawed, or even if not, whether it will gain any degree of credibility and acceptance.

Acknowledgements

Many thanks to Renee Koeller for the 1999 paper that served as a model and motivation, identified several problem areas needing redress, and "ignited" this effort. Valuable additional discussion early on and coaching on thermodynamics subtleties was also received from Shankar Nataraj, also much appreciated. Thank you, Shankar. Joe Slusser has "enabled" this tutorial in numerous ways as coach, sounding board, data resource, and liaison to ASTM Committee G4 — Many thanks, Joe.

References

[1] ASTM Committee G4 on Compatibility and Sensitivity of Materials in Oxygen Enriched Atmospheres, Subcommittee G4.01, **Standard G74 Standard Test Method for Ignition Sensitivity of Materials to Gaseous Fluid Impact**, American Society for Testing and Materials, *Annual Book of Standards,* Vol. 14.02, Oct, 29, 1983, Latest version 2001 in Vol. 14.04, 7 pages.

[2] ASTM Committee G4 on Compatibility and Sensitivity of Materials in Oxygen Enriched Atmospheres, Subcommittee G4.01, **Standard G175-03 Standard Test Method for Evaluating the Ignition Sensitivity and Fault Tolerance of Oxygen Regulators Used for Medical and Emergency Applications**, American Society for Testing and Materials, *Annual Book of Standards,* Vol. 14.04, 2003, 14 pages..

[3] Compressed Gas Association, *CGA G-4.4 Oxygen Pipeline Systems*, (EIGA 13/02), Fourth Edition, Compressed Gas Association, Arlington VA, 12/4/2003, 70 pages.

[4] Werley, B. L., **"Sonic, Supersonic and Other Extreme Velocities in Oxygen Systems,"** Presented at the ASTM Committee G-4 Seminar, Fall 1998, Cocoa Beach, Air Products and Chemicals Inc., Allentown PA, 1999, 20 pages.

[5] Werley, B. L., **"Estimating Maximum Gas Velocities in Oxygen System Valves,"** Presented at the Spring 1998 Seminar of ASTM Committee G-4 (22 April 1998), Atlanta GA, Air Products and Chemicals Inc., Allentown PA, 1998, 17 pages.

[6] Werley, B. L., **"A Perspective on Gaseous Impact Tests: Oxygen Compatibility Testing on a Budget",** *Flammability and Sensitivity of Materials in Oxygen-Enriched Atmospheres: Sixth Volume, ASTM STP 1197*, Dwight D. Janoff and Joel M. Stoltzfus, Eds., American Society for Testing and Materials, Philadelphia, 1993, pp. 27-42.

[7] Werley, B. L., **"Are Current Fire-Test Procedures for Medical-Oxygen Gas Regulators Adequate?**", Prepared for the Fall 2002 meetings of ASTM Committee G-4, 10-12 September 2002, Huntsville AL, 2002, 12 pages.

[8] Wilson, D. B., Barragan, M., and Beeson, H. D., **"A Parametric Modeling Study of Temperature Dynamics of Contaminated or Damaged Softgoods in Compressed Oxygen"**, *Flammability and Sensitivity of Materials in Oxygen-Enriched Atmospheres: Tenth Volume, ASTM STP 1454*, T. A. Steinberg, H. D. Beeson, and B. E. Newton, Eds., ASTM International, West Conshohocken, PA, 2003, pp. 319-332.

[9] Leslie, I. H., **"Thermodynamic and Fluid Mechanic Analysis of Rapid Pressurization in a Dead-End Tube",** *Flammability and Sensitivity of Materials in Oxygen-Enriched Atmospheres: Fifth Volume, ASTM STP 1111*, Joel M. Stoltzfus and Kenneth McIlroy, Eds., American Society for Testing and Materials, Philadelphia, 1991, pp. 399-413.

[10] Koeller, R. M., **"The Effect of 'Real' Gamma on Oxygen Compatibility Calculations,"** Presented at the Spring 1999 Seminar Series of ASTM G-4 in Seattle WA, Air Products and Chemicals, Inc., Allentown, PA, 1999.

[11] Barragan, M., Wilson, D. B., and Stoltzfus, J. M., **"Adiabatic Compression Of Oxygen: Real Fluid Temperatures,"** *Flammability and Sensitivity of Materials in Oxygen-Enriched Atmospheres: Ninth Volume, ASTM STP 1395,* T. A. Steinberg, B. E. Newton, and H. D. Beeson, Eds., American Society for Testing and Materials, West Conshohocken, PA, 2000, pp. 256-265.

[12] Van Wylen, G. J., and Sonntag, R. E., *Fundamentals of Classical Thermodynamics*, 3rd Edition, SI Version, John Wiley & Sons, 1985.

[13] **"Tables of Thermodynamic and Transport Properties,"** Chapter 8: *The Thermodynamic Properties of Oxygen,* Perganion Press, 1960: pp. 369-436.

[14] Russian thermo tables book Selover

[15] Wagner, W., and de Reuck, K. M., *Oxygen International Thermodynamic Tables of the Fluid State —9*, International Union of Pure and Applied Chemistry, Blackwell Scientific Publications, Oxford, 1987.

[16] Friend, D. G., *NIST Standard Reference Database 12: NIST Thermophysical Properties of Pure Fluids, Version 3.0*, National Institute of Standards and Technology, Standard Reference Data Program, Gaithersburg, MD, 1992.

[17] Lemmon, E. W., McLinden, M. O., and Huber, M. L., *NIST Reference Fluid Thermodynamic and Transport Properties—REFPROP, Version 7.0*, National Institute of Standards and Technology, Standard Reference Data Program, Gaithersburg, 2002.

[18] E.W. Lemmon, M.O. McLinden and D.G. Friend, "**Thermophysical Properties of Fluid Systems**" in *NIST Chemistry WebBook, NIST Standard Reference Database Number 69*, Eds. P.J. Linstrom and W.G. Mallard, June 2005, National Institute of Standards and Technology, Gaithersburg MD, 20899 (http://webbook.nist.gov)

[19] John, J. E. A., *Gas Dynamics*, Allyn and Bacon, Inc., Boston, 1969, pp. 222-230, 97-99 and throughout.

[20] Kennard, E, H., Kinetic Theory of Gases, First Edition, McGraw-Hill Bok Company, New York and London, 1938, pp. 51, 364.

[21] Lewis, B. and von Elbe, G., *Combustion. Flames and Explosions of Gases*, Academic Press, New York, 1961, p. 326..

[22] Steiner, J. C., and Mirsky, W., **"Experimental Determination of the Dependence of the Minimum Spark Ignition Energy Upon the Rate of Energy Release",** *Transactions of the Society of Automotive Engineers*, Paper 660346, 1966, pp. 392-407.

[23] Janoff, D., Pedley, M. D., and Bamford, L. J., **"Ignition of Nonmetallic Materials by High Pressure Oxygen III: New Method Development",** *Flammability and Materials in Oxygen-Enriched Atmospheres: Fifth Volume, ASTM STP 1111*, Joel M.Stoltzfus and Kenneth McIlroy, Eds., American Society for Testing and

Materials, Philadelphia, 1991, pp. 60-74.

[24] Santay, A. J., Becker, Jr., I. D., and Werley, B. L., **"Design Strategies for Polymer-Lined Flex-Hose Distance/Volume Pieces,"** *Flammability and Sensitivity of Materials in Oxygen-Enriched Atmospheres: Eighth Volume, ASTM STP 1319,* William T. Royals, Ting C. Chou, and Theodore A. Steinberg, Eds., American Society for Testing and Materials, 1997, pp. 93-107

[25] Werley, B. L., Hansel. J. G., ands Buchter, W. C., "**TNT Equivalency Concepts**", Presented at the Spring 1998 Seminar of ASTM Committee G-4 (22, 23 April 1998), Atlanta GA, Air Products and Chemicals, Inc., Allentown PA, 1998, 14 pages.

[26] Becker, R., *Z. Physik*, 8, 321(1922)

[27] Lewis, B. and von Elbe, G., op cit., page 512.

[28] Werley, B. L., **"An Oxygen Index Update",** *Flammability and Sensitivity of Materials in Oxygen-Enriched Atmospheres: Third Volume, ASTM STP 986*, D.W.Schroll, Ed., American Society for Testing and Materials, Philadelphia, 1988, pp. 248-261.

[29] Gugliemini, C.J., Kadri, S.H., Martrich, R.L., Slusser,J.W., Vora, J., Werley, B.L., and Woytek, A.J., **"Flammability of Metals in Fluorine and Nitrogen Trifluoride,"** *Flammability and Sensitivity of Materials in Oxygen-Enriched Atmospheres; Seventh Volume, ASTM STP 1267,* DwightD.Janoff, WilliamT. Royals, and MohanV.Gunaji, Eds., American Society for Testing and Materials, Philadelphia, 1995, pp. 107-127.

[30] Wolf, G. L., and Simpson, J. I., **"Oxidant O_2 and Oxidant N_2O Indices of Flammability and Their Additive Effect",** *Flammability and Sensitivity of Materials in Oxygen-Enriched Atmospheres: Third Volume, ASTM STP 986*, D.W.Schroll, Ed., American Society for Testing and Materials, Philadelphia, 1988, pp. 420-426

[31] Wolf, G. L., Simpson, J. I., **"Flammability of Endotracheal Tubes in Oxygen and Nitrous Oxide Enriched Atmospheres,"** *Canadian Journal of Anesthesiology* , Vol. 34, No. 3-II, May 1987 Supplement, pp. S127-S128.

[32] Guy, Keith W. A., *The Explosive Decomposition of Nitrous Oxide*, doctoral thesis, University of London, Imperial College of Science and Technology.

[33] Janoff, D., Bamford, L. J., Newton, B. E., and Bryan, C. J., **"Ignition of PTFE-Lined Flexible Hoses by Rapid Pressurization with Oxygen",** *Flammability and Sensitivity of Materials in Oxygen-Enriched Atmospheres: Fourth Volume, ASTM STP 1040*, Joel M.Stoltzfus, FrankJ.Benz, and Jack S.Stradling, Editors., American Society for Testing and Materials, Philadelphia, 1989, pp. 288-308.

[34] Ducrocq, J., Barthelemy, H., and Roy, D., **"A Fluid Flow Analysis of the Gaseous Impact Test,"** *Flammability and Sensitivity of Materials in Oxygen-Enriched Atmospheres: Ninth Volume, ASTM STP 1395,* T. A. Steinberg, B. E. Newton, and H. D. Beeson, Eds., American Society for Testing and Materials, West Conshohocken, PA, 2000,pp. 224-239.

[35] Bradley, J. N., *Shock Waves in Chemistry and Physics*, John Wiley & Sons, New York, and Methuen & Co, Ltd, London, 1962, pp. 45-51 and throughoutHughes, W. F., and Brighton, J. A., *Fluid Dynamics*, Third Edition, Schaums's Outline Series, McGraw-Hill, New York, 1999, pp. 197-200 and throughout.

[36] Hughes, W. F., and Brighton, J. A., *Fluid Dynamics*, Third Edition, Schaums's Outline Series, McGraw-Hill, New York, 1999, pp. 197-200 and throughout

[37] Streeter, V. L., *Handbook of Fluid Dynamics*, First Edition, McGraw-Hill Book Company, Inc., New York, 1961..

[38] Newton, B. E., and Forsyth, E. T., **"Cause and Origin Analyses of Two Large Industrial Gas Oxygen Valve Fires"**, *Flammability and Sensitivity of Materials in Oxygen-Enriched Atmospheres: Tenth Volume, ASTM STP 1454*, T. A. Steinberg, H. D. Beeson, and B. E. Newton, Eds., ASTM International, West Conshohocken, PA, 2003, pp. 268-289.

[39] Presti, J. B. and DeSimone, C. J.**,** Jr., "**Oil Contamination in Oxygen Systems**," DDC-AD6S6126 General Dynamics Electric Boat Div. Final Report No. U413-67-109, Contract NObs-94416, Project SF013-08-14, Task 3917, General Dynamics, Groton, Conn., 1967.

[40] Sears, F. W., and Zemansky, M.W., *College Physics*, Third Edition, Addison-Wesley Publishing Company, Reading Massachusetts, U.S.A., 1960, p. 377.

Appendix A

Entropy-Parameter-Free Compression for Nonthermodynamists

There are three models of oxygen of interest here for thermodynamic rapid compression/expansion analysis. Real oxygen, and two forms of ideal oxygen (oxygen of constant heat capacity or variable heat capacity). The ideal gases will be examined first

Real and ideal oxygen are often drawn as thermodynamic surfaces in three space. In conditions of current interest to OSPs, either ideal-gas surface is very reminiscent of a portion of a cone, upper portion of Figure A-1. The surface of a real gas can be much more complex, lower portion of Figure A-1. These surfaces are often shown in two-space as a series of slices through the surface. As is also the case for other gases, oxygen is taken as a collection of "equilibrium" states. Each "state" is taken as fully characterized by its pressure, temperature and volume. Any two of these parameters may be taken as independent variables in defining the third. In addition, any two are independent in also defining a fourth property each state has—an internal energy, which allows the definition of still other dependent thermodynamic properties such as enthalpy and entropy. Not every property is directly measurable.

The entire surface is taken as being in equilibrium at every point. Among the importance of the equilibrium is that without equilibrium, there is technically no uniform pressure or temperature parameter defined. Therefore, during an actual rapid compression, pressure, temperature and even volume (even over certain sub-regions) may not be definable, the process may not be (probably is not) in equilibrium, but nonetheless may settle (usually very quickly) to an equilibrium state adequately predicted by that which an equilibrium process would experience, and therefore equilibrium results may still be meaningful to the design of an oxygen system.

There are numerous methods to establish these states mathematically. Equations of state (EoS) seek to predict any parameter from the other two. In papers in the ASTM G4 collegium to date, the Virial EoS, Peng-Robinson EoS, Soave-Redlich-Kwong EoS, and van der Waals EoS have all been used. One can measure specific states or interpolate between experimental points either linearly or with more sophisticated formulas. Software is also available and in this effort, software based on a modified Benedict-Webb-Rubin equation of state or a more general type of Helmholtz energy equation of state is used.

To estimate how oxygen behaves during rapid pressurization, one must tease from these various data the series of states it will move through when pressurized with no external addition or loss of heat. In some software, one can track this as the constant entropy condition and obtain predictions that way. However, although the entropy parameter is elegant and its constant value is typically, maybe always, used in textbooks to derive the equations for adiabatic processes, it is subtle and is not mandatory. This section will forego use of the entropy parameter in deriving the several ideal-gas equations, in hopes of giving a simpler more mechanical perspective, more

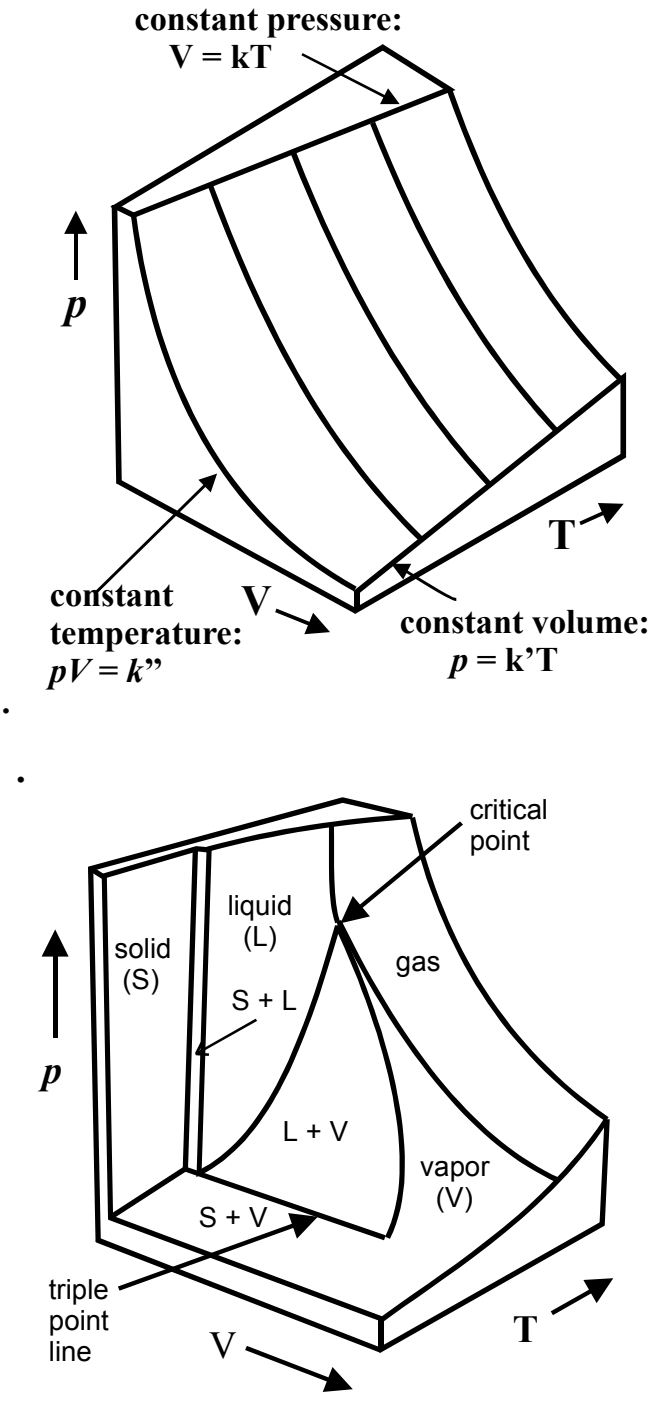

FIG. A-1—*Example ideal-gas (upper) and real-gas (lower) thermodynamic surfaces. (Patterned after Sears and Zemansky* [***40***]*, page 377, with enhancements.)*

meaningful to some like the writer.

Ideal Oxygen/Constant Specific Heat Case

Ideal oxygen of constant specific heat is the simplest to analyze and will be addressed first. Ideal gas obeys the mathematical equation:

$$PV = nRT$$

also

$$PV/n = Pv = RT$$

Where:

P = absolute pressure
V = volume
n = number of moles
v = V/n = molar volume
R = universal gas constant
T = absolute temperature

Also for an ideal gas the internal energy is only a function of temperature. As a result the internal energies along each hyperbola (each slice) represented by constant PV product in the upper part of Figure A-1 have a constant internal energy at every point.

Compression by Vessel Volume Reduction

Perhaps the most easily analyzed compression is like that in a piston and cylinder where the vessel volume is forcibly reduced. This scenario is shown in Figure A-2. The lowest curve (green) in the figure exhibits ideal gas behavior of isotemperature and isoenergy. Consider point *a* in Figure A-2 at an initial pressure P_i = 15 psia and initial volume V_i = 300 ft^3 and at initial temperature T_i = 70°F = 530°R. This gas can be compressed in many ways, but we are interested in adiabatic compression in which no net heat is transferred in or out of the system.

First, let's approximate the compression of the gas in two stages. The first stage is reduction of the volume in one step (N=1) from point *a* through *b* through *c* through *d* to the value still at constant temperature at point *e* of Figure A-2, Part A. This corresponds to the compression process A to B to C to D to E of Figure A-2, Part B. Since the internal energy of this ideal gas is constant along the curve, as we do work to compress the gas we have to transfer out an amount of heat $Q_{a\text{-}e}$. To compress this gas, work must be performed upon it in the amount:

$$\text{Work} = \int P(-dV) = \int (-nRT/V)dV = nRT \text{ Ln } (V_a/V_e) = Q_{a\text{-}e} \qquad \text{(A1)}$$

This is the area under the lower curve, abcde (green on digital copies) from point *a* to point *e*.

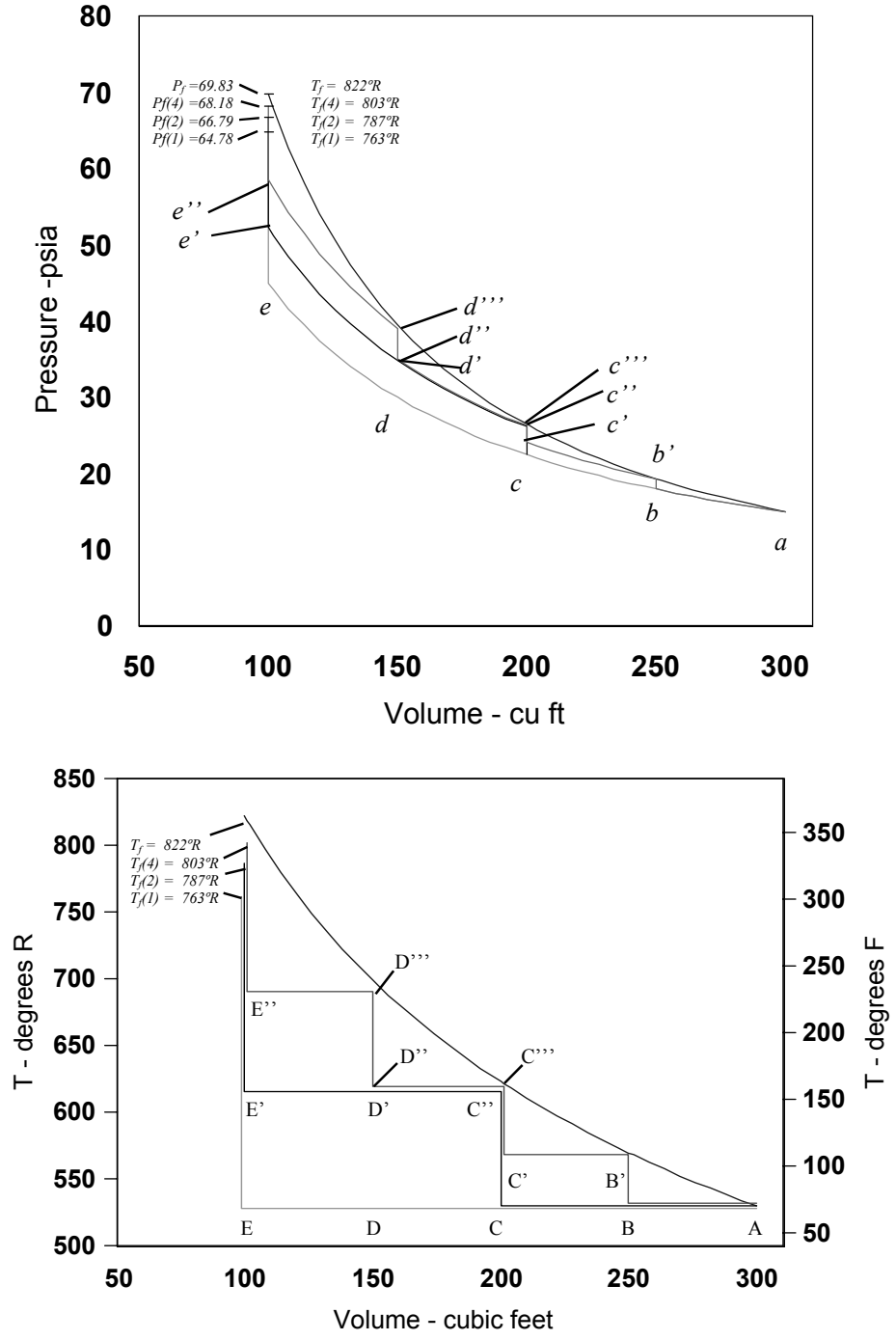

FIG. A-2—*Adiabatic compression estimates using decreasing vessel volume. (Some lines are shifted slightly to avoid overlap.)*

Now holding the volume constant at point *e*, we transfer Q_{a-e} back into the gas at the constant specific heat rate to yield an overall net zero heat loss and provide a first estimate of the final temperature, $T_f(1)$, Figure A-2, Part B.

$$Q_{T(1)-e} = \int nC_v dT = nC_v[T_f(1) - T_E] = nRT_A \text{ Ln } (V_a/V_e) \quad \text{(A2)}$$

And since $T_A = T_E$,

$$T_f(1) - T_A = (RT_A/C_v) \text{ Ln } (V_a/V_e) \quad \text{(A3)}$$

At constant volume, the final first-estimate pressure, $P_f(1)$ is given by

$$P_f(1) = [T_f(1) / T_E] P_e = [T_f(1) / T_A] P_e \quad \text{(A4)}$$

For the actual starting conditions of Figure A-2, this would estimate the final temperature as 763ºR (up from 530ºR at point E) and the pressure as 64.78 psia (up from 45 psia at point *e*).

As a second approximation (N=2) this same exercise will be repeated by dividing the work calculation into two parts as are also shown in Figure A-2 (black curve on digital copies) and re-addition of the incremental work-produced heat after each step. The first segment uses the same equation as for the previous example but only to half the final volume (the piston is half way to its destination). The corresponding equations are:

$$\int P(-dV) = \int (-nRT/V)dV = nRT \text{ Ln } (V_a/V_c) = Q_{a-c} \quad \text{(A5)}$$

$$Q_{a-c} = \int nC_v dT = nC_v(T_{C''} - T_C) = nRT_A \text{ Ln } (V_a/V_{c''}) \quad \text{(A6)}$$

Transferring this heat back into the gas at *c* yields the temperature at a new point *c''*

$$T_{C''} - T_A = (RT_A/C_v) \text{ Ln } (V_a/V_{c''}) \quad \text{(A7)}$$

The temperature at this point *C''* is 615.96ºR. At constant volume the pressure at point *C''*, 26.14 psia, is given by

$$P_{c''} = [T_{C''} / T_C] P_c = [T_{C''} / T_A] P_c \quad \text{(A8)}$$

The point *c''* becomes the starting point for another compression starting on a different isotemperature/isoenergy curve through *c''*. This leads through point d' and finally to *e'* at which a pressure greater than at point *e* exists. As a result of the transfer of heat back into the gas at point *c*, the pressure is greater throughout the second step of this second estimate, than during the second half of the first estimate, and so the work performed on this second portion is greater than for the corresponding portion of the first path. The set of equations that correspond

to (A5) through (A8) are:

$$\int P(-dV) = \int (-nRT/V)dV = nRT \text{ Ln } (V_{c''}/V_{e'}) = Q_{c''\text{-}e'} \quad \text{(A9)}$$

$$Q_{c''\text{-}e'} = \int nC_v dT = nC_v(T_{E'} - T_{C''}) = nRT_{E'} \text{ Ln } (V_{c''}/V_{e'}) \quad \text{(A10)}$$

Transferring this heat back into the gas at *e'* yields the final temperature at a new point $T_f(2)$:

$$T_f(2) - T_{E'} = (RT_{E'}/C_v) \text{ Ln } (V_{c''}/V_{e'}) \quad \text{(A11)}$$

In this case, at constant volume, the final pressure is

$$P_f(2) = [T_f(2) / T_{E'}] P_{e'} = [T_f(2) / T_{C''}] P_{e'} \quad \text{(A12)}$$

In summary:

$$T_f(2) = T_i + \Sigma \Delta T = T_A + [T_f(2) - T_{E'}] + [T_{C''} - T_A] \quad \text{(A13)}$$

$$T_f(2) = T_A + (RT_{E'}/C_v) \text{ Ln } (V_{c''}/V_{e'}) + (RT_A/C_v) \text{ Ln } (V_a/V_{c''}) \quad \text{(A14)}$$

If the volume were compressed only slightly, so that the temperature increase were very small, then $T_{E'} \approx T_A$, and then

$$T_f(2) = T_A + (RT_{A'}/C_v) [\text{Ln } V_a - \text{Ln } V_{e'}] \quad \text{(A15)}$$

The previous two exercises can be repeated by dividing the volume interval *a-e* (300 – 100 ft^3) into three segments, and obtaining an estimate for a final pressure, $P_f(3)$, and temperature $T_f(3)$ but that will be skipped here to avoid a confusing drawing. Instead, the sequence of equations that obtain for dividing the compression into four segment in pursuit of the estimate for final pressure, $P_f(4)$, and final temperature $T_f(4)$ will be considered.

Without repeating all four sets of equation, the work under the original curve for a to b is calculated as heat equivalent $Q_{a\text{-}b}$ and added back to define point *b'*. A new isotemperature/ isoenergy curve through *b'* is defined and the work under it from b' to c' is determined as heat equivalent $Q_{b'\text{-}c'}$ which is added back to define *c'''* (only slightly greater than *c''* in pressure). A new isotemperature/isoenergy curve through *c'''* is defined and the work under it from *c'''* to d'' is determined as heat equivalent $Q_{c'''\text{-}d''}$ which is added back to define *d'''*. A new isotemperature/isoenergy curve through *d'''* is defined and the work under it from *d'''* to *e''* is determined as heat equivalent $Q_{d'''\text{-}e''}$ which is added back to define $T_f(4)$ and therefore $P_f(4)$.

$$T_f(4) = T_A + (RT_{E''}/C_v) \text{ Ln } (V_{d'''}/V_{e''}) + (RT_{D''}/C_v) \text{ Ln } (V_{c'''}/V_{d''}) + \\ + (RT_{C'}/C_v) \text{ Ln } (V_{c'}/V_{b'}) + (RT_A/C_v) \text{ Ln } (V_a/V_b) \quad \text{(A16)}$$

As with Equation (A14), if the total compression is small so that the temperature at each step changes little, then a simplified expression similar to equation (A15) can be derived.

$$T_f(4) = T_A + (RT_A/C_v)\,[\text{Ln } V_a - \text{Ln } V_e] \tag{A17}$$

In early calculus courses, one learns that integrals are in general, established by increasing the number of segments in an estimate like this indefinitely. Regardless of the number of segments the compression is resolved into, the temperature rise for k^{th} segment is of the form;

$$\Delta T_{(k+1)-k} = T_{(k+1)} - T_k = (RT_k/C_v)\,\text{Ln}\,(V_{(k+1)}/V_k) \tag{A18}$$

And,
$$\Delta T_{(k+1)-k}/T_k = (T_{(k+1)} - T_k)/T_k = (R/C_v)\,\text{Ln}\,(V_{(k+1)}/V_k) \tag{A19}$$

So that, if we let $k \to \infty$

$$\text{Lim } \Sigma\Delta T_{(k+1)-k}/T_k = \text{Lim } \Sigma(T_{(k+1)} - T_k)/T_k = \text{Lim } \Sigma\Delta(R/C_v)\,[\text{Ln } V_{(k+1)} - \text{Ln } V_k] \tag{A20}$$

As the interval approaches zero length, the summations approach integrals and the arguments approach differentials:

$$\int \text{Lim } \Delta T_{(k+1)-k}/T_k = \int d(T_k)/T_k = (R/C_v)\int d(\text{Ln } V_k) \tag{A21}$$

So that,
$$\text{Ln}(T_f/T_i) = (R/C_v)\text{Ln}\,(V_f/V_i) \tag{A22}$$

And,
$$T_f/T_i = (V_f/V_i)^{R/Cv} \tag{A23}$$

This equation produces the upper (blue) curve of Figure A-2. And the final temperature for this calculation is 822°R, which is greater than each of the previous estimates.

Substituting $V = nRT/P$ and $T = PV/nR$ into Equation (A23) yields the following two equations respectively:

$$T_f/T_i = (P_f/P_i)^{R/(Cv+R)} \tag{A24}$$

$$P_i V_i^{(Cv+R)/Cv} = P_f V_f^{(Cv+R)/Cv} \tag{A25}$$

All three of these equations are valid for calculating ideal gas conditions during adiabatic processes.

The physical meaning of this analysis is that as the number of segments increases the saw tooth nature of the estimates smoothes and converges to a final equation and to the final curve which was produced with that same equation. With each increase in the number of seg-

ments, additional area is nibbled from the space between the final curve and the saw teeth. Therefore, the final temperature can be calculated by integrating the work/area under the final curve and adding that amount of heat energy to the gas at point e.

One can now calculate final temperatures based on the specific heat capacity at constant volume by running an approximating sum of individual steps (for example in a spread sheet) along the lines of Equation A16 using as many segments as needed for accuracy. Or with more convenience, one can use the equivalent Equations A23, A24 and A25 and plug into them three of the four variables (initial temperature and either initial and final pressure or initial and final volume). Because integrals are limiting sums, one can also use a spreadsheet and "pipeline" Equations A23, A24 or A25. To do this one can segment any of the variables: pressure, volume or temperature and insert any two of the initial parameters into any suitable equation and use it along with a first step parameter to calculate the remaining first-step parameter. Then one uses the first step parameters as the initial conditions for a second application of the formula and so forth. This is a trivial benefit when the heat capacity is constant, but we will soon see that the heat capacity is not always constant.

Compression by Gas Addition

A second, perhaps more important, mechanism of compression is when a gas is admitted to a fixed-volume system. This happens whenever a valve to a high pressure system is opened and is a major source of risk in many oxygen systems. The released incoming gas compresses any gas already present downstream and in some cases with little or no mixing of the incoming and existing gases. As a result the resident gas may experience heating much the same as if being compressed by a piston except that there is no piston position by which to sense its current volume. Instead, the pressure of the system, rather than the geometric volume, is the sensible (observable) variable. This scenario is shown in Figure A-3. The lowest curve (green again on digital copies) in the figure again exhibits the same ideal gas behavior of isotemperature and isoenergy as for Figure A-2. Consider point *a* in Figure A-3 again at an initial pressure $P_i = 15$ psia and initial volume $V_i = 300$ ft^3 and at initial temperature $T_i = 70°F = 530°R$. This gas will again be compressed adiabatically in which no net heat is transferred in or out of the system.

In this example, for correspondence with the analysis of Figure A-2, it will again be compressed in up to four pressure increments. Pressure addition will first bring it to the final pressure achieved in Figure A-2 (69.83 psia), then pressure will be increased in two equal steps, and finally the pressure will be raised in four equal steps. This requires that the ideal gas curve be extended further than in Figure A-2 up to the final pressure point. The work of compression in each step will again be the area under the pressure curve, which is now represented as the area subtended between the ideal gas curve and the ordinate (or volume) axis, and the increments in the volume over which the work increments are calculated are now of different lengths.

These same data of Figure A-3 Part A are again exhibited with the axes exchanged so that pressure is the ordinate and volume is the abscissa in Figure A-4. In this case the work per-

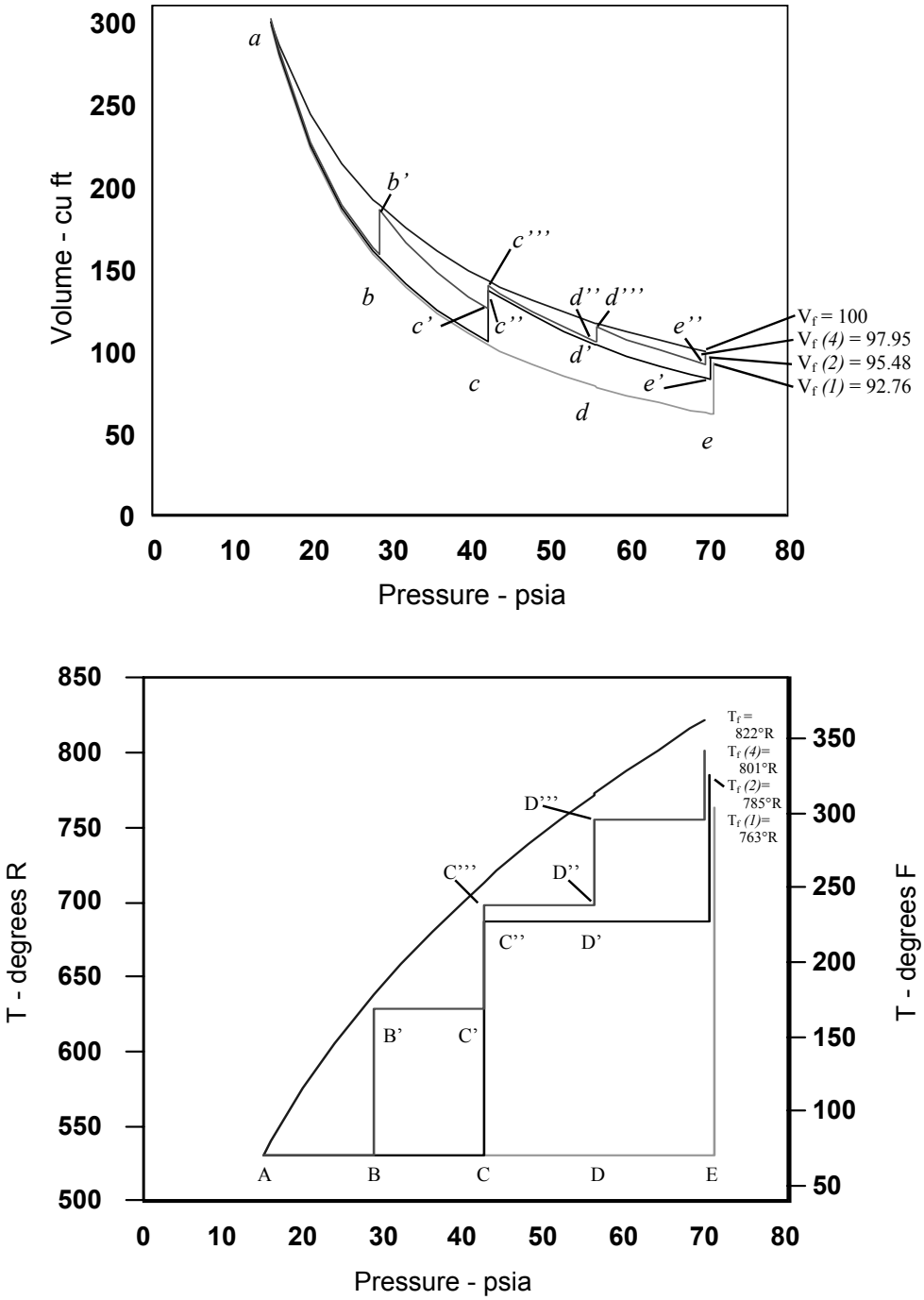

FIG. A-3—*Adiabatic compression estimates using gas addition.*
(Some lines are shifted slightly to avoid overlap.)

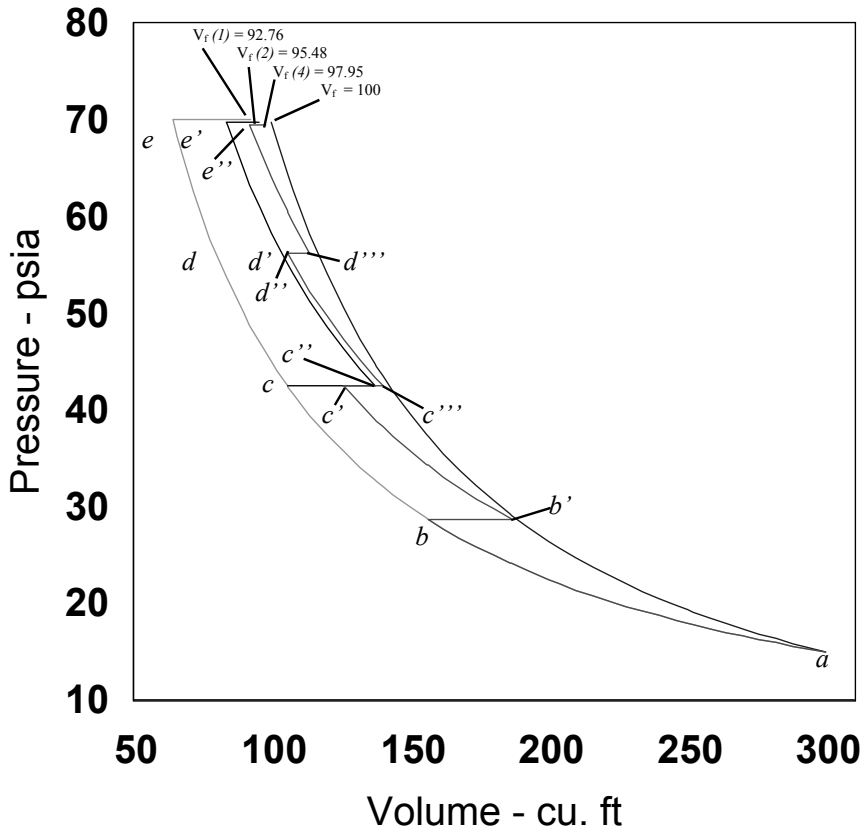

FIG. A-4—*Adiabatic compression estimates using gas addition*.

formed during compression is again the area below the curve and the lower limit of the volume is now 64.4 cubic feet.

First let's approximate the compression of the gas in two stages. The first is reduction of the volume in one step (N = 1) from *a* to *b* to *c* to *d* to the final value at constant temperature at point *e*. Since the internal energy of this ideal gas is constant along the curve, as we do work to compress the gas we have to transfer out an amount of heat $Q_{a\text{-}e}$. To compress this gas, work must be performed upon it in the amount:

$$\text{Work} = \int PdV = \int (nRT_i/V)dV = nRT_i \text{ Ln } (V_e/V_a) = Q_{a\text{-}e} \qquad \text{(A26)}$$

This is the area under the green curve of figure A-4 from point *a* to point *e*. However, since the measurable variable is pressure, recall that PV = nRT and therefore

$$dV = (-nRT/P^2)\, dP \qquad \text{(A27)}$$

Therefore, the integral of (A26), which is the area to the left of the curve, can be replaced with

$$\text{Work} = \int PdV = \int P\,(-nRT/P^2)\,dP = \int (-nRT/P)\,dP = nRT\,\text{Ln}\,(P_a/P_e) = Q_{a\text{-}e} \qquad \text{(A28)}$$

Now holding the pressure constant at point *e*, we transfer $Q_{a\text{-}e}$ back into the gas at constant pressure by making the calculation with the constant-pressure specific heat rate to yield an overall net zero heat loss and provide a first estimate of the final temperature, $T_f(1)$, Figure A-3, Part B. However, in this case as the heat is returned, the volume increases as the temperature rises. The gas must do mechanical work which is also at the expense of the heat, $Q_{a\text{-}e,}$

$$Q_{T(1)\text{-}e} = \int nC_p dT = nC_p[T_f(1) - T_E] = nRT_A\,\text{Ln}\,(P_a/P_e) \qquad \text{(A29)}$$

And since $T_A = T_E$,

$$T_f(1) - T_A = (RT_A/C_p)\,\text{Ln}\,(P_a/P_e) \qquad \text{(A30)}$$

At constant pressure, the final first-estimate volume, $V_f(1)$ is given by

$$V_f(1) = [T_f(1) / T_E]\,V_e = [T_f(1) / T_A]\,V_e \qquad \text{(A31)}$$

For the actual starting conditions of Figures A-3 and A-4, this would estimate the final temperature as 763ºR (up from 530ºR at point E) and the volume as 92.76 cubic feet (up from 64.44 cubic feet at point *e*).

As a second approximation (N=2) this same exercise will be repeated by dividing the work calculation into two parts as are also shown in Figure A-3 and A-4 (black curve on digital copies) and re-addition of the incremental work-produced heat after each step. The first segment uses the same equation as for the previous example but only to half the final pressure (Fgure A-3), however, Figure A-4 shows that this is at more than the half way point in the volume reduction (the volume is at less than 200 cu ft). The corresponding equations are:

$$\int PdV = \int P\,(-nRT/P^2)\,dP = \int (-nRT/P)\,dP = nRT\,\text{Ln}\,(P_a/P_c) = Q_{a\text{-}c} \qquad \text{(A32)}$$

$$Q_{a\text{-}c} = \int nC_p dT = nC_p[T_{C''} - T_C] = nRT_A\,\text{Ln}\,(P_a/P_c) \qquad \text{(A33)}$$

Transferring this heat back into the gas at constant pressure at *c* yields the temperature at a new point *c''* which is at a greater volume than that at point *c*. Figure A-3, Part B exhibits this higher temperature at corresponding point C''.

$$T_{C''} - T_A = (RT_A/C_p)\,\text{Ln}\,(P_a/P_c) \qquad \text{(A34)}$$

The temperature at this point *C''* is 785ºR. At constant pressure the volume at point *C''*, 95.48 cubic feet, is given by

$$V_{c''} = [T_{C''} / T_C] V_c = [T_{C''} / T_A] V_c \quad (A35)$$

The point *c''* becomes the starting point for another compression starting on a different isotemperature/isoenergy curve through *c''*. This leads through point *d*' and finally to *e'* at which a pressure greater than at point *e* exists. As a result of the transfer of heat back into the gas at point *c*, the pressure is greater throughout the second step of this second estimate, than during the second part of the first estimate, and so the work performed on this second portion is greater than for the corresponding portion of the first path. The set of equations that correspond to (A5) through (A8) are:

$$\int PdV = \int P\,(-nRT/P^2)\,dP = \int (-nRT/P)\,dP = nRT\,Ln\,(P_{c''}/P_{e'}) = Q_{c''\text{-}e'} \quad (A36)$$

$$Q_{c''\text{-}e'} = \int nC_p dT = nC_p(T_{E'} - T_{C''}) = nRT_{E'}\,Ln\,(P_{c''}/P_{e'}) \quad (A37)$$

Transferring this heat back into the gas at *e'* yields the final temperature at a new point $T_f(2)$:

$$T_f(2) - T_{E'} = (RT_{E'}/C_p)\,Ln\,(P_{c''}/P_{e'}) \quad (A38)$$

In this case, at constant pressure, the final second-estimate volume, $V_f(2)$ is given by

$$V_f(2) = [T_f(2) / T_{E'}]\,V_{e'} = [T_f(2) / T_{C''}]\,V_{e'} \quad (A39)$$

In summary:

$$T_f(2) = T_i + \Sigma\,\Delta T = T_A + [T_f(2) - T_{E'}] + [T_{C''} - T_A] \quad (A40)$$

$$T_f(2) = T_A + (RT_{E'}/C_p)\,Ln\,(P_{c''}/P_{e'}) + (RT_A/C_p)\,Ln\,(P_a/P_{c''}) \quad (A41)$$

If the volume were compressed only slightly, so that the temperature increase were very small, then $T_{E'} \approx T_A$, and then

$$T_f(2) = T_A + (RT_A/C_p)\,[Ln\,P_a - Ln\,P_{e'}] \quad (A42)$$

The previous two exercises can be repeated by dividing the pressure interval *a*-*e* (69.83–15 psia) into three segments, and obtaining an estimate for a final pressure, $P_f(3)$, and temperature $T_f(3)$ but that will again be skipped here to avoid a confusing drawing. Instead, the sequence of equations that obtain for dividing the pressure interval into four segments in pursuit of the estimate for final pressure, $P_f(4)$, and final temperature $T_f(4)$ will be considered.

Without repeating all four sets of equation, the work under the original curve for a to b

is calculated as heat equivalent $Q_{a\text{-}b}$ and added back to define point *b'*. A new isotemperature/ isoenergy curve through *b'* is defined and the work under it from b' to c' is determined as heat equivalent $Q_{b'\text{-}c'}$ which is added back to define *c'''* (only slightly greater than *c''* in volume). A new isotemperature/isoenergy curve through *c'''* is defined and the work under it from *c'''* to d'' is determined as heat equivalent $Q_{c'''\text{-}d''}$ which is added back to define *d'''*. A new isotemperature/isoenergy curve through *d'''* is defined and the work under it from *d'''* to *e''* is determined as heat equivalent $Q_{d'''\text{-}e''}$ which is added back to define $T_f(4)$ and therefore $P_f(4)$.

$$T_f(4) = T_A + (RT_{E''}/C_p)\,\mathrm{Ln}\,(P_{d'''}/P_{e''}) + (RT_{D''}/C_p)\,\mathrm{Ln}\,(P_{c'''}/P_{d''}) + \\ + (RT_{C'}/C_p)\,\mathrm{Ln}\,(P_{c'}/P_{b'}) + (RT_A/C_p)\,\mathrm{Ln}\,(P_a/P_b) \qquad \text{(A43)}$$

As with equation (A14), if the total compression is small so that the temperature at each step change little, then a simplified expression similar to equation (A15) can be derived.

$$T_f(4) = T_A + (RT_{A'}/C_p)\,[\mathrm{Ln}\,P_a - \mathrm{Ln}\,P_{e''}] \qquad \text{(A44)}$$

Again appealing to early calculus training, one learns that integrals are in general, established by increasing the number of segments in an estimate indefinitely. Regardless of the number of segments the compression is resolved into, the temperature rise for k^{th} segment is of the form;

$$\Delta T_{(k+1)\text{-}k} = T_{(k+1)} - T_k = (RT_k/C_p)\,\mathrm{Ln}\,(P_{(k+1)}/P_k) \qquad \text{(A45)}$$

And,
$$\Delta T_{(k+1)\text{-}k}/T_k = (T_{(k+1)} - T_k)/T_k = (R/C_p)\,\mathrm{Ln}\,(P_{(k+1)}/P_k) \qquad \text{(A46)}$$

So that, if we let $k \to \infty$

$$\mathrm{Lim}\,\Sigma\Delta T_{(k+1)\text{-}k}/T_k = \mathrm{Lim}\,\Sigma(T_{(k+1)} - T_k)/T_k = \mathrm{Lim}\,\Sigma\Delta(R/C_p)\,[\mathrm{Ln}\,P_{(k+1)} - \mathrm{Ln}\,P_k] \qquad \text{(A47)}$$

As the interval approaches zero length, the summations approach integrals and the arguments approach differentials:

$$\int \mathrm{Lim}\,\Delta T_{(k+1)\text{-}k}/T_k = \int d(T_k)/T_k = (R/C_p)\int d(\mathrm{Ln}\,P_k) \qquad \text{(A48)}$$

So that,
$$\mathrm{Ln}(T_f/T_i) = (R/C_p)\mathrm{Ln}\,(P_f/P_i) \qquad \text{(A49)}$$

And,
$$T_f/T_i = (P_f/P_i)^{R/Cp} \qquad \text{(A50)}$$

This equation produces the upper (blue) curve of Figure A-3. And the final temperature for this calculation is 822°R, which is greater than each of the previous estimates and duplicates the fi-

nal temperature derived in the case for volume reduction compression.

Substituting P = nRT/V and T = PV/nR into Equation (A50) yields the following two equations respectively:

$$T_f/T_i = (V_f/V_i)^{R/(Cp-R)} \qquad (A51)$$

$$P_i V_i^{Cp/(Cp-R)} = P_f V_f^{Cp/(Cp-R)} \qquad (A52)$$

All three of these equations are valid for calculating ideal gas conditions during adiabatic processes. All share similar but not identical structure to equations A24, A23 and A25, respectively.

The physical meaning of this analysis is again that as the number of segments increases the saw tooth nature of the estimates smoothes and converges to a final equation and to the final curve which was produced with that same equation. With each increase in the number of segments, additional area is nibbled from the space between the final curve and the saw teeth. Therefore, the final temperature can be calculated by integrating the work/area under the final curve and adding that amount of heat energy to the gas at point e.

As in the analogous earlier derivation of this appendix, one can now calculate final temperatures based on the specific heat capacity at constant pressure by running an approximating sum of individual steps (for example in a spread sheet) along the lines of equation A44 using as many segments as needed for accuracy. Or with more convenience, one can use the equivalent equations A50, A51 and A52 and plug into them three of the four variables (initial temperature and either initial and final pressure or initial and final volume). Because integrals are limiting sums, one can also use a spreadsheet and "pipeline" equations A50, A51 or A52. To do this one can segment any of the variables pressure, volume or temperature and insert any two of the initial parameters into any suitable equation and use it along with a first step parameter to calculate the remaining first-step parameter. Then one uses the first step parameters as the initial conditions for a second application of the formula and so forth. This is again a trivial benefit when the heat capacity is constant, but we will see that real-gas heat capacity is not always constant.

Coordinating the Two Sets of Equations

There is an analogous structure between the two sets of equations, A23-A25 and A50-A52. These two sets of equations represent two different, yet both valid, ways to do the calculation. Consequently the two sets should yield the same results, since the predicted behavior of the gas does not depend on the way its behavior is calculated. The respective equations can only yield the same results if the respective exponents are equal., or if :

For Eqs 25, 52: $(Cv+R)/Cv = (Cp/(Cp-R)$ which implies $Cp - Cv = R$

For Eqs. 24, 50: $R/(Cv+R) = R/Cp$ which implies $Cp - Cv = R$.

For Eqs. 23, 51: $R/Cv = R/(Cp-R)$ which again implies $Cp - Cv = R$.

Using this requirement on Eqs. 25 and 52,

$$P_i V_i^{(Cv+R)/Cv} = P_f V_f^{(Cv+R)/Cv} = P_i V_i^{Cp/(Cp-R)} = P_f V_f^{Cp/(Cp-R)} = PV^{Cp/Cv} = PV^{\gamma}$$

:

Where

$$\gamma = Cp/Cv = (Cv+R)/Cv = Cp/(Cp-R) \quad \text{A53)}$$

When C*p* and C*v* are constant, then γ is also constant and can be used to reframe Equations 23-25 and 50-52 in the form of Equations 1-3:.

$$T_f/T_i = (P_f/P_i)^{(\gamma-1)/\gamma} \quad \text{(A54)}$$

$$T_f/T_i = (V_i/V_f)^{(\gamma-1)} \quad \text{(A55)}$$

$$P_i V_i^{\gamma} = P_f V_f^{\gamma}, \quad (P_f/P_i) = (V_i/V_f)^{\gamma} = (V_f/V_i)^{-\gamma} \quad \text{(A56)}$$

This set of equations is currently used to estimate adiabatic temperatures, but heat capacities are not constant, gases are often compressible, and other factors can introduce significant errors in the estimates.

The Relationship of C_p to C_v

The analysis of the previous section declares that for an ideal gas of constant heat capacities:

$$Cp = Cv + R \quad \text{(A57)}$$

There is a physical significance to this relationship that is worth examining.

Figure A-5 again exhibits the same isothermal/isoenergy curve (bottom/green on digital copies) and adiabatic compression curve (top/blue on digital copies) as presented in Figures A-2 and extended in A-3 and A-4.

In the limit, the work/heat energy (W_1) represented by the area under the adiabatic curve a-d divided by the constant heat capacity C_v was introduced at constant volume into the system at point b. This produced a temperature rise and in turn a pressure rise to point d.

In related fashion, the work/heat energy (W_2) represented by the area of the curve under the curve a-d-c divided by the heat capacity C_p, was introduced at constant pressure into the gas at point c. This is the same work/energy (W_1) as in the case just reviewed (from a-d) plus the work at constant pressure from point d to point c. It both produced a temperature rise and resultant volume increase from point c to point d. The temperature rise and final pressure were both the same as those in the earlier case.

These work energies can be related

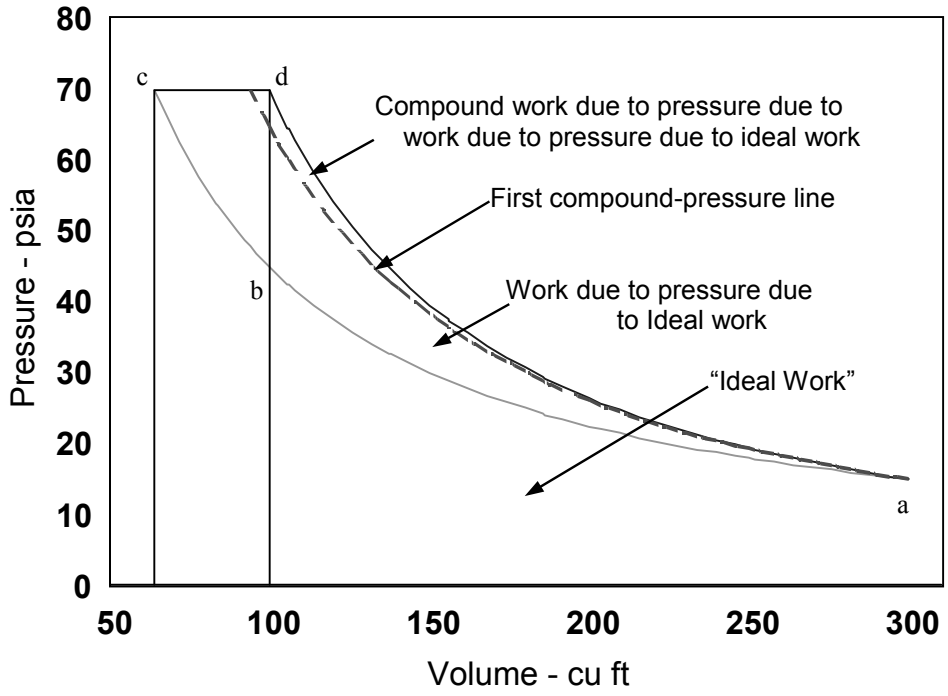

FIG. A-5—*Adiabatic compression estimates using gas addition*.
(Duplicate data to Fig, A-4)

$$\Delta T = T_f - T_i = W_1/Cv = W_2/C_p = \{W_1 + [P_d(V_d - V_c)]\} / C_p \quad (58)$$

Also $P_d = P_c = P_f$ and $P_d V_d = RT_d$, and $P_d V_c = RT_c = RT_i$, so that, from the third and fifth terms above,

$$\Delta T = W_1/Cv = \{W_1 + [P_d(V_d - V_c)]\} / C_p \quad (59)$$

And,

$$C_p W_1 = C_v W_1 + C_v[P_d(V_d - V_c)]\} \text{Or,} \quad (60)$$

$$C_p W_1 = C_v W_1 + C_v(RT_d - RT_c) \quad (61)$$

Re-arranging by dividing by W_1, and substituting

$$C_p = C_v + (C_v/W_1)R(T_d - T_c) \quad (62)$$

Substituting C_v/W_1 for $1/(T_d - T_b)$ which also equals $1/(T_d - T_c)$, and again

$$C_p = C_v + R(T_d - T_c)/(T_d - T_c) = C_v + R \quad (63)$$

This important relationship ($C_p = C_v + R$) is often used to convert and "simplify" the form of Equations A23-A25 and A50-A52 into the form employing the ratio $C_p/C_v = \gamma$ which yields the equations (1-3).

Adiabatic Compression and Compound Interest

Figure A-5 also illustrates the relationship of the various work energies involved in adiabatic compression. Again consider the same curves from Figures A-2, A-3 and A-4 are important. In addition a middle (dashed)curve (red on digital copies) on Figure A-5 shows the pressure that would be produced at any point if the work/heat component under the ideal curve up to that point were reintroduced at that point. The work under the lower ideal curve is labeled as the "Ideal work". The region between the bottom and middle curves (green and red on digital copies) is additional pressure that results due to the ideal work. The work represented by the area between these curves (green and red) is labeled the "Compound work due to the ideal work". If the work represented by the area between the bottom and middle curves up to any point was reintroduced at that point, there would be another curve between the middle and top (red and blue on digital copies) curves representing increased pressure due to the compound work due to the ideal work, and it would define yet another work and area. The region between the middle and top (red and blue) curves is labeled "compound work due to compound work".

The compound work is directly analogous to compound interest earned on investments. In this analogy the ideal work is related to the principal. Simple interest is the amount of extra work (money) due to the principal. And compound interest is the interest earned on the interest resulting from the principal. Similarly the compound work is the work done against additional pressure that results from the pressure that results from the ideal pressure. The final curve represents infinite compounding.

Greater interest (work and temperature) result if the principal is larger (if the starting pressure is higher) and if the investment is allowed to earn for a longer period of time (if the volume reduction is greater) and if the interest is calculated over shorter periods (if the compression is broken into smaller volume increments).

This graphically illustrates that most of the pressure rise (and therefore temperature rise) of oxygen at lower amounts of compression results from the ideal isothermal pressure. However, as the total volume change increases, the compound work and pressure can ultimately come to dominate the final values.

Ideal Gas / Variable Heat Capacity Case

Heat capacities are typically not the same for all gases nor are they even close to constant for real gases. Leslie [***9***] and, for comparison, Barragan et al. [***11***], treat this prospect in a mathematically straightforward (if not simple) way for some adiabatic cases with ideal gases using variable heat capacity and find it results in a much better estimate (for at least one common set of initial pressure and temperature) of compression temperatures (compared to equation

of state predictions) than does the ideal gas model. Remember that in Figure A-5, the work/heat equivalent of W_1 (the area under the curve from "a" to "d"), acts on the gas continuously to increase its temperature and pressure from point "b" to point "d". Similarly the work/heat equivalent of W_2 (the area under the curve from "a" to "d" to "c") acts on the gas at point "c" and increases its volume and temperature to the same point "d". If the heat capacities had a different value or a variable value, the resulting final temperature and pressure would simply shift. They would shift down if the heat capacity were greater (because W_1 would be smaller and it would be divided by a larger specific heat number so W_1/C_v would also be smaller. Similarly, W_2 would be smaller and it would be divided by a larger specific heat number so W_2/C_p would be smaller). If the heat capacity were less, then W_1/C_v and W_2/C_p would be larger and the temperature increase would be greater.

The ideal work (the isothermal work) would be identical to that in the previous derivation. However, the net work values W_1 and W_2 would be smaller, because as the ideal work increments were being added to the gas they would each produce less pressure rise and therefore less "work due to the ideal work" as well as less compound work, also. Therefore a larger heat capacity acts to reduce the numerator and increase the denominator of the W/C ratios.

Figure A-6 exhibits an ideal gas isotherm and a series of adiabatic compression curves that approximate the behavior of several gases using ideal models of constant but differing heat capacity. The ideal work (the area under the lowest [green on digital copies] curve) in each of these is identical. This region between the lowest (the isotherm) and highest curves represents the principal range of compression heating that occurs with ideal gases.

The solid (final pressure) and dashed (ideal work) curves labeled nitrogen trifluoride are for a large molecule with a large heat capacity and therefore small value of γ, about 1.16. The solid (final pressure) and dotted (ideal work) curves labeled argon and helium, are for small molecules with small heat capacities and therefore large value of γ, about 1.67. The intermediate solid (final pressure) and dashed (ideal work) curves labeled oxygen, are for a mid-sized molecule with a middling heat capacity and middling value of γ, about 1.40.

Similarly, notice the relative sizes of the compound work. Compound-pressure could shift and change the final pressure as indicated in Figure A-6 (by the dotted lines below each adiabat). As heat capacity decreases, γ increases, and the relative amount of compound pressure and compound work increases. As heat capacity increases, the relative amount of compound pressure and compound work decreases.

A similar result applies when one considers heat capacities that may be variable for any individual gas. Here again, if the heat capacity increases variably with temperature, then the marginal effect of compression is to produce lesser temperature rise. If it were to decrease variably with temperature (something many real gases apparently do not typically do at common temperatures of interest), then higher temperature rises would result.

Real gases have significant variations in heat capacity. And so to better estimate the behavior of real oxygen, the ideal gas model is often assumed to have a variable heat capacity. In the papers presented in the ASTM collegium [***9,11***] the variations that have been assumed are

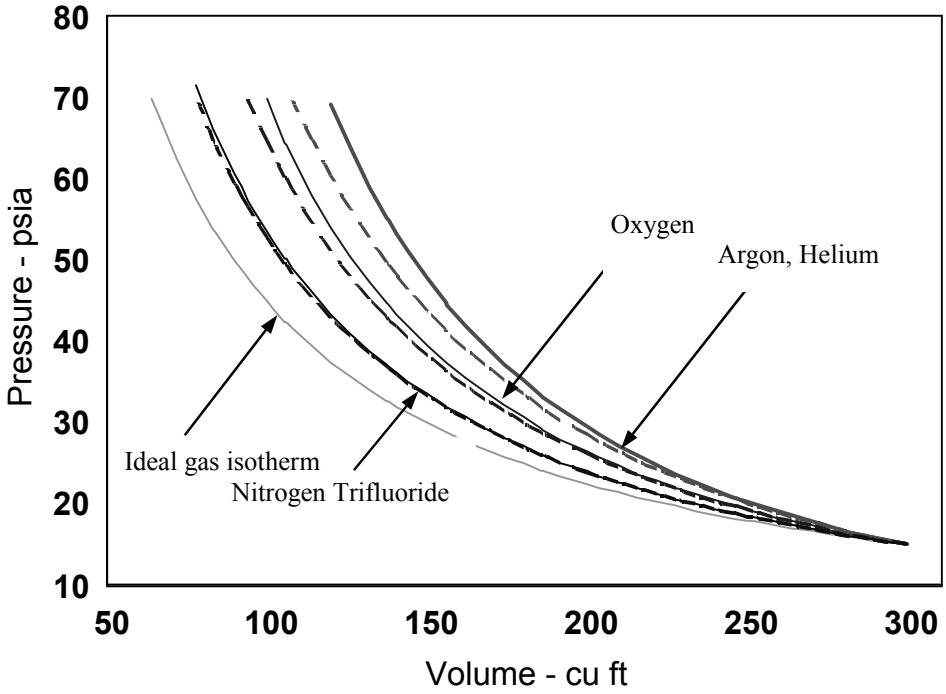

FIG. A-6—*Ideal gas adiabatic compression and first compound pressure estimates (dashed) for gases of differing constant specific heat.*

those of real oxygen as a function of temperature at atmospheric pressure. No comments are offered as to whether heat capacity should, or should not, vary with pressure, but Barrow [***42***] indicates it does, and the NIST databases indicate they can vary a lot. Referring again to Figure A-5, a variable heat capacity simply means that differing amounts of temperature rise result from each successive element of work/heat that are cumulatively introduced at points "b" and "c". However, we have seen that for both these heats to produce the same temperature at point "d", for ideal gases with constant heat capacities, $C_p = C_v + R$.

Apparently theoretical efforts to predict specific heat as a function of temperature are very complex. It appears therefore that real data for the variation are established and then the data are fit to empirical equations of simpler form for use in actual calculations.

There are numerous equations (for example those chosen by Leslie [***9***], Barragan et al [***11***], Van Wylen [***12***], and Abbot [***41***]) used to represent specific heat capacity. The upper group of curves of Figure A-7 show these and others for $C_p(T)$ for oxygen, and although all are of much different algebraic structure, all generate similar data. Indeed, these data are also compared to those for real oxygen at atmospheric pressure as is also shown as symbols extracted from the NIST 12 DB (up to its 1500 K limit).

The writer's efforts located only equations for $C_p(T)$ in these references. There appears

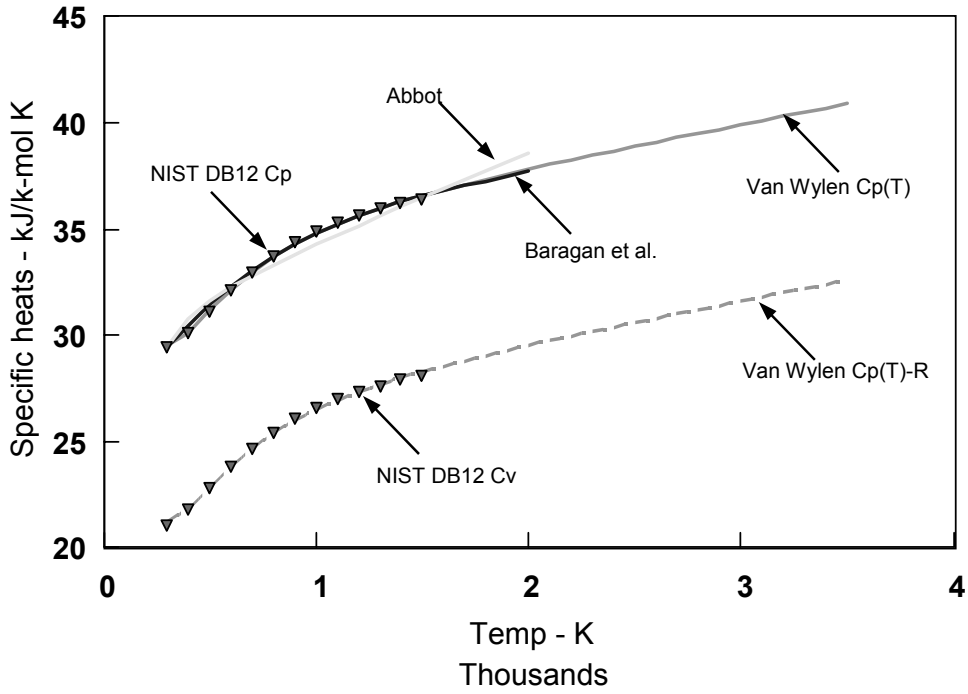

FIG. A-7—*Variations in specific heat of oxygen with temperature.*

(but is not stated) an assumption that because ideal gas of constant heat capacity obeys the relationship $C_p = C_v + R$, that therefore:

$$C_v(T) = C_p(T) - R \tag{A64}$$

Examining the lower curves of Figure A-7, one can see how that $C_v(T)$ compares to $C_p(T)$, the upper curves, at comparable conditions. The dashed upper curve is based on $C_p(T)$ from Van Wylen [***12***] is shown again with R subtracted from it for $C_v(T)$ and the set of symbols overlaid on it are extracted for $C_v(T)$ for real oxygen at atmospheric pressure from NIST DB12. The writer does not know how NIST 12 makes its calculation. Nonetheless the symbols and the Van Wylen curve are in excellent accord. This suggests Equation A64 is correct and is why the approximate calculations can improve the estimate of real gas behavior, *provided the effect of pressure on heat capacity is small*.

One can see that at atmospheric pressure, $C_p(T)$ for temperatures of interest is bracketed by a max and min value for all temperatures of interest to OSPs (That is, up to a few thousand K). In the units most of the equations used (J/lbmolK), the lowest $C_p(T)$ was 29.4 (at T = 300K) and the highest was 40.9 at T = 3500K. Similarly the lowest $C_v(T)$ was 21.1 (at T=300K) and the highest was 32.6 at T = 3500K. Therefore the higher the starting temperature, the lower will be the adjusted relative final adiabatic rise.

The lower specific heat capacity values on Fig A-7 result in γ ratios per equation A53 that are both approximately 1.4. This is the same value at these conditions as the exponent γ used to estimate adiabatic temperature for ideal oxygen in most text books and in ASTM Committee G4 standards. The upper specific heat values result in γ ratios per Equation A53 of approximately 1.25 indicating the magnitude of temperature predictions using a variable heat capacity should be less at higher temperatures, as has been observed.

As a result, when predicting temperatures for this quasi-real oxygen, one would proceed as in the examples for ideal oxygen of constant specific heats (Appendix sections titled *Compression by Vessel Volume Reduction* and *Compression by Vessel Volume Reduction*) in calculating the work energy on the gas as the amount of heat that must be reintroduced into the oxygen. In this case the two equations below apply as they did in Equations A2 and elsewhere (for compression through volume reduction) and Equation A-29 and elsewhere (for compression through gas addition).

$$\int nC_v dT \quad \text{and} \quad \int nC_p dT \tag{A65}$$

However, in this case where the specific heats are not constants, they are functions of temperature. So these become:

$$\int nC_v(T) dT \quad \text{and} \quad \int nC_p(T) dT \tag{A66}$$

Therefore at each step, one would have to insert a suitable formula for $C_v(T)$ or $C_p(T)$ and then solve the integral. The several formulas considered for oxygen so far and exhibited in Figure A-7 are:

From Leslie [***9***] (sourced to Van Wylen and Sonntag [***12***]:

$$C_{po} = 8.9465 + (4.8044 \times 10^{-3}\theta^{1.5}) - (42.679\theta^{-1.5}) + (56.615\theta^{-2}) \tag{A67}$$

For use over the range 540-6300 R, with C_{po} in Btu/lb-mole-R, and θ in T(Rankine)/180.

$$C_{po} = 37.432 + (0.020102\theta^{1.5}) - (178.57\theta^{-1.5}) + (236.88\theta^{-2}) \tag{A68}$$

For use over the range 300-3500 K, with C_{po} in kJ/kmol-K, and θ in T(Kelvin)/100.

From Barragon [***11***]:

$$C_p \text{ (vapor)} = 25.46 + 1.519 \times 10^{-2}T - 0.7151 \times 10^{-5}T^2 + 1.311 \times 10^{-9}T^3 \tag{A69}$$

Yielding results as J/mol K, and the source of the equation is a cited text [***13***].

From Abbott and Van Ness [***41***]:

$$C_p^{ig} = 3.639 + 0.506 \times 10^{-3} \times T - 0.227 \times 10^{5} \times T^{-2} \qquad (A70)$$

where "ig" indicates ideal gas and the results apply to 2000 K, with presumably the same units as above.

These formulae are not challenging to integrate, however once the integral is found, one may find it challenging, or at least onerous, to solve for T_f explicitly. In one case the integral is a fourth power equation. In fact there may not be an explicit solution for T_f for some of them.

One can numerically manually integrate the Equations A65-66 and produce a table. Then use it to look up the starting condition and subtract that starting value from the higher temperature values until a solution is found at each step.

Also, one could approximate the specific heat curve with a simpler (less precise) curve for which it is easier to obtain a simpler explicit integral. And the mathematically astute may have other approaches also.

However, this is not as daunting as it is onerous to the OSP. For oxidant system design usage, sufficient precision is possible with a numerical integration approach using popular spreadsheet software. Divide the pressure or volume interval into segments and treat the gas as ideal over each segment and of locally constant specific heat, where the local specific heat is predicted by the empirical equations of choice. The precision can then be improved to any needed degree by shrinking the segment lengths.

This latter approach was used to estimate the comparable quasi-real gas calculation of Leslie [***9***] and Barragon et al. [***11***] as linear and Log/Log versions both shown in Figure A-8 for $\gamma_i = 1.393$, $\gamma_f = 1.26$ (blue on digital copies), along with ideal gas curves for γ values of 1.4, 1.393 and 1.26 (the latter are bracketing values of γ for the range of specific heats in Fig, A-7), and points are added for the corresponding real gas curve calculated by NIST DB 12. For this "quasi-real" ideal oxygen gas, since the exponent starts out at room temperature at a γ value near 1.393 the initial heating during compression will initially follow the ideal and real gas curves (of slope m = 0.282 on the Log/Log plot). Then as the gas temperature and the specific heats increase, the exponent will decrease as γ decreases and the adiabatic curve will shift towards the bracketing curve of $\gamma = 1.26$ and slope on the Log/Log plot of m = 0.206. The real gas data points fit nicely on the quasi-real approximation for compression at these specific conditions.

This spread sheet approach was also used by Koeller [***10***] in which one assumes the gas behaves as an ideal gas of constant specific heat capacity over small increments of compression and similarly "pipelines" the calculation. Each increment employs a different polytropic exponent suited to its specific interval. In Koeller's case the polytropic equation employed the ratio of specific heats, γ, in assigning the real exponent. This worked well for these conditions and

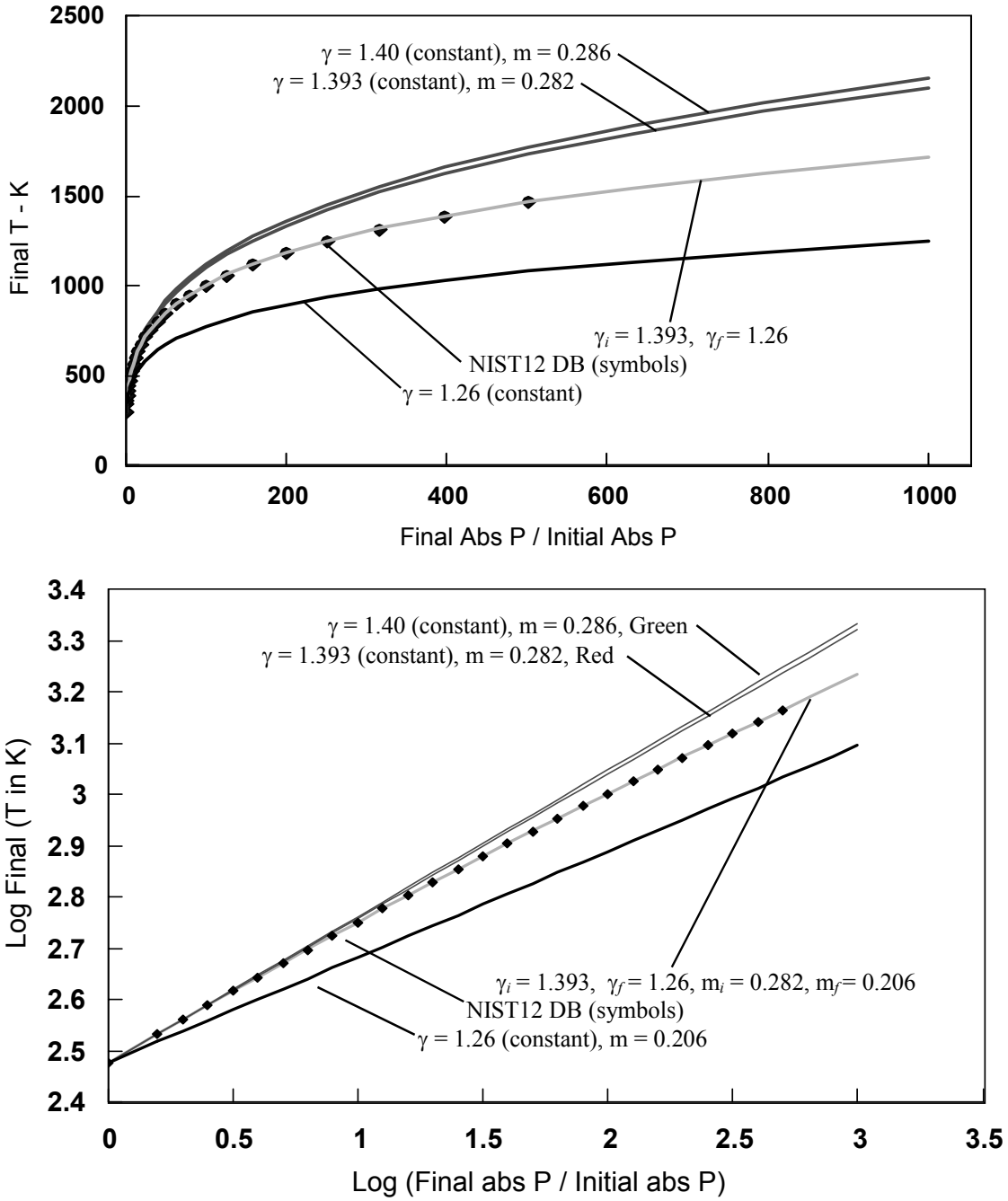

FIG. A-8—*Replication of Calculation in Leslie* [***9***] *and Barragon et al.* [***11***].

others for which $C_P = C_v + R$, but proved a problem for some other conditions. However, in the analysis here the polytropic equation can also use the equivalent derived exponents R/C_p or $R/(C_v+R)$ or $(\gamma-1)/\gamma$. per (Equation A50, A24 and A54, respectively)

The spread sheet that would perform this calculation based on addition employs the equation

$$T_f/T_i = (P_f/P_i)^{R/Cp} = (P_f/P_i)^{R/(Cv+R)} = (P_f/P_i)^{(\gamma-1)/\gamma} \quad \text{(A71)}$$

The pressure interval $(P_f - P_i)$ is divided into k parts each $(P_f - P_i)/k$ long. The k applications of the equation are used each employing the Equation (A66) above with the starting point of each being the end point of the one before it and the value of C_p used to calculate the exponent being the value of $C_p(T)$ at the start of the segment.

As a result the final term of $T_{f(k)}$ is a product (Π) of the form:

$$T_f = T_{f(k)} = \prod [P(_j)/P(_{j-1})]^{R/C_p[T(_{j-1})]} \quad \text{(A72)}$$

Where Π signifies the product and $P_{(j)}$ is the pressure of the j^{th} interval and $T_{(J)}$ is the temperature of the j^{th} interval

This form of product is very easy to convert into a spreadsheet with each cell multiplying against the previous cell result.

The use of a variable specific heat produced a good approximation of real oxygen for starting conditions near atmospheric pressure and room temperature. This is perhaps the most frequent set of starting conditions confronted. However, it is by no means the only starting conditions of interest.

Figure A-9 exhibits a wider range of the $C_p(T)$ and $C_v(T)$ data exhibited in Figure A-7 (which started out at room temperature (300K) from the NIST 12 DB software for the atmospheric pressure starting condition. It also exhibits $C_p(T)$ and $C_v(T)$ data for several other starting pressures and at lower temperatures, and the differences are quite significant. These suggest that $C_p(T)$ is reasonably close at higher temperatures regardless of pressure. Therefore the use of atmospheric pressure $C_p(T)$ is a good approximation of the specific heat that is experienced during common adiabatic compression. The types of estimates reviewed so far should indeed be close to real gas estimates.

However, a "quasi-real" calculation would need to be much more sophisticated if starting conditions at high pressure or low temperature approaching the liquid or supercritical threshold are desired. In this region clearly, $C_P \neq C_v + R$, and the errors of assuming equality can be large. At low temperatures, the C_p rapidly increases towards the condensation point. Would this introduce widely different or spurious estimates? The calculation that would be needed to approximate real gas in these other cases is becoming more complex than has been reviewed so far and would also need to include additional complicating factors related to the properties of real gas (like internal energy) to be reviewed it the next section.

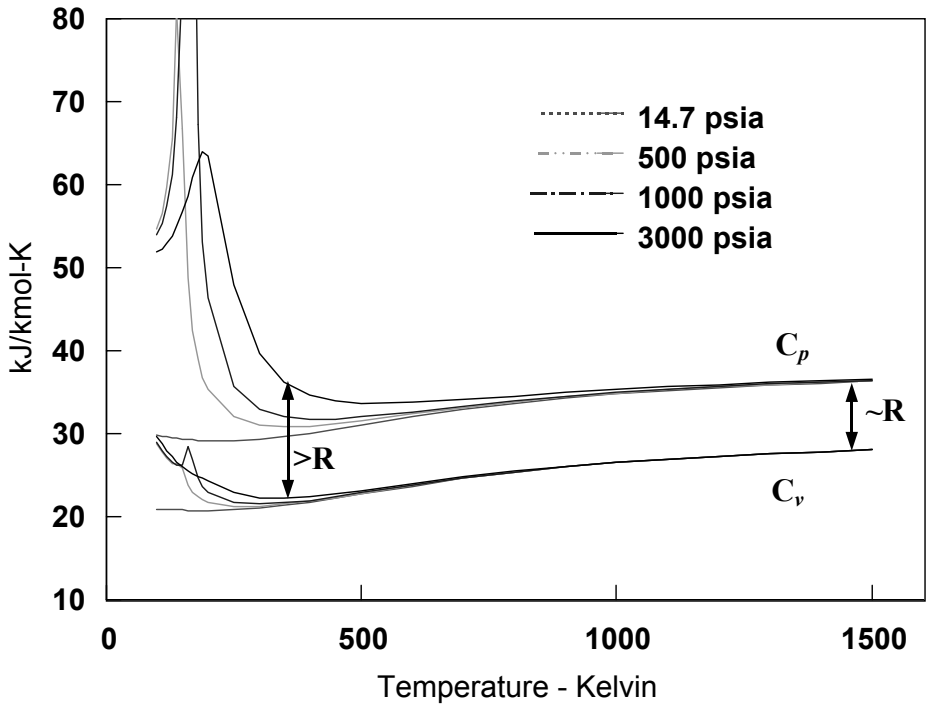

FIG. A-9—*Real $C_p(T)$ Versus Pressure From NIST DB 12.*

Real Oxygen / Everything Variable Case

Real gas apparently breaks the rules for all of the estimates reviewed so far. Specific heat capacities are not constant and they vary not only with temperature, but with pressure, also, especially at low temperatures. The gas is not ideal and does not precisely obey the PV = nRT equation, especially at low temperatures (although in cases at higher temperature is only a little different). Specific heats are not precisely tied to each other therefore, $C_v(T) \neq C_p(T) - R$] although their relation is close in some cases, and as Fig A-9 indicates specific heat varies greatly at lower temperatures and higher pressures. Internal energy is not a function of temperature alone.

In the case of simple compression of atmospheric-pressure room-temperature oxygen, the upper graph of Figure A-10 shows how pressure and volume for isothermal ideal gas differ from the real case based on NIST software. This figure is of the higher pressure, lower volume properties for compression from 14.7 psia and 70°F. *The starting point is far off the left edge of the figure*. The lower group of three curves include one for isothermal ideal gas (green in digital copies) of constant specific heat ($\gamma = 1.4$), which also exhibits constant internal energy.

The curve (red in digital copies) on the upper graph of Figure A-10, which lies just

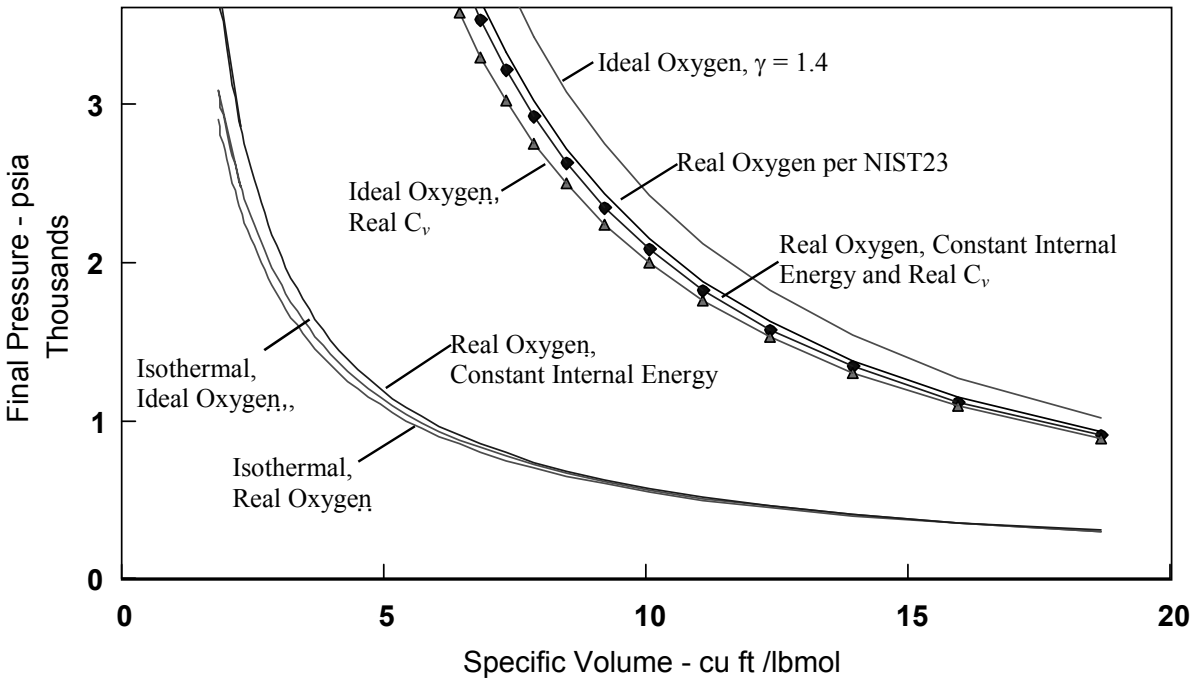

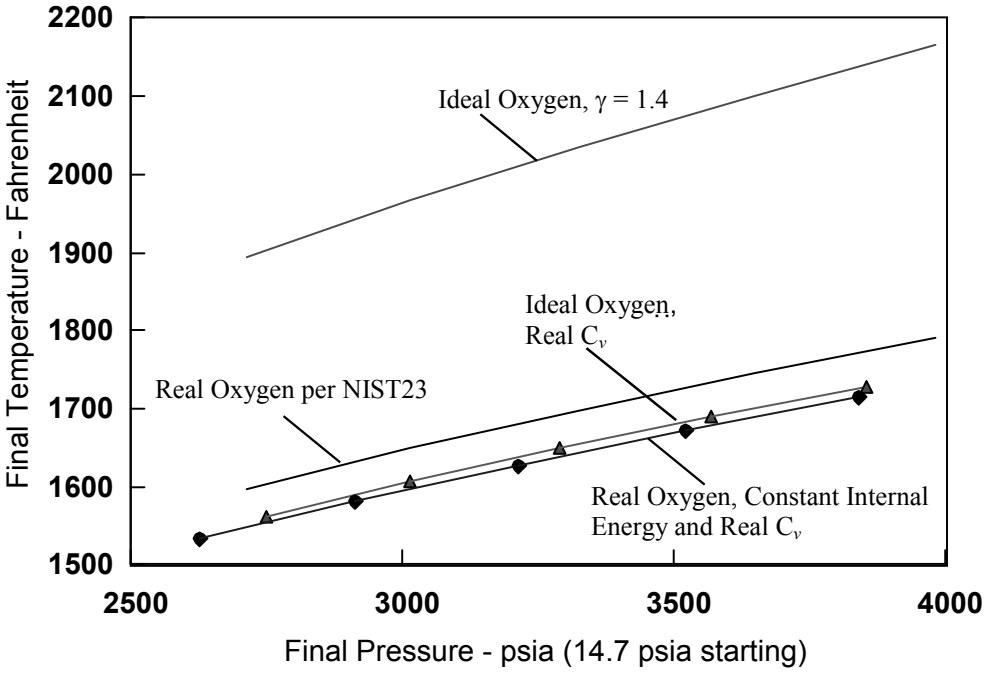

FIG. A-10—*Real Oxygen Calculations Performed Several Ways*.

slightly below the ideal gas curve is for similar isothermal real oxygen per the NIST23 DB. However, this curve does not exhibit constant internal energy. If one were to integrate the work energy below this curve continuously to generate the adiabatic compression as was done in the earlier examples, one would have to also determine the change in internal energy and compensate the result at each increment.

The curve (blue in digital copies) which lies just slightly above the ideal gas curve is for similar real gas of constant internal energy and is from NIST23 DB. This means its temperature is changing as volume decreases, in this case increasing until at 3600 psia it has increased from 70°F to about 1700°F. In this case, integrating the work under the curve would yield a slightly different work energy than for the green ideal gas curve below it and since it starts at a slightly greater temperature, when the work is divided by the local specific heat, it would yield a different resulting adiabatic compression temperature and pressure estimate than would result using ideal gas as a starting point.

The dashed curve (green on digital copies) at the top is the adiabatically compressed ideal oxygen related to the solid ideal-gas curve. This is equivalent under the previous analyses to incrementally integrating the work under the ideal gas curve and re-introducing it continuously into the gas at a constant specific heat (related to $\gamma = 1.4$). A solid (black on digital copies) curve under it is the real compressed oxygen from NIST23 db. The dashed curve (green on digital copies) with triangle symbols is based upon numerical integration (about 30 increments) of the work under the solid real oxygen curve of constant internal energy with re-introduction of the heat into the oxygen using a variable specific heat for real oxygen from NIST23 DB. This yields a result a little lower than the real result. Finally, the dotted curve (blue on digital copies) with circle symbols is the pseudo-real oxygen approximation obtained by numerically integrating the work under the real oxygen curve of constant internal energy but reintroducing it into the oxygen at a variable specific heat consistent with that of real oxygen, and its pressure is a little closer to the "correct" result, probably within the expected error for this type of calculation.

The lower graph of Figure A-10 exhibits the corresponding final temperatures in the neighborhood of 3600 psia for the four calculations with similar color and symbol coding. In this case the ideal gas approximation and constant internal energy (dotted blue on digital copies) approximations are almost identical.

NIST 23 was chosen to facilitate these calculations rather than NIST12 because it allows more flexible extraction of data at constant internal energy.

In this case, we see confirmation for Leslie's [***9***] conclusion that the variations in specific heat are more important to estimating final temperature than is compressibility...at least at his starting conditions. At a 3600 psia final pressure, ideal gas yielded 2092°F, real gas yielded 1739°F, ideal gas with variable specific heat yielded 1693°F, a numerical estimate for real gas yielded 1683°F, and Leslie's empirical formula yields 1752°F.

Real Oxidants and Realism

The body of work examined herein is intended to support guidance and wisdom to Oxidant Safety Practitioners through voluntary consensus safety standards which for forty years, have focused on the ideal gas model. Leslie [***9***], Barragan, et al. [***11***] and Koeller [***10***] sought to explore whether the risk of adiabatic compression of real oxygen differed from the ideal gas model enough to warrant any guidance at all. Clearly their results prove the Ideal Gas Model, as good as it is generally, is not *always* an adequate approximation.

Historically, even the polytropic equation (as applied to ideal-gas, constant heat capacities, adiabatic compression) has been problematic for many to use and led to frequent subtle misuse[A1] . When ASTM Committee G4 published its first standards suggesting the use of the polytropic equation to predict peak heat of compression temperatures, caution led to the inclusion of a table of typical results with it for the most commonly experienced compression (from 70°F, 14.7 psia), and that was later augmented with a PC Utility and example graphs. Leslie's complex calculations were not trivial but did allow for approximating compression for one set of starting condition, and was simplified with a modified polytropic equation.

To make valid quasi-real estimates like Leslie's one needs the heat capacities to differ by the constant, R, yet we have seen that this is not the case for higher pressures and temperatures below ambient. So should OSPs calculate temperatures with the equation of state that Barragan et al suggest, and should they consider more than just peak compression temperatures, branching out as Koeller did?

The calculations reviewed herein are sufficiently onerous that one might do well to, instead, become practiced in the use of the NIST databases, but even the NIST databases include their own set of challenges. However, the pursuit of realism involves the rejection of that which is impractical and begs the question: How best can guidance and wisdom be delivered to the "qualified technical personnel" within the OSP community for use with the diverse skill sets they provide?

This tutorial proposes that three kinds of graphs (similar to, if not in fact, Moliere diagrams) can best serve this purpose. They can be vetted and validated and provided to the community in an existing or new standard, learned readily by the community, and used by the community with minimal risk of subtle misinterpretation. These figures characterize real oxygen by the relationships between temperature and pressure, temperature and volume, and pressure and volume during isentropic (adiabatic) compression. And being based on data for real oxygen from the NIST databases, to the extent that the NIST data are accurate, would prevent some of the flawed estimating that can be so misleading.

. Figure A-11 exhibits a series (a family) of isentropic (adiabatic) curves as log-log plots of data from the NIST12 DB that span the range of temperature as a function of pressure of

[A1] In 1897 Peukert applied an empirical polytropic-like equation to the estimation of lead-acid battery capacity relating capacity to draw rate, draw time and starting capacity. Today there are still web sites that seek to tutor on the use on this equation owing to its continued and frequent misuse.

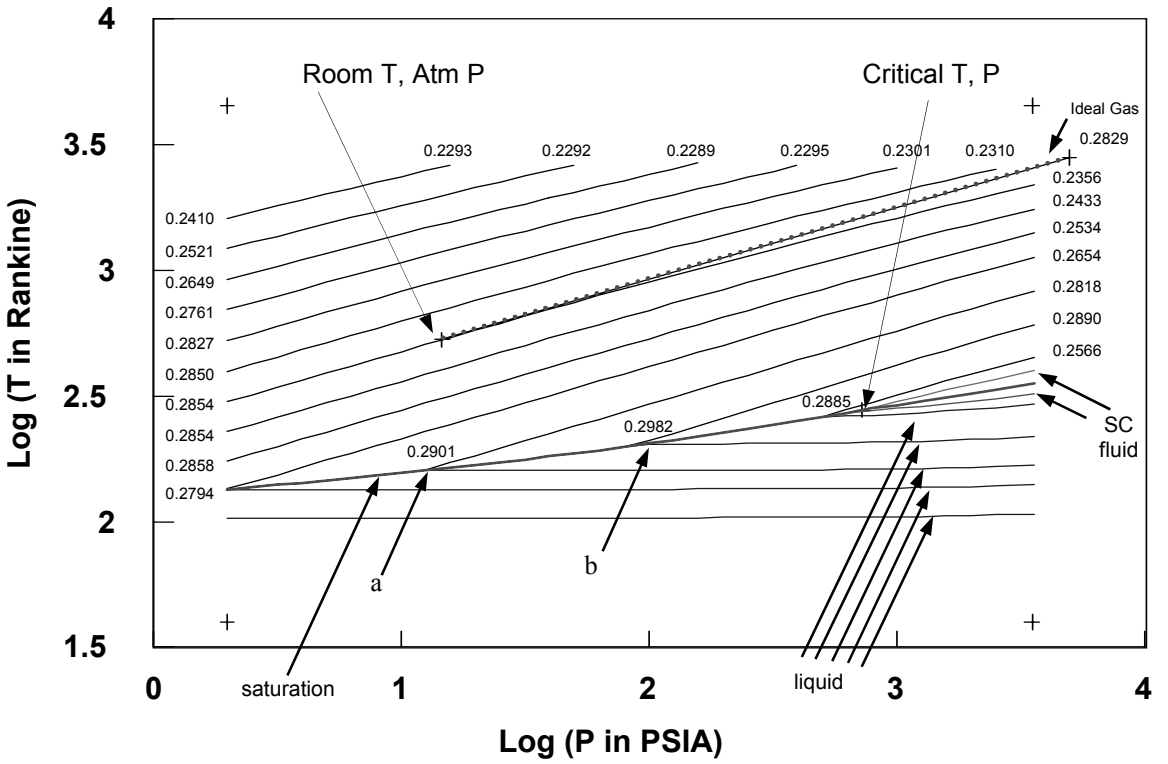

FIG. A-11—*Real-Oxygen Adiabatic Temperature Versus Pressure From NIST12 DB.*

greatest interest today (from approximately 2 psia to 5000 psia, and –360°F to 2200°F). Exhibited are curves for gaseous, liquid, saturated, and supercritical oxygen. Recall that for polytropic-equation data, a straight line relationship results from log-log plots and with real oxygen at high temperatures the slope decreases as the gas heat-capacity increases.

Figure A-11 also flags (1) the starting conditions for 70°F and 14.7 psia, (2) where supercritical oxygen begins, as well as (3) where the ideal-gas oxygen compression example in Leslie [***9***] ends at 5000 psia and 1568 K, forming a straight-line slope (ΔLog T/ΔLogP) of 0.2829.

One can now apply the same approach as Leslie [***9***]. He found that a log-log plot of real pressure and temperature for compression of room-temperature atmospheric-pressure oxygen yielded only slight curvature (the value of the governing exponent and curve slope changed only slightly), and so could be approximated as a straight line with a new weighted empirical exponent. His approximate curve would begin at the room temperature (300K) point and slope upward to the right lying below the ideal gas curve shown om Figure A-11. This same reasoning now suggests that his approach would also work to approximate this entire family of real semi-straight "curves". Indeed, despite the complex way in which the work energy and specific heat capacity and internal energy are varying (even at high pressure and low temperature), the

resulting curves are all remarkably straight segments, even those in the regions where the oxygen is liquid (blue on digital copies) or supercritical (green on digital copies). This means that on average, and to an even greater degree locally, virtually all of these "curves" (line segments) can be approximated as polytropic equations. And therefore, whether or not there is an analysis that relates the exponent involved to γ or other simple or complex parameters, *the same mathematical approach can be used*.

Figure A-11 also shows labels indicating what the value of the empirical polytropic exponent (that is, the slope, m_{TP}, of this log-log temperature-versus-pressure, TP, curve) is locally at the beginning and end of each gas curve. These are the limiting slopes for each curve that is used in the equation:

$$T_f/T_i = (P_f/P_i)^{m_{TP}} \tag{A73}$$

which is analogous to Equation A54.

Indeed the same empirical approach can be used with Figure A-11 to estimate the adiabatic heating of liquid fluid and saturated gas/liquid. Furthermore, when evaluating gas expansion, Figure A-11 visually shows where the process changes as condensation begins at the saturation boundary. These will be covered in detail in a later section. Indeed, one can even avoid the math by simply reading the data and interpolating the curves where great accuracy and precision are not required. The main drawback with this figure is the difficulty of reading log-log plots with sufficient precision and accuracy (and is addressed in the main text).

Notice that for the upper gas curves (black on digital copies, above the saturation curve) at higher pressures and temperatures, where the oxygen is a gas or supercritical fluid:

$$\sim 0.2289 \leq m_{TP} \leq \sim 0.2982 \tag{A74}$$

These values are all close to the ideal-gas value Leslie reported of 0.2829, but the nature of exponential functions is that these variations can still be crucially important.

The lower liquid curves (blue on digital copies) at lower temperatures and pressures where oxygen is a liquid or supercritical fluid have the slope being nearly flat $m_{TP} \sim 0$, but with a small positive slope and the slope is progressively smaller the lower the temperature.

For the regions where oxygen is a transitional supercritical fluid (the triangular region of the curves, green on digital copies, that fans out from the critical point on Figure A-11) ,the curves shown have slopes of much greater variability:

$$\sim 0.03 \leq m_{TP} \leq \sim 0.29 \tag{A75}$$

This "supercritical triangle" is shown in greater detail in Fig A-12. Just as oxygen passing through the boiling point curve goes through a transition from high density to low density, and from high heat capacity to low heat capacity, the "supercritical triangle" exhibits a region in which constant-pressure oxygen goes through its largest, if more diffuse, changes in these same parameters. It is in this region that supercritical fluids most seriously exhibit the unique proper-

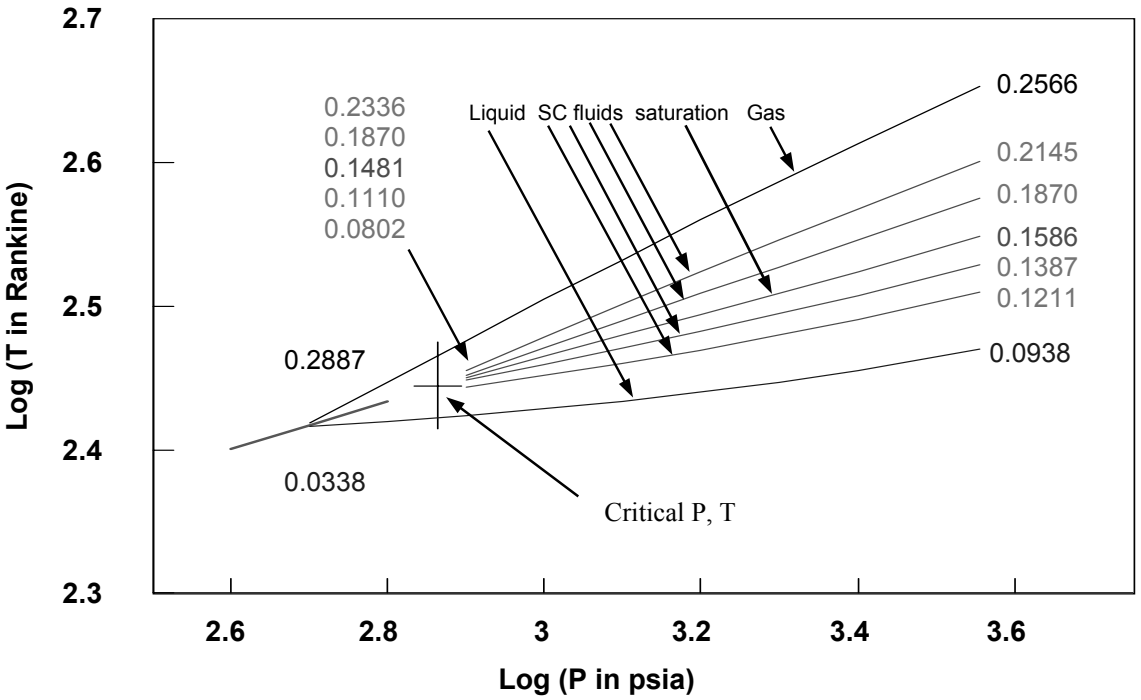

FIG. A-12—*Real-Oxygen Adiabatic Temperature Versus Pressure From NIST12 DB.* (*In Region of Supercritical Triangle*)

ties that make them most interesting for extraction and cleaning and the like.

The exponents and slopes of the gas (black curves on digital copies) are larger than for the liquid (blue in digital copies) curves because the gas compresses more and is therefore affected by more compression-work energy. Above the critical pressure the gas and liquid curves which are then above the supercritical fluid pressure follow the same general trend and have similar properties such as density and specific heat as for the gases and liquids at respective lower pressures. Those among them that also exceed the critical temperature are then considered supercritical fluids having a single phase.

The saturation curve (red in digital copies) represents the boiling point condition up to the NIST12 DB critical pressure of 731.43 psia and critical temperature of -181.424° F. Along this curve there can be both liquid and gas fractions present in any relative degree. The NIST 12 DB does not predict adiabatic compression for starting points along this line because it depends on the relative fraction (the "Quality") of gas to liquid present.

For example, take a gas at the boiling point "a" on Figure A-11. Adiabatic compression would produce a pressure rise along the gas (black) curve at an initial slope (adiabatic exponent) of 0.2901 (it is heating at a rate slightly greater than does room temperature, atmospheric pressure oxygen, albeit from a lower temperature starting point). If the oxygen at point "a" were

liquid, it would produce a much smaller pressure rise along the liquid (blue) curve of initial adiabatic exponent ~0. If there were both liquid and gas present at the correct proportion the pressure would initially increase along the intermediate (red) saturation curve.

If the liquid fraction were large and dominant, the compression of the liquid would heat less than the gas but its large specific heat would swamp the work energy on the gas. As the compression progressed, gas would condense until at some point it would become entirely liquid (for example at point "b"), then the liquid would compress thereafter along a liquid (blue) curve. If that point were indeed to be at "b", then fully liquid oxygen would compress along a curve of initial slope (adiabatic exponent) of ~0 until it achieved its final pressure.

If the gas fraction at "a" were large and dominant, the compression heating of the gas would swamp the liquid specific heat. As the compression progressed, liquid would evaporate until at some point it would become entirely gas (for example at point "b"), then the gas would compress thereafter along a gas (black) curve. If that point were indeed to be at "b", then the fully gaseous oxygen would compress along a curve of initial adiabatic exponent of 0.2982 until it achieved its final pressure.

If the ratio of gas-to-liquid were in just the right range, then the adiabatic compression would track the saturation (red) curve to the point of supercriticality. In this case, as the two components passed through the supercritical threshold, the ratio of gas-to-liquid would dictate whether the resulting supercritical fluid would track along a higher supercritical fluid (green) curve (lower density and specific heat and higher slope) or lower supercritical fluid (also green) curve (higher density and specific heat capacity and lower slope),or even (if just right) track along the satruation (red) curve which follows the condition near the peak specific heat (as is the case for the red curve below the critical point).

Figure A-13 exhibits fluid-quality data from the NIST12 DB to show how this proceeds. Nine curves are shown from Figure A-11 and quality data are exhibited for five pressures on each. The quality data are the fractional amount of oxygen in the gas state. At 2 psia, all nine curves have the same pressure and temperature. Curve 1 (C1) is completely gaseous (Quality equals unity), and Curve 9 (C9) is completely liquid (Quality equals zero). The seven intermediate curves (C2-C8) represent mixtures having both gas and liquid present.

As curve 1 is compressed it remains gaseous up to the 501 psia point and finally achieves a temperature of about 668°F at the final pressure shown, a temperature that might prove hazardous in some oxygen systems. This final point is technically a supercritical state.

As curve 9 is compressed it remains liquid up to the final pressure point and finally achieves a temperature of about –319°F, a temperature that is only about 6F° greater than it was initially. Although above the critical pressure, it is not above the critical temperature to qualify as supercritical in the NIST DB.

At approximately 12.6 psia, Curve 2 has gone from 89.3% gas to 100% gas and then compresses further as a gas to a final temperature of about 370°F. Curve 8 has gone from about 9.6% gas to 0% gas (completely liquid) and then compresses as a liquid to a final temperature of about –292°F.

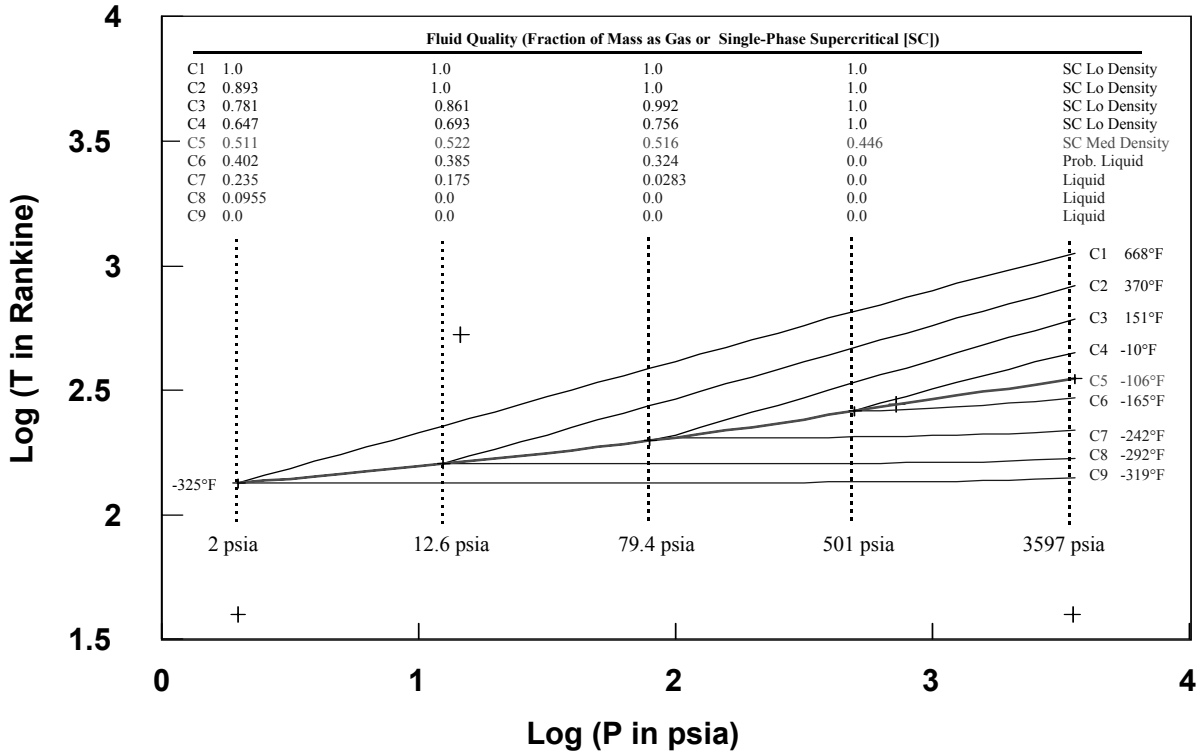

FIG. A-13—*Real-Oxygen Quality During Adiabatic Processes From NIST12 DB.*

At approximately 79.4 psia, Curve 3 has gone from 78.1% gas to 86.1% gas at 12.6 psia, and then to 99.2% gas. It soon becomes complete gas and compresses further as a gas to a final temperature of about 151°F. Curve 7 has gone from about 23.5% gas to 17.5% gas at 12.6 psia and then to 2.8% gas (nearly completely liquid). It soon becomes completely liquid and compresses as a liquid to a final temperature of about –242°F.

At approximately 501 psia, Curve 4 has gone from 64.7% gas at 2 psia to 69.3% gas at 12.6 psia, to 75.6% gas at 79.4 psia, and then to 100% gas. It compresses after that as a gas to a final temperature of about –10°F. Curve 6 has gone from about 40.2% gas at 2 psia to 38.5% gas at 12.6 psia to 32.4% gas at 79.4 psia and then to 0% (completely liquid) at 501 psia. After that it compresses as a dense single phase and supercritical fluid to a final temperature of about –165°F.

Curve 5 follows the saturation (boiling point) curve beginning as 51.1% gas at 2 psia, to 52.2% gas at 12.6 psia, to 51.6% gas at 79.4 psia, and to 44.6% at 501 psia. After that it becomes a supercritical fluid and follows an extrapolated curve close to the conditions of maximum heat capacity ending at a final temperature of –106°F.

Although most of the conditions depicted would not be of major fire concern to an

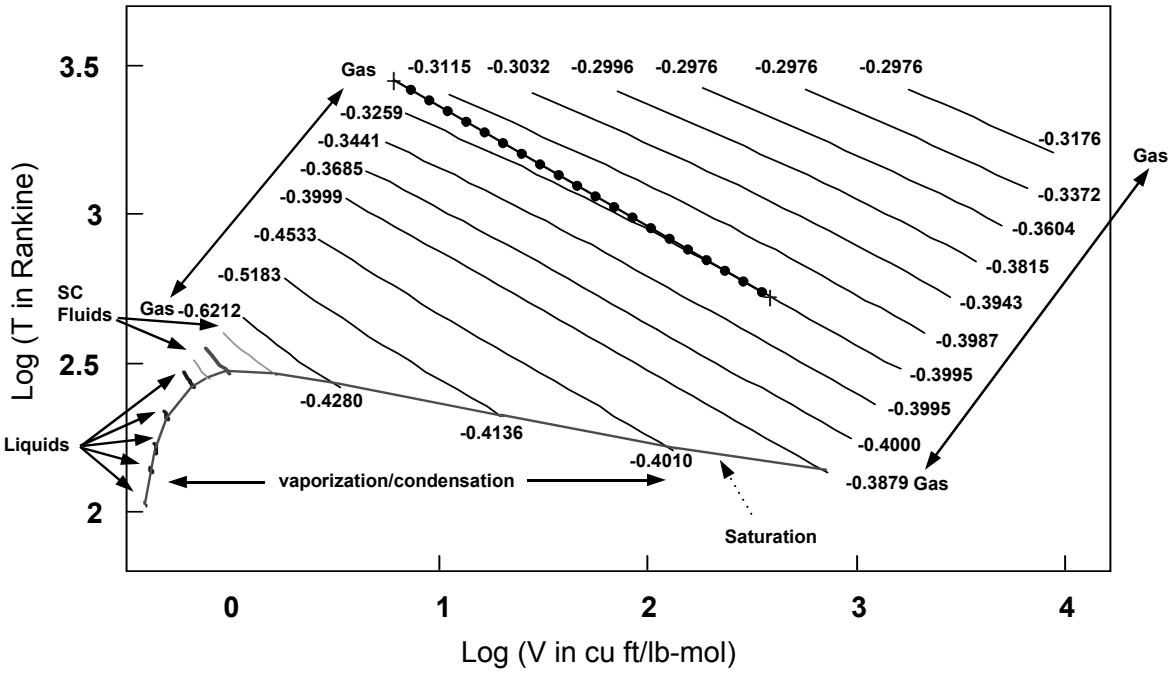

FIG. A-14—*Real-Oxygen T vs.V During Adiabatic Processes From NIST12 DB.*

OSP, because oxygen has a low-temperature boiling point and critical point, other oxidants and diluents may be of more concern.

The Analogs

The previous section concentrated on the real relationship between temperature and pressure during adiabatic compression, ultimately justifying the empirical Equation A73 while surmising that where the curve is relatively straight or over short portions that are reasonably straight, the exponent is defined by its slope: m_{TP}. This relation allows one to estimate peak temperature when pressurizing a system by adding gas. However, The compressed gas volume is also changing and one might be interested in the relation between volume and temperature and finally between the pressure and volume

Figures A-14 and A-15 are the exact same data points as for Figure A-11 in combination with volume data from the NIST 12 database that were used to produce Figure A-11. Also indicated on each are calibrations points for 70°F, 14.7 psia, the critical pressure and temperature of oxygen, and the adiabatic ideal gas compression point used by Leslie [***9***] of 5000 psia, 1568 K (2822°R).

Notice both figures have fairly straight lines for the temperature/volume and pressure/

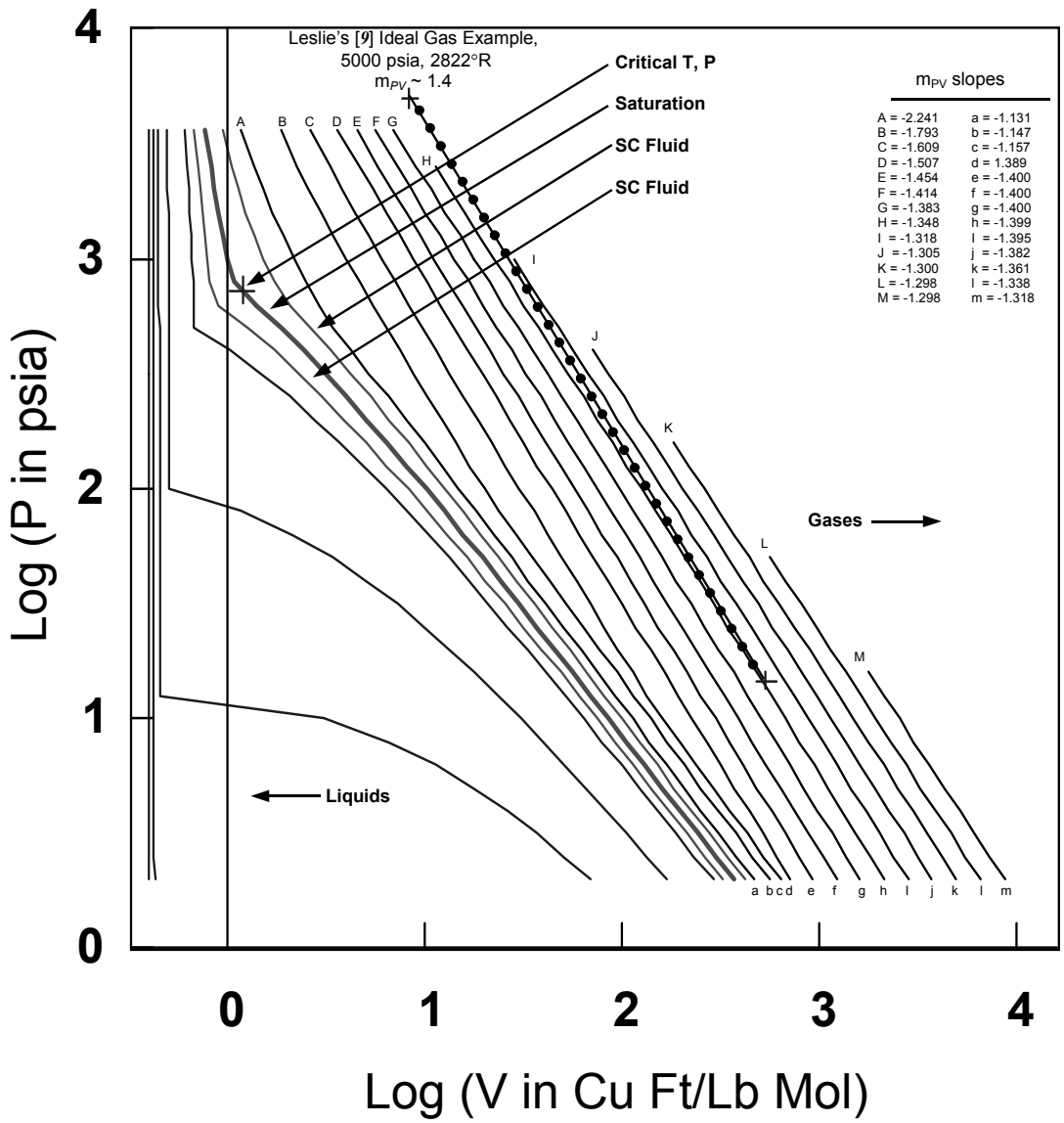

FIG. A-15—*Real-Oxygen V vs.P During Adiabatic Processes From NIST12 DB.*

volume curves where gas is present, respectively, that correspond to the fairly straight temperature/pressure gas curves of Figure A-11.

On Figure A-14, the slope of the ideal gas curve is given by the exponent of Equation (3) (calculated as $1-\gamma$, and in Leslies' example would be -0.395) and the empirical approximation variable related to any two points between (V_i, T_i) and (T_f,V_f) is m_{TV} which in some re-

gions may is very close to -0.395. Local values of m_{TV} are shown at the ends of the gas curves on Figure A-14 (black on digital copies).

Similarly, on Figure A-15, the slope of the ideal gas curve is given by the exponent of Equation (1) (calculated as $-\gamma$, and in Leslie's example would be –1.395) and the empirical approximation variable related to any two points between (P_i,V_i) and (P_f,V_f) is m_{PV} which in some regions may is very close to –1.395. Local values of m_{PV} are shown at the ends of the gas curves on Figure A-15 (black on digital copies).

For ideal gas of constant heat capacity (and $\gamma \sim 1.4$) and the real oxygen data herein, the following are analogous:

Ideal Gas, Const C_p, C_v	**Real Fluid, Empirical**
$T_f/T_i = (P_f/P_i)^{(\gamma-1)/\gamma}$	$T_f/T_i \sim (P_f/P_i)^{m_{TP}}$
$T_f/T_i = (V_f/V_i)^{(1-\gamma)}$	$T_f/T_i \sim (V_f/V_i)^{m_{TV}}$
$P_f/P_i = (V_f/V_i)^{-\gamma}$	$P_f/P_i \sim (V_f/V_i)^{m_{PV}}$

Although ideal oxygen with constant heat capacity allows all three adiabatic exponents to be expressed in terms of the single constant γ, no similar number can construct the three approximation adiabatic exponents. But there is a relation among them.

Figures A-11, A-14 and A-15 are constructed from the exact same data point sets. For example, the end points of each respective curve relate to the same sets of P, V, and T. Hence for any two points: $(P_i,V_i,T_i,)$ and $(P_f,V_f,T_f,)$ and given the relationships for the Real Fluid, Empirical entries above:

$$T_f/T_i \sim (P_f/P_i)^{m_{TP}} \quad \text{(Eq. A73)}$$

$$T_f/T_i \sim (V_f/V_i)^{m_{TV}} \quad (76)$$

$$P_f/P_i \sim (V_f/V_i)^{m_{PV}} \quad (77)$$

Taking the logarithms:

$$\text{Log } T_f/T_i \sim m_{TP} \text{ Log } (P_f/P_i) \quad (78)$$

$$\text{Log } T_f/T_i \sim m_{TV} \text{ Log } (V_f/V_i) \quad (79)$$

$$\text{Log } P_f/P_i \sim m_{PV} \text{ Log } (V_f/V_i) \quad (80)$$

And eliminating $\text{Log } T_f/T_i$ from the first two yields:

$$m_{TP} \text{ Log } (P_f/P_i) \sim m_{TV} \text{ Log } (V_f/V_i) \quad (81)$$

$$\text{Log } (P_f/P_i) \sim m_{TV}/m_{TP} \text{ Log } (V_f/V_i) \quad (82)$$

Therefore,

$$m_{TV}/m_{TP} \text{ Log } (V_f/V_i) \sim m_{PV} \text{Log } (V_f/V_i) \quad (83)$$

And

$$m_{PV} \sim m_{TV}/m_{TP} \quad (84)$$

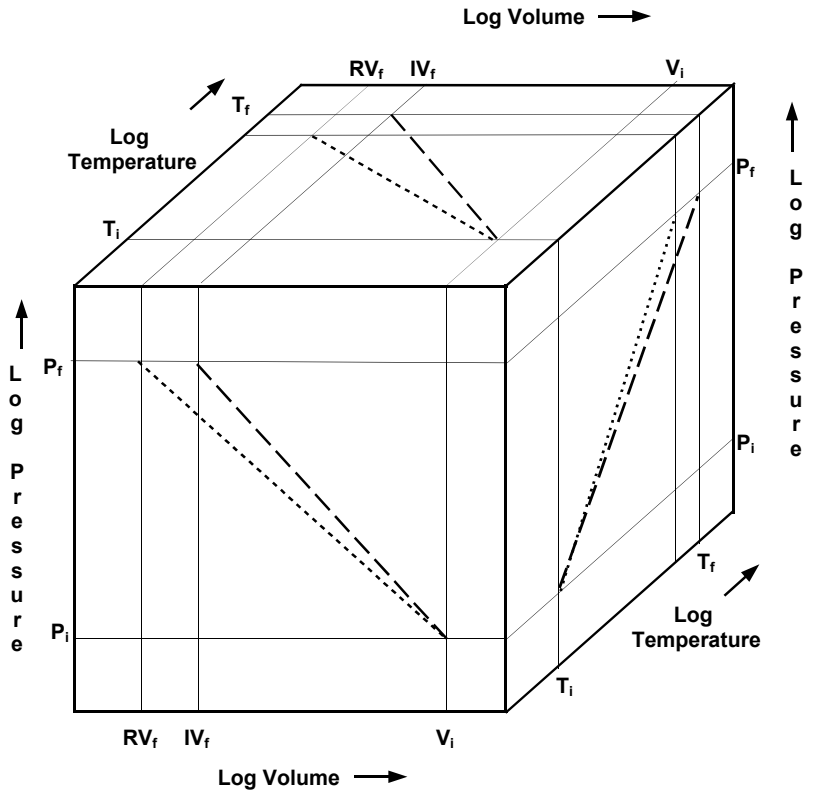

FIG. A-16—*Relationships among* m_{PV}, m_{TV}, and m_{TP} .

Figure A-16 exhibits the relationships between the three slopes three-dimensionally. Any two can predict the third but the three can not be based on a single parameter, except for those cases where $C_p = C_v + R$, for which the ratio $C_p/C_{v=}\gamma$ ties all three together as cited in Equations (1), (2), and (3).

Correction: Mea Culpa

In the 2007 versions of this tutorial, This commentator naively drew an analogy to the effect that for real oxygen (and elsewhere in this tutorial for other real materials), the tutorial should refer to the controlling empirical parameter as the "adiabatic exponent" (AE) and structured it in analogy with that for ideal gas. It also used the diphthong, Æ (pronounced as a long A with an E flavor as in "maelstrom"), to represent it in equations. As a result, γ, was a parameter that was used to approximate Æ. Hence locally and to a lesser extent generally, by analogy to equations A56, A54, and A55 and others:

$$P_i V_i^{Æ} = P_f V_f^{Æ} \qquad \text{(A85)}$$

$$T_f/T_i = (P_f/P_i)^{(Æ-1)/Æ} \quad \text{(A86)}$$

$$T_f/T_i = (V_f/V_i)^{(1-Æ)} \quad \text{(A87)}$$

Figure A-11 listed approximate starting and ending Æ for each straight curve segment and Æ was cited in analyzing numerous scenarios. *It now appears analogy was an incorrect tactic to apply*. This section now (2016) seeks to correct this and other potential lesser errors.

The Bottom Line

The mathematics applicable to estimating maximum gas temperature produced during adiabatic compression vary in complexity and subtlety. Often the most common estimates are adequate (and conservative) to design safe oxygen systems. However there are cases where the errors are important. The writer concludes that when considering the range of skill sets among oxygen safety practitioners, the most practical approach is to vet, validate and provide capsule views of real oxygen behaviors akin to those presented in Figure A-11, A-14, and A-15. These allow qualitative understanding and along with a suitable methods to read the temperature with adequate accuracy and precision, such as large fold-open graphs, high-definition graphic files, or computer algorithms, can provide a robust quantitative understanding.

Appendix B

Additional Math

This appendix addresses related calculations that are based on or incorporate those techniques in Appendix A. These following calculations mimic the series performed by Koeller [***10***] and specifically examines the use of the parameter real γ. Since adiabatic compression and expansion can also be extracted directly from software such as the NIST DBs (by specifying isentropic conditions and choosing the entropy at the initial conditions to specify for the starting parameters). Hence the use of spreadsheet analysis is not crucial. However, for some of the following calculations the results are not thermodynamic properties or do not solve in closed form and hence spreadsheet calculations are quite useful. To this end, some equations are assessed for their abilities to be pipelined in a spreadsheet analysis.

Adiabatic Expansion

Adiabatic expansion is the reverse of compression. All of the math is analogous and therefore the use of real γ is acceptable for these cases where $C_p = C_v + R.$. There are issues related to the handling of supercritical, two-phase and condensing fluids but these are addressed in detail in the earlier parts of the text and appendices.

In analyzing real-versus-ideal expansion, the starting points coincide at the higher pressure point and then may diverge as the pressure decreases.

Spreadsheets based upon real γ can often break the expansion into smaller expansions and pipeline the calculation in which the starting point for each increment is the ending point for the previous increment and each increment applies the real γ that is appropriate to the specific interval. Each approach includes the effect of variations in specific heat.

Adiabatic expansion can also be estimated with an empirical polytropic equation using Figures A11 and A12 (to estimate the correct $m_{TP)}$ for the case of greatest interest (T vs. P) by taking the initial condition to be to the right of the final condition. It can also be estimated for the cases of Figures A14 (T vs. V) and A15 (P vs.V) by taking the initial condition to be at the higher pressure point and reading the respective slopes M_{TV} and M_{PV}.

NIST12 DB has a built-in procedure for generating tables and plots of temperature and pressure for any value of entropy. The entropy can be determined from any point in the expansion.

Distance/Volume Piece Design

Distance/volume piece design is a case of adiabatic gas compression [***24***]. In final slug containment (FSC) designs, one starts with an initial gas slug that fills a system (typically a polymer-lined hose and upstream fittings) to which a fire-resistant end-piece is attached that

also contains the gas, and then one compresses both the gas in the hose and end piece into the end piece. The end-piece volume is chosen so that the entire hot gas slug at the final pressure will fit into the end-piece with a safety factor to spare. Absent buoyancy and percolation, the end piece then absorbs the heat of compression and protects the hose. As the gas slug cools, its shrinks and recedes even further into the end-piece.

Sometimes there are end-pieces required on both ends of the hose and so the volume of gas in the hose and in both end pieces must all be compressed into one of the end pieces at the final pressure. The derivations of these cases are from the polytropic pressure/volume equation (1). Therefore (since $-\gamma$ is analogous to m_{PV}) substitution of empirical $-m_{PV}$ for ideal γ is appropriate in both as follows:

Single Ended Case:

Replace: $V_{DVP} = k(V_u+V_h)/[(P_f/P_i)^{1/\gamma} - k)]$ with $V_{DVP} = k(V_u+V_h)/[(P_f/P_i)^{-1/m_{PV})} - k)]$ (B1)

Double Ended Case:

Replace: $V_{DVP} = kV_h/[(P_f/P_i)^{1/\gamma} - 2k)$ with $V_{DVP} = kV_h/[(P_f/P_i)^{-1/m_{PV}} - 2k)$ (B2)

Where in both
V_{DVP} = Volume of distance/volume piece
k = safety factor as a fractional final volume
V_u+V_h = volume of hose and upstream hardware (not including DVP)

A major problem with FSC-designed DVPs is that the required DVP volume increases with *decreasing* final pressure. If a DVP is designed to contain the final slug of a gas compressed to a pressure, P, it will be too small to contain the final slug if the pressurization is stopped at any lower level. And for even a minor incremental pressure change, where the risk is negligible, the DVP volume specified is the maximum, and may even be larger than the hose.

In Temperature Controlling (TC) designs, one starts with an initial gas slug that fills a system (typically a polymer-lined hose and upstream fittings) to which a fire-resistant end-piece is attached that also contains the gas, and then one compresses both the gas in the hose and end piece(s) into the endpiece. The end-piece volume is chosen so that when the entire initial gas slug is compressed to a specified temperature, it will fit into the end-piece with a safety factor to spare. Absent buoyancy, and percolation, only the end piece is then exposed to temperatures at-and-above the threshold elevated temperature, and it absorbs the heat of compression and protects the hose. As in the previous case, sometimes there are end pieces required on both ends of the hose and so the volume of gas in the hose and in both end pieces are all compressed into one of the end pieces. The derivations of these are from the polytropic temperature/volume equation (3). Therefore (since $1-\gamma$ is analogous to m_{TV}) substitution of empirical $(1- m_{TV})$ for ideal γ is again appropriate in both as follows:

$$\text{Single Ended Case: } V_{DVP} = [V_u + V_h] X /[(1/k) - X)] \quad \text{(B3)}$$

$$\text{Double Ended Case: } V_{DVP} = V_h X)/[(1/k) - 2X)] \quad \text{(B4)}$$

Where in both,
V_{DVP} = Volume of distance/volume piece
k = safety factor as a fractional final volume
$X = [T_i/T_L]^{[1/\gamma -1)]} = [T_i/T_L]^{[-1/m_{TV}]}$ for polytropic analysis where:
empirical $(1\text{-}m_{TV})$ has been substituted for γ, or alternatively,
$X = V_L/V_i$ where,
from a suitable database, V_L and V_i are the specific volumes of oxygen at T_L and T_i, respectively during isentropic compression .
T_i = Initial absolute temperature
T_L = Limiting absolute temperature

If the final temperature does not exceed the threshold temperature, no DVP is needed. This approach solves the major problem with FSC designs, in that it provides dimensions that are correct for every contingency. However, these TC designed DVPs do suffer in that the size of DVP required increases dramatically with increasing initial temperature. There actually comes a point where for an initial temperature below the threshold limit but approaching the threshold limit, it is not physically possible to install a large enough DVP to contain the pressurized gas, because the DVP adds initial volume faster than it contains the compressed volume. Therefore there are clear initial temperatures for which one cannot protect against compression hazards, among these are the degenerate cases where the starting temperature is above the limit temperature.

The four Equations, B1 to B4, do not pipeline in spread sheet analysis, as such. If one divides the pressure interval or temperature interval into segments and applies the equations to the first segment, the result is a DVP value. To calculate the second segment requires input values to be the final condition of the first segment. For Equations B-1 and B-2, the necessary data are the volume of the combined gas slug at the end of the first segment. In the case of the Equations B3 and B4, it requires the temperature of the combined gas slug at the end of the first segment. None of these are provided.

Since both types of designs involve straight forward compression, pipelined spread sheet estimates are possible based on empirical data or γ as appropriate. In the case of the preferred TC designs, in which the ratio of the specific volume at the limit temperature to the specific volume at any initial temperature ($V_L/V_i = X$) is calculated and then length or volume of the required DVP including safety factor as a function of hose volume is calculated using Equation B3 or B4 as needed.

Similarly, data from NIST12 or NIST 23 DB can be used for the calculation, and one needs the starting molar volume at the initial temperature and can then extract an isentropic fi-

nal molar value at the limit temperature and then apply similar calculation using Equations B3 or B4 to obtain the final DVP length or volume as a fractional multiple of the hose volume including a safety factor.

For both design types, figures based on these methods are presented and discussed in the main text (and a PC algorithm similar to that already proposed could be developed to help extract the actual data).

TNT Equivalency

Mechanical TNT equivalency is often taken by OSPs as the maximum adiabatic work that an expanding fluid can accomplish [***25***]. When there is combustion in an expansion, there can be cases where hot materials such as particles can be in good heat transfer and can produce heating and a greater amount of work from the fluid, but in the cases of interest here, the adiabatic work absent combustion is a practical limit. Following the release of a fluid at pressure, adiabatic expansion is assumed. The gas can do work on itself, and it can do work on its environment. If the ambient is a vacuum, all of the work will be accomplished on the gas itself. The typical calculation is integration of the pressure with volume. When an incident has resulted that is consistent with a certain energy release, then precise calculations may be needed to ensure that the candidate hypothesis would produce the required damage as a minimum.

A previous analysis the writer participated in was based on the polytropic equation (1) and produced several appearances of the parameter γ in the TNT equivalency equations. This yields the equations:

$$E = \int PdV = [(1/\gamma\text{-}1)]\ [(P_iV_i) - (P_fV_f)] \tag{B5}$$

And when released into a background pressure (typically atmospheric pressure, P_a:

$$E = \int PdV - \int P_a dV = \{[(1/\gamma\text{-}1)]\ [(P_iV_i) - (P_fV_f)]\} - \{P_aV_i[(P_i/P_f)^{1/\gamma} - 1]\} \tag{B6}$$

$$\text{Or, } E = \{[1/(\gamma\text{-}1)]\ [(P_iV_i) - (P_f{}^{([\gamma-1]/\gamma)}\ V_iP_i{}^{1/\gamma})]\} - \{P_aV_i[(P_i/P_f)^{1/\gamma} - 1]\} \tag{B7}$$

Substitution of real γ (where $C_P = C_V + R$) for γ would be appropriate. However substitution of the negative of the real empirical slope, $-m_{PV}$, from Figure 7 for γ is always preferable and yields the Equations (20-22) in the main text..

These equations are valid wherever real γ or γ are constant or where a reasonably average or weighted value is inserted. Values to insert can be chosen using Figure 7 or data directly from a thermo database. When γ is variable (but still conforms to $C_P = C_V + R$), or when $-m_{PV}$ is being used the calculation can be pipelined by breaking the pressure range into segments and using the output of each segment as the input for the next segment, however, the end point must be calculated separately.

In the case of TNT equivalencies, very often to the point of being common, the initial temperature of a vessel will be near room temperature. In this case, if the vessel pressure

is sufficient, then adiabatic cooling in the fluid during expansion can at some point produce fractional liquefaction of the fluid. And as the fluid converts to liquid, any liquid produced yields a reduction in the pressure and is often taken to reduce expansion thereafter. *However this does not terminate the energy release* ***and in some cases liquid can have greater release***. than ideal gas predictions.

Therefore, when one does TNT equivalencies along adiabats shown on Fig 7, if the initial temperature is high (for expansions beginning to the upper left region) then the average exponent (real- or ideal-γ ,or $-m_{PV}$) may be inserted into the equation to obtain reasonable results. When an adiabat is used that intersects the vapor/liquid saturation curve (red on digital copies), then the calculation should be broken into two portions at that point, one a first stage in which the fluid is expanded along the respective (black on digital copies) gas curve with an exponent given for the upper portion of the curve) and a second expansion in which the exponent reflects the slope of the vapor/liquid saturation curve (red on digital copies). Furthermore for expanding fluid in the hybrid supercritical transition, the appropriate γ would apply until the critical point was reached, then the γ for the saturation curve would apply. Note that in some cases, when the fluid passes through the critical point, *the value of* γ may actually change to *increase* the energy release per unit volume. Since there is a small curvature to the saturation curve, more precise calculation may factor in several γ values along the saturation curve or a pipelined calculation.

However, Equations (B5-B7) do not allow for pipelined calculations directly. To pipeline, one must use the output conditions from the segment as the input conditions for the next segment. Equations (B5-7) do not provide end-point pressures. However, one can estimate endpoints using Figures 4-7 and the related algorithm can help establish both the "bendpoint" pressure and values of γ.

Perhaps, the best way to estimate TNT equivalency may be to perform real-fluid calculations using the NIST databases, during an adiabatic process, any work done on or by the fluid is reflected in a change in internal energy. One enters the initial conditions of pressure and temperature and obtains the range of initial properties including the initial and therefore constant entropy. Then one enters the initial entropy and final pressure and obtains the range of final properties. Since heat transfer is taken as zero, the energy released, the real PdV integral is given as the change in internal energy. Data reported in the main discussion take this approach and consider its applicability at various pressures, including where condensation and/or flash may occur.

Maximum Achievable Velocities

In calculating maximum achievable velocity, the potential energy of pressure is converted into the kinetic energy of a gas stream. In calculating the total pressure of a moving gas stream, the kinetic energy of the stream is converted into the potential energy of pressure. The same equation and analysis applies for both with the independent and dependant variables reversed.

Previously derived equations [***4, 5***] for these calculations were based on three terms. Work done by the upstream pressure, work done by the gas on itself and work done by the gas on the downstream system. The work done on itself was predicted using the previously derived equation for the TNT equivalency of a gas in vacuum. That equation incorporated a constant γ for ideal oxygen gas and therefore, since real γ (when $C_p = C_v + R$) is a suitable replacement for it, the γ present in the equations that were derived may also be replaced with γ for real gas. Those equations would then take the following forms.

In Reference [***5***], Max. Achievable Velocity is given in its Equation (14) as:

$$v_d = \{[(2/m)(P_u V_u - P_d V_d)[\gamma/(\gamma-1)]\}^{0.5} \qquad \text{(B8)}$$

In this case one is interested in how velocity varies in a system with a fixed and constant up-stream pressure at a constant upstream temperature and a variable lower downstream pressure. Therefore, this equation can be simplified. One can use the relationships $P_u V_u^{\gamma} = P_d V_d^{\gamma}$ and $P_d V_d = nRT_d$ and some units conversion to reduce this to:

$$v_d = \{10.73 \times 2 \times 144 \times T_u [\gamma/(\gamma-1)][\, 1 - (P_d/P_u)^{[(\gamma-1)/\gamma]}]\}^{0.5} \qquad \text{(B9)}$$

Where v_d is in f/s, and T_u is in °R. These equations are both acceptable for use with real- or ideal-γ values over intervals where they are constant or over intervals where a reasonably constant average value is taken. *Caution: they are not acceptable for use in doing pipelined spread sheet calculations with variable* real- or ideal-γ *to approximate real gas where* $C_p \neq C_v + R$). Since the velocity is related to the ∫PdV work being done, γ may be replaced by $-m_{PV}$ values taken from Figure 7 or a suitable database for improved real gas estimates.

When using the Equations (B-8 and (B-9), there is an assumption that the interval over which they are applied begins with a zero gas velocity. Therefore in dividing up any range of input values, one cannot use the output of the first interval (which will be nonzero) as the input for the second interval which is taken as zero.

In the case of a real-gas analysis using a thermo database, one would follow the math steps as worked through in the earlier papers [***4, 5***]. In that analysis, there are three nonzero contributors (algebraic terms cited as Stage 2, Stage 3 and Stage 5) to the maximum velocity that a pressure differential can produce.

The Stage 2 term is the work done on an arbitrary gas slug by the upstream pressure, $P_u V_u$. The Stage 3 term is the work the slug does on itself during an expansion. This Stage 3 work is the same as the energy that would be calculated to estimate a TNT equivalency for an explosion in vacuo. And the Stage 5 work is the work the gas slug must do on the downstream gas pressure, $P_d V_d$. The sum of Stage 4 and Stage 5 are the same energy term that would be used to estimate the TNT equivalency of the expanding slug in an ambient pressure equal to the downstream pressure. In the previous section on TNT equivalency, the last term was taken as atmospheric pressure.

The maximum final kinetic energy of the slug is the sum of the three terms. Therefore a real-oxygen analysis would insert the real oxygen adiabatic expansion (the internal energy change) between the two pressures from a NIST or other DB to the Stage 2 and Stage 5 terms and equate it to the kinetic energy term, $mV_d^2/2$, from which the velocity can be solved.

Total Pressure

In calculating the total pressure of a moving gas stream, the kinetic energy of the stream is converted into the potential energy of pressure. Equations (B8-9) are again applicable and uses the same analysis. In this case the pressure corresponding to P_u is the total pressure P_T, and the pressure corresponding to the pressure, P_d is the incident pressure P_i

Rearranging Equation B-8 yields:

$$P_T / P_i = [(v_i^2[\rho_i/2g_c(\gamma/(\gamma-1))P_i] +1\}^{\gamma/(\gamma-1)} \quad \text{(B10)}$$

In this case, one is perhaps most interested in how the total pressure (the stagnation pressure) varies in a system with a fixed and constant incident pressure at a constant incident temperature and a variable incident velocity. Therefore this equation can be simplified. One can use the relationships $P_T V_T^{\gamma} = P_i V_i^{\gamma}$ and $P_i V_i = nRT_i$ and some units conversion to reduce Equation B9 to:

$$P_T / P_i = \{[v_i^2 x(\gamma-1)/(10.73x2x144xT_i x\gamma)]+1\}^{\gamma/(\gamma-1)} \quad \text{(B11)}$$

Where v_i is in f/s, and T_i is in °R. These equations are both acceptable for use with real- and ideal γ over intervals where $C_p = C_v + R$ and where they are constant or over intervals where a reasonably constant average value is taken. *Caution: they are not acceptable for use in doing pipelined spread sheet calculations with variable γ to approximate real gas.*

When using the Equations (B10-11), there is an assumption that the interval over which they are applied ends with a zero gas velocity. Therefore in dividing up any range of input values, one cannot use the output of the first interval (which will be zero velocity) as the input for the second interval which is taken as nonzero.

In the case of a real-gas analysis using a thermo database, one would follow the math steps as worked through in the earlier papers [***4, 5***]. In that analysis, there are three nonzero contributors (algebraic terms cited as Stage 2, Stage 3 and Stage 5 in the earlier papers) to the maximum velocity that a pressure differential can produce. In the previous section on maximum achievable velocity, these three terms were calculated then equated to the kinetic energy term to extract a velocity. In this case one takes the velocity and converts it into a kinetic energy, then apportions it over the three potential energy terms

The Stage 2 term is the work done by an arbitrary gas slug by the upstream pressure, $P_u V_u$. The Stage 3 term is the work the slug does on itself during an expansion. This Stage 3 work is the same as the energy that would be calculated to estimate a TNT equivalency for an explosion in vacuo. And the Stage 5 work is the work the gas slug must do on the downstream gas pressure, $P_d V_d$. The sum of Stage 4 and Stage 5 are the same energy term that would be used to estimate the TNT equivalency of the expanding slug in an ambient pressure equal to the

downstream pressure. In the previous section on TNT equivalency, the last term was taken as atmospheric pressure.

In determining the maximum real total pressure for this tutorial, the kinetic energy was combined with the work done on the gas slug by the incident pressure behind the slug (P_iV_i), and a spread sheet table was prepared of sums of the other two terms P_tV_t + TNT Equivalency (based on internal energy change using NIST data) was created and the solution was taken as the term in which the former equaled the latter.

Appendix C

Adiabat.exe: Structure and Standards

This tutorial was initially posted publicly in early 2007 and as described in the main text the writer had coded and posted with it an associated non-validated (i.e. "As is" and "Use at your own risk") draft software algorithm as both a teaching aid and for estimating peak "real" adiabatic compression temperatures: adiabat.exe. The writer had hoped that ASTM Committee G4 would validate and adopt it as a PC utility based on this concept or even this very code. This appendix is to describe the software details and potential user options.

Adiabat.exe was first written in Microsoft Visual Basic 3.0 (VB3.0). As of this writing, there is a review of the history of Visual Basic and it successor on Wikipedia at:

http://en.wikipedia.org/wiki/Visual_basic .

VB3.0 is an older (1993) 16-bit version of the Visual Basic language (the software achieved 32 bit status in VB 4.0 in 1995 and ultimately a final version 6.0 (in 1998) issued before being phased out and replaced by something called VB.NET. There are several reasons for preserving this older software approach. This is the same language used for the withdrawn ASTM G4 software including G4Math.exe Versions 1.0-1.2 first issued in 1991. As a result ASTM G4 purchased a copy of the software and was therefore licensed to distribute a balloted version of this software and its support files, if it should desire. ASTM may not own a later version but the writer owns VB3.0, VB4.0 and VB6.0 versions.

With the widespread adoption of 64-bit PCs, the oldest 16-bit VB3.0 software (useable on 32-bit PCs) became unusable to many, although there may be some 32-bit PCs still in use with the working G4Math software on them. It was easy to upgrade the code to 32-bit software that will run equally well on 32-bit PCS (apparently even with the latest Windows10 Operating systems), and on 64-bit PCs in 32-bit "Compatibility Mode". Adiabat.exe has been similarly upgraded to 32 bit operation and renamed adiabat32.exe.

Software such as adiabat.exe and adiabat32.exe (namely software without ongoing support) needs to be robust if not bulletproof. And that is easier to achieve if the source language is not in the debug stage. Furthermore, although later versions of Visual Basic have much more power and many more Internet bells and whistles, they come with a much greater degree of complexity. Visual Basic 3.0-6.0 is a known quantity. Finally, these versions allow for the avoidance of formal installation and modification of a user's registry file which entails many risks. One can insert a CDRom or USB key or copy a folder of files to a hard drive and run the program from it without installation. To remove the file from the system, one can just remove the CDRom or USB key or delete any folder that the files were copied to.

This software basically reads and analyzes a Log/Log graph. One loads a graphics file produced by a spreadsheet into it and it allows for the reading of various points on the surface

and reports various related calculations in assorted units with sufficient resolution that one can read graphical data like those on Figure 4 and estimate the "real" behavior of fluids without having to do actual math with polytropic equation, or equations of state, or even databases like NIST 12 and 23. Thus making "real" fluid property data readily available to "Qualified Technical Personnel" at all levels of training. However, where greater resolution is needed these other alternatives can still be used.

The adiabat32.exe (and adiabat.exe) file is the heart of the program along with assorted support files and data files. The user is cautioned below about the support files and is advised how to produce a limited number of data files of his own.

Support Files

Adiabat.exe and adiabat32.exe both come with several support files (.DLLs, .OCX, etc.). For example for adiabat.exe they are: Ddeml.dll, Ver.dll, and Vbrun300.dll. These files are placed in the same, hopefully dedicated, folder/directory (for example (\adiabat or \adiabat32) that contains. adiabat.exe (or adiabat32.exe for 64 bit PCS systems). There are several reasons for doing this.

This renders the operations of the program complete within the folder/directory. One installs the program simply by copying the files into the dedicated folder/directory and "uninstalls it simply by deleting the entire folder/directory. There are no risky changes made to the Windows registry. Whenever the program is operated it uses the exact support files for which it was developed and debugged,.. and thereby avoids incompatibility issues the commentary on the Internet refers to as "dll-hell".

Some advanced PC users like to place the support files into the Windows System directory. This has several advantages in theory, but their benefits can be elusive in practice. The writer recommends against his approach for all but the most advanced and skillful PC users. An example will illustrate.

The concentration of the support files in the Windows System Directory allows the computer to avoid multiple copies of the same file on the system. In the old days when disk space was scarce, this was an important consideration, but is irrelevant today for small programs like these. It allows all software to use the latest and presumably best versions of the support files. However, this is a mixed virtue.

In theory, the latest version of a support file is the best and is all anyone should need. But with Visual Basic in the past the promise has not been realized. When the writer wrote his first software in Visual Basic 4.0 and installed it on an intranet and in various PC's system directories and registries, it broke (read that as "crashed") all of the Visual Basic 3.0 applications present. The upgrades did not upgrade (this is one of the very valid sources of much of the legitimate and deserved animosity towards Microsoft software in the world). This does not appear to happen when each application is used with the exact support files it was developed with (and debugged with, as happens in many standards groups). When software might be used for safety purposes, software complexity should be avoided, even for "as is" and "use at your own risk"

software.

In the past, departures from this cautious approach in search of the latest glitz have caused problems for persons attempting to use ASTM 's G4Math.exe software. The writer is not aware of any PC issues with those whose installed G4Math in the recommended way.

User-Produced Data Files

Both adiabat.exe and adiabat32.exe come with 12 graphic datafiles in windows metafile (.wmf for adiabat.exe) or Windows enhanced metafile (.emf for adiabat32.exe) format:

Oxidants	Diluents	Miscellaneous
o2.(wmf or emf)	argon.(wmf or emf)	capsule.(wmf or emf)
f2.(wmf or emf)	he.(wmf or emf)	blank.(wmf or emf)
nf3.(wmf or emf)	n2.(wmf or emf)	o2argon.(wmf or emf)
n2o.(wmf or emf)	co2.(wmf or emf)	cf4.(wmf or emf)

Each of these is menu selectable in the software. The menu also lists several user file options: user1, user2, user3, user4, user5, user6. All in either .wmf or .emf format. These files are all the same in that they do not contain data and only carry a message that they may be replaced by files the user creates to exploit the software.

Creating Data Graphic Files

The data files for both adiabat.exe and adiabat32.exe were created in a Lotus 123 spreadsheet by extracting data from various NIST software as described in the tutorial. Logarithms of each point were extracted. Each matrix of log/log adiabatic curves (isentropic curves) were joined with six other data points:

1. .301 (~2 psia), 1.6 (~40°R, -420°F) Lower left calibration point
2. .301 (~2 psia), 3.657 (~4540°R, 4080°F) Upper left calibration point
3. 3.55 (~3550 psia), 1.6 (~40°R, -420°F) Lower right calibration point
4. 3.55 (~3550 psia), 3.657 (~4540°R, 4080°F) Upper right calibration point
5. 1.1673 (~14.7 psia), 2.7243 (~530°R, ~70°F) Ambient calibration point
6. The critical point pressure and temperature for the subject fluid

These calibration points were formed with "+" (crosses) made of short line segments and did not use the "+" symbols in the Lotus 123 symbol sets, because that symbol was not large enough to be readily seen after conversion to a .wmf or .emf graphic.

A plot of the data was prepared in Lotus 123 Release 9 with the limits on the abscissa (log pressure in log psia) of 0 to 4 (1-10,000 psia), and on the ordinate (log [T in Rankine]) of 1.5 to 4.0 (31.6 to 10,000°R). Grids and the like inside the frame are optional, but ticks are not allowed on the outside of the axis.

The plot was Selected, Copied and Pasted into a Corel PrintOffice Version 5 (5.00.203) software. The pasted file was Ungrouped twice ("Arrange, Ungroup") and the background mats were deleted. The scales on both axis were selected and deleted. An identifier was typed into the upper left corner. The figure was then Selected and grouped ("Arrange, Group"). Then it was saved in Windows metafile format, and during the "Save As" step, one must select the "Save as Type: Windows Metafile (WMF) [or Window Enhanced metafile (EMF)] option" and also check the "Selected only" checkbox and then save the file to the \adiabat folder/directory. Users must assign the names: user1, user2, user3, etc. Files created this way should open when selected from the dropdown menu in adiabat.exe or adiabat32.exe and clicking on the calibration points should yield reports approximating the points cited above to within the pixel error of the PC.

An example copy of the Lotus 123 spread sheet that was used for pure oxygen is included in the adiabat folder as o2.123